Universität Basel

Fakultät für Psychologie

Robust pipelines for extensive analyses of large genetic and brain imaging datasets linked to complex human behavior

A cumulative dissertation submitted to the Faculty of Psychology, University of Basel, in partial fulfillment of the requirements for the degree of Doctor of Philosophy by

Jana Petrovska

from Skopje, North Macedonia

Basel, 2020

Universität Basel

Fakultät für Psychologie

Approved by the Faculty of Psychology at the request of

Professor Dr. med. Andreas Papassotiropoulos

Professor Dr. med. Dominique J.-F. de Quervain

Date of the doctoral examination: 24.02.2020

Dean of the Faculty of Psychology

Universität
Basel

Fakultät für
Psychologie

Declaration of scientific fairness

I Jana Petrovska hereby declare that the present work was written independently without the help of third parties and without the use of any means other than those indicated. Sources used for help are marked as such. The manuscripts published or submitted for publication in journals were prepared in cooperation with the co-authors and were not published elsewhere by any of the participants, submitted for publication, or submitted to any other examination authority as a qualification paper. These are the following manuscripts:

- Petrovska, J., Coynel, D., Fastenrath, M., Milnik, A., Auschra, B., Egli, T., Gschwind, L., Hartmann, F., Loos, E., Sifalakis, K., Vogler, C., de Quervain, D. J.-F., Papassotiropoulos, A. & Heck, A. (2017). The NCAM1 gene set is linked to depressive symptoms and their brain structural correlates in healthy individuals. *Journal of Psychiatric Research*, *91*, 116-123.

- Petrovska, J., Loos, E., Coynel, D., Egli, T., Papassotiropoulos, A., de Quervain, D. J.-F. & M., Milnik, A. Recognition memory performance can be estimated based on few specific brain networks.

- Heck, A., Milnik, A., Vukojevic, V., Petrovska, J., Egli, T., Singer, J., Escobar, P., Sengstag, T., Coynel, D., Freytag, V., & Fastenrath, M., Demougin, P., Loos, E., Hartmann, F., Schicktanz, N., Bizzini, B. D., Vogler, C., Kolassa, I.-T., Wilker, S., Elbert, T., Schwede, T., Beisel, C., Beerenwinkel, N., de Quervain, D. J.-F. & Papassotiropoulos, A. (2017). Exome sequencing of healthy phenotypic extremes links TROVE2 to emotional memory and PTSD. *Nature Human Behaviour, 1(4)*, 1-10.

Jana Petrovska

Basel, 23.01.2020

Abstract

The rapid technological and methodological advances in genetics, molecular biology and brain imaging in the last decades have enabled the current wide-spread application of brain-wide and genome-wide analyses of potential biological substrates of complex behavioral traits, such as psychological processes and psychiatric disorders. This thesis addresses methodological and statistical issues emerging from the large scale, complexity and explorative nature of brain-wide and genome-wide analyses. Furthermore, it points out additional steps for increasing the confidence in findings resulting from such extensive analyses. It does so by introducing two studies investigating the genetic bases of depressive symptoms and the brain imaging underpinnings of recognition memory performance, respectively. In the first study we aggregated genome-wide data of genetic variation to groups of genes and used inferential statistics to associate them with depressive symptoms. We also replicated the results in an independent sample and used imagining genetics to validate and extend our findings. In the second study, we decomposed the voxel-wise brain activation contrast of looking at previously seen vs. new pictures into 12 brain networks, based of which we evaluated recognition memory performance using prediction analysis. We used stable and reproducible data-driven decomposition and we trained and tested our prediction model in different samples, insuring higher generalizability of our findings. These two studies offer additional insight into the biological underpinnings of complex behavioral traits. Importantly, the applied analyses were carefully tailored to the specific research questions and integrated into robust pipelines for replication and validation of the initial results.

Acknowledgments

I would like to take this opportunity to thank my supervisors, Prof. Andreas Papassotiropoulos and Prof. Dominique J.- F. de Quervain, for providing me with the possibility to take this PhD journey filled with exciting and diverse projects. Their great passion for science made me feel very proud and fortunate to be part of the divisions! I am deeply grateful for all their guidance, support, motivation and encouragement, as well as their sincerity and kindness. I would also like to thank Dr. Angela Heck, who helped me take my first steps into the field of genetic research. She was an excellent mentor from whom I learned a great deal! I am also grateful to Dr. Annette Milnik for teaching me so much about coding and statistical analysis. Thank you, Annette, for all your time, effort and patience! I would also like to express my appreciation to Dr. David Coynel for all his help with the brain imaging analyses, especially at the beginning, and for offering advice and support nearly instantaneously after an email! Furthermore, I would like to thank my officemate Dr. Virginie Freytag and Dr. Vanja Vukojevic for being very helpful, friendly and supportive, as well as all the other colleagues that made the workplace so pleasant and productive.

On a more technical note, I would like to thank all who contributed to the creation of the large, diverse datasets that I had the privilege to work with. This thesis (and so much more) would not be possible without them. Thank you for the high-quality data, crucial for robust research!

I would also like to thank my family for their great and continuous enthusiasm encouragement and support. Finally, I am very thankful to my partner, Thomas David, for all his patience and care! ***Thank you all!***

Table of Contents

Abbreviations

BOLD: Blood oxygenation level-dependent signal, 17

DNA: Deoxyribonucleic acid, 8
DTI: Diffusion tensor imaging, 17

FA: Fractional anisotropy, 18
fMRI: Functional magnetic resonance imaging, 10
FWER: Family-wise error rate, 23

GM: Grey matter, 17
GWAS: Genome-wide association study, 14

IC: Independent component, 25
ICA: Independent component analysis, 25

LD: Linkage disequilibrium, 14

MADRS: Montgomery Asberg Depression Rating Scale, 12
MDD: Major depressive disorder, 12
MRI: magnetic resonance imaging, 8

SNP: Single nucleotide polymorphism, 14

WM: White matter, 17

1 Introduction

Over the last few decades, there has been substantial progress in the investigation of the biological underpinnings of complex human behavior. The rapid technological and methodological advances in genetics, molecular biology and brain imaging throughout the years have greatly contributed to this endeavor. Innovations in high-throughput genotyping have provided the possibility for rapidly generating high-density datasets of genetic variability throughout the genome ("genomics") (Brown & Botstein, 1999; Bumgarner, 2013; Goodwin et al., 2016; Metzker, 2010). Additional high-throughput technologies have been developed, capable of generating extensive datasets of distinct molecular information, e.g., deoxyribonucleic acid (DNA) methylation or gene expression, on a global scale ("-omics") (Hasin et al., 2017). Furthermore, the development of non-invasive magnetic resonance imaging (MRI) technology has enabled the production of large datasets of estimates of brain anatomy and neural function with high spatial resolution (Belliveau et al., 1991; Lerch et al., 2017). These technological advances have been followed by the creation of an abundance of analytical software for the utilization of large (gen)omics and brain imaging data. Furthermore, there has been an increasing initiative for data and technology sharing in these fields, making diverse datasets, as well as state-of-the-art analytical tools quickly accessible to the scientific community (Bycroft et al., 2018; Craig et al., 2011; Kannan et al., 2016; Nichols et al., 2017; Sullivan, 2010; Thompson et al., 2014; Van Essen et al., 2013).

These developments have enabled the current widespread application of extensive brain-wide and genome-wide analyses in search of potential biological substrates of complex behavioral traits, such as psychological processes and

neuropsychiatric disorders. For example, there are over 20,000 experiments including brain-wide analysis of brain function or structure only in the BrainMap database - http://brainmap.org/ (Laird et al., 2005; Vanasse et al., 2018) and over 500 publications with genome-wide search for genetic background of psychology-related traits only in the GWAS Catalog - https://www.ebi.ac.uk/gwas/ (Horwitz et al., 2019). While hypothesis-driven studies targeting specific genes or brain regions of interest can certainly extend our understanding of the biological underpinnings of complex behavior, extensive genome-wide and brain-wide approaches have proven essential for many novel discoveries (Horwitz et al., 2019; Papassotiropoulos & de Quervain, 2011; Poldrack & Farah, 2015).

However, specific methodological and statistical issues appear due to the large scale, complexity and the explorative nature of such extensive approaches, many of which are common to both brain imaging and genomics (Lazar, 2016). In this thesis, I will present two studies applying extensive analyses of potential genetic and brain imaging substrates of complex behavior, respectively, and address some of those issues. First, I will provide a brief description of some of the different *levels of analyzing* brain-wide and genome-wide datasets, ranging from single units to pathways and networks. Next, I will introduce two distinct *types of analysis*, i.e., inference and prediction, as well as their purpose in the context of neuroscientific research. Finally, I will discuss some potential ways in which the initial analyses can be integrated into *robust analytical pipelines*, in order to insure more meaningful, high-confidence results. The two studies that will serve as examples are listed below.

- **Study 1**: Petrovska, J., Coynel, D., Fastenrath, M., Milnik, A., Auschra, B., Egli, T., Gschwind, L., Hartmann, F., Loos, E., Sifalakis, K., Vogler, C., de Quervain, D. J.-F., Papassotiropoulos, A. & Heck, A. (2017). The NCAM1 gene set is linked to depressive symptoms and their brain structural correlates in healthy individuals. *Journal of Psychiatric Research*, *91*, 116-123.
- **Study 2**: Petrovska, J., Loos, E., Coynel, D., Egli, T., Papassotiropoulos, A., de Quervain, D. J.-F. & M., Milnik, A. Recognition memory performance can be estimated based on few specific brain networks.

In Study 1, we conducted a genome-wide search for groups of genes, i.e., gene sets, associated with depressive symptoms in a large sample of healthy young adults (*N* = 2'099). While several gene sets were significantly associated with depressive symptoms in this sample, we *robustly* identified the NCAM1 Interactions gene set as relevant for our trait of interest due to its association with depressive symptoms and their structural brain correlates in an additional independent sample (*N* = 1'523 and *N* = 658, respectively). I contributed to designing the experiment, analyzing the data and writing the paper for this study.

In Study 2, we used whole-brain functional MRI (fMRI) data from 1'410 healthy young adults that performed a picture-recognition task. We robustly estimated the task performance based on the fMRI-derived brain activation. First, we decomposed the brain activation contrast of previously seen vs. new pictures from 56'764 voxels, i.e. three-dimensional pixels, into 12 *robust* and *replicable* brain networks by performing data-driven dimensionality reduction in two independent samples of participants (*N* = 645, *N* = 665). Next, we estimated recognition memory performance based on the 12

networks in a third independent sample (N = 100). I contributed to designing the experiment, analyzing the data and writing the paper for this study.

2 Complex behavioral traits

Common neuropsychiatric disorders and the psychological processes associated with them are complex behavioral traits influenced by a combination of interacting genetic and environmental factors. As such, they have notable heritability and diverse (neuro)biological and behavioral correlates (Assary et al., 2018; Murray et al., 2017; Otte et al., 2016; Papassotiropoulos & de Quervain, 2011). In the next paragraphs I will briefly introduce two such complex traits, depressive symptoms and recognition memory, as their biological underpinnings were the object of investigation in Study 1 and Study 2 of this PhD thesis, respectively.

2.1 Depressive symptoms

Major depressive disorder (MDD) is a highly debilitating psychiatric disorder, with a lifetime prevalence of about 20%. It is characterized by experiencing a minimum of one depressive episode with a duration of at least two weeks, including notable changes in mood, interests, pleasure and cognition, as well as vegetative symptoms (Otte et al., 2016). Depressive symptoms are continuously distributed throughout the general population and symptoms below the diagnostic threshold for depression are related to the same risk factors as full-blown depressive episodes (Ayuso-Mateos et al., 2010). Therefore, utilizing the continuous spectrum of depressive symptomatology may provide additional insights into the complex underpinnings of depression. Depressive symptoms can be measured by standardized psychological instruments, such as the Montgomery Asberg Depression Rating Scale (MADRS) (Montgomery & Asberg, 1979) or the Beck Depression Inventory (Beck et al., 1996). In Study 1, we

obtained MADRS scores of young healthy individuals and used them to investigate the genetic basis and the neural correlates of depressive symptoms.

2.2 Recognition memory

Recognition memory is a complex psychological process entailing the identification of an event and the judgement of its previous occurrence, which has a vital role in our daily life (Mandler, 1980). The nature and the neural features of recognition memory have been the object of extensive scientific research and debate (Squire et al., 2007; Yonelinas, 2002). However, studies on the neural underpinnings of recognition memory typically investigate the general neural mechanism associated with recognition memory processes (Carlesimo et al., 2015; Frithsen & Miller, 2014; Horn et al., 2016; Kim, 2010; Scalici et al., 2017; Skinner & Fernandes, 2007; Spaniol et al., 2009; Vilberg & Rugg, 2008; Yonelinas et al., 2005). More research is needed on neural systems underlying interindividual differences in recognition memory performance in healthy individuals (though please see de Chastelaine, Mattson, Wang, Donley, & Rugg, 2016). In Study 2 of this PhD thesis, recognition memory performance was assessed by subjecting our participants to an image-based memory test while recording their brain activation in the MRI scanner, in order to estimate interindividual differences in memory performance based on the fMRI signal.

3 Extensive analyses of the biological underpinnings of complex human behavior

In the next paragraphs, I will outline some important analytical considerations when investigating the neural and genetic underpinnings of complex behavioral traits in an extensive manner. Notably, both brain imaging and genetic data can be analyzed on multiple levels, ranging from single units to pathways, networks and overall measurements. Furthermore, one faces some similar analytical challenges when working with these two modalities (Lazar, 2016). First, I will review some of the levels of analysis of genomics and brain-wide imaging data, respectively. Second, I will discuss the types of analysis that can be applied to each modality.

3.1 Level of analysis: From single units to pathways and networks

3.1.1 Genome-wide approaches

The most widely used contemporary approach for investigating the genetic underpinnings of complex traits is conducting a genome-wide association study (GWAS). The majority of GWASes conducted to date rely on DNA microarray chip technology to rapidly produce data for a large number of predetermined single nucleotide polymorphisms (SNPs), i.e., interindividual differences in a single base pair of the DNA sequence, throughout the genome (Bumgarner, 2013; Chee et al., 1996). Microarray technologies profit from the naturally existing correlational structure between DNA variants, termed linkage disequilibrium (LD) (Gibbs et al., 2003). Namely, SNPs tagged by the microarray are usually in high LD with additional variants, thus capturing information beyond a single base pair. However, array-based

technologies are typically limited to tagging common variants, found in over 1% of the general population (Visscher et al., 2017). More recently developed whole exome and whole genome sequencing technologies can produce extensive exome-wide and genome-wide data for both common and rare genetic variants (Kiezun et al., 2012; Sanders et al., 2017). Nevertheless, due to the longer use and lower financial cost of microarrays compared to sequencing technologies, array-based datasets still remain more prevalent.

An array-based GWAS usually tests the association between a heritable trait and each of around one million SNPs throughout the genome (Corvin et al., 2010). Furthermore, by applying genotype imputation, i.e., a method of inferring genotypes at untagged locations based on LD patterns, the number of tested variants can be greatly increased (Das et al., 2016; Marchini et al., 2007). Thus, GWAS is a large-scale method for investigating the genetic underpinnings of a given trait. This approach has proven successful for identification of common SNPs associated with many complex traits and diseases, such as type 2 diabetes, height, body mass index, memory performance, neuroticism, schizophrenia and MDD (Fuchsberger et al., 2016; Lam et al., 2019; Li et al., 2017; Locke et al., 2015; Luciano et al., 2018; Nagel et al., 2018; Papassotiropoulos et al., 2011; Papassotiropoulos et al., 2006; Pardinas et al., 2018; Ripke et al., 2014; Wood et al., 2014; Wray et al., 2018). However, most of the identified genetic variants have small effect sizes. This notion can be problematic for GWASes considering that their results need to surpass stringent statistical correction for false-positive findings due to the large number of association tests conducted (Pe'er et al., 2008; Price et al., 2015). Therefore, a very large number of participants is typically needed in order to gain sufficient statistical power for GWAS-based detection of common variants associated with complex traits (Sullivan et al., 2018).

Furthermore, GWAS findings do not offer any information regarding the biological mechanisms underlying the identified genetic associations (Visscher et al., 2017).

Methods for secondary analysis of GWAS summary statistics, such as gene-level and gene-set analysis (GSA), can increase the statistical power for investigating the genetic underpinnings of complex traits and disorders and place association findings in a wider biological context (Wojcik et al., 2015). Gene-level analyses combine GWAS statistics (or raw genetic variance) per gene, and associate each gene with a given trait (e.g. de Leeuw et al., 2015). GSA aggregates single variants to genes and genes to groups of genes (also known as gene sets or pathways) based on prior knowledge regarding their biological or functional properties and investigates the association of each gene set with a trait of interest (de Leeuw et al., 2016; Wang et al., 2010). This method has been successfully utilized to identify genetic underpinnings of complex behavioral traits and disorders, such as working memory, episodic memory, schizophrenia and bipolar disorder (Heck et al., 2014, 2015; Lips et al., 2012; Nurnberger et al., 2014). GSA was also used in Study 1 contributing to this PhD thesis, in which we aggregated GWAS summary statistics to 1'411 gene sets in search of genetic basis of depression scores in healthy young adults (Petrovska et al., 2017).

3.1.2 Brain-wide approaches

Within the last few decades, the neural underpinnings of complex human behavior have been predominantly investigated using MRI. MRI technology utilizes the magnetic properties of the nuclei of hydrogen atoms in order to create images of soft tissues in the human body, including the brain (Plewes & Kucharczyk, 2012). A typical

MRI scanner produces three-dimensional images with a rather high spatial resolution, e.g., 1 mm^3 or better for T1-weighted anatomical images (Lusebrink et al., 2017).

Contemporary MRI technology provides diverse possibilities for non-invasive large-scale investigation of the human brain. MRI techniques based on the distinct structural properties of grey matter (GM) are used for estimation of cortical thickness, surface area and volume (Lerch et al., 2017). Importantly, MRI is also used for investigating brain function. fMRI technology typically relies on a measure of the magnetization difference between oxygenated and deoxygenated hemoglobin in the brain, termed blood oxygenation level-dependent (BOLD) signal. The BOLD signal is considered to reflect changes in the levels of oxygen consumption within a brain region and is used as an estimate of brain activation (Gauthier & Fan, 2019). Since its development nearly three decades ago, fMRI has become one of the most prevalent brain imaging techniques in neuroscientific research (Roalf & Gur, 2017; Rosen & Savoy, 2012). Another widely-used MRI technique is diffusion tensor imaging (DTI). DTI relies on the specific nature of the dispersion of water molecules in white matter (WM) throughout the brain, in order to make inferences regarding the structural properties of WM tracts connecting brain regions (Basser, 1995; Beaulieu, 2002).

Initially, the majority of quantitative MRI studies investigating the neural underpinnings of complex human behavior have estimated to which extent individual brain regions are implicated in a specific function or trait (Chen & Glover, 2015). However, it has been well-established that interacting brain areas, rather than single regions, are enabling cognitive processes and complex behavior (Bressler & Menon, 2010; Fuster, 2000; Misic & Sporns, 2016). Therefore, additional analytical strategies, complementary to the regional approach, have been developed in order to investigate the structural connectivity and functional interactions between brain regions. Structural

connectivity has been predominantly estimated by DTI analysis. DTI measurements, such as fractional anisotropy (FA) and mean diffusivity, have been linked to cognition and neuropsychiatric disorders like schizophrenia and MDD (Coynel et al., 2017; Jiang et al., 2017; Kelly et al., 2018; Takeuchi et al., 2011). Furthermore, functional interactions between brain regions, assessed by connectivity analyses of fMRI data (reviewed in Friston, 2011; Reid et al., 2019), have been implicated in cognitive processes such as memory, learning, attention, cognitive control, reward processing and language (Legon et al., 2016; McIntosh et al., 1999; Salimpoor et al., 2013; Spielberg et al., 2015; Stephan et al., 2003; Vossel et al., 2016; Xu et al., 2015). For example, an increased connectivity from the amygdala to the hippocampus has been found during the encoding of emotional pictures in healthy young adults (Fastenrath et al., 2014). Not only individual connections, but large-scale networks including connectivity between multiple brain regions are recruited by complex behavioral tasks, as well as during rest (Damoiseaux et al., 2006; Fox et al., 2005; Smith et al., 2009). Network-level brain activation has also been related to cognitive outcomes, such as working memory performance, emotional memory and speed of recollection (Egli et al., 2018; Fornito et al., 2012; Loos et al., 2019).

In Studies 1 and 2 we investigated structural properties of brain tracts and network-level brain activation, respectively, as potential neural underpinnings of complex behavioral traits. In Study 1, we identified brain tracts related to depressive symptoms using DTI analysis. Specifically, we obtained brain-wide FA values, reflecting WM properties (e.g. fiber density), as well as coherence within a voxel (Beaulieu, 2002), and associated them with our behavioral trait. Depressive symptoms were associated with decreased FA within the forceps minor and the left superior temporal longitudinal fasciculus. In Study 2, we decomposed the fMRI contrast of

looking at previously seen vs. novel pictures into 12 independent components, potentially representing distinct functional brain networks, based on which we estimated memory performance.

3.2 Type of analysis: Inference and prediction

Traditionally, neuroscientific research has relied on inferential statistical approaches, such as null hypothesis significance testing, for data analysis. More recently, predictive approaches have been adopted as a popular alternative (Bzdok & Ioannidis, 2019; Gabrieli et al., 2015; Woo et al., 2017; Yahata et al., 2017). While contemporary prediction analyses can rely on highly complex pattern-learning algorithms, it is actually the purpose of the analysis, rather than the applied tool, that makes the key distinction between prediction and inference. For example, ordinary linear regression can be used for both prediction and inference. Therefore, the decision whether to apply inference or prediction should depend on the specific research question and the motivation for its investigation (Bzdok & Ioannidis, 2019). Inference can provide insight into the importance, and somewhat the nature, of the contribution of given variable(s) to a certain outcome. Inferential statistics are suitable for identifying genetic variants, genes, gene sets, brain regions or networks related to a given (behavioral) trait (e.g. Egli et al., 2018; Heck et al., 2014, 2015; Papassotiropoulos et al., 2006). Prediction approaches evaluate how well can a model built based on the relation between given variables and an outcome of interest reproduce that outcome. Predictive models have already been successfully used for the estimation of complex brain-related behavioral traits, such as emotional arousal, emotional memory performance and alcohol misuse (Loos et al., 2019; Whelan et al., 2014). On the one hand prediction allows higher

generalizability of the results compared to inferential approaches, but on the other hand it is typically used in a “black box” manner without explanatory power or insight into the contribution of individual predictors (but also see Yarkoni & Westfall, 2017). Therefore, inferential and prediction approaches have distinct and complementary roles in neuroscientific research. In Study 1 of this PhD thesis, we used an inferential approach in order to identify gene sets and brain tracts associated with depressive symptoms, while in Study 2 we applied prediction analysis for the estimation of memory performance based on brain activity. Of note, in Study 2 we used a linear model, rather than a more complex predictive algorithm, in order to maximize the transparency and generalizability of our results (Bzdok & Ioannidis, 2019).

4 From initial results to robust findings

4.1 Results replication

Replication of the initial results in an independent sample is widely accepted as the gold standard for confirming the validity of novel discoveries in scientific research and (lack of) replicability is a major concern across scientific disciplines, including neuroscience and genetics (Boekel et al., 2015; Ioannidis, 2005; Jasny et al., 2011; Marigorta et al., 2018; Plomin et al., 2016; Poldrack et al., 2017; Schmidt, 2009). When possible, independent replication should be conducted as part of the initial analytical pipeline, in order to insure higher robustness of the results before they are shared with the scientific community. However, independent replication is not always feasible, particularly when working with large and complex datasets that require a lot time, financial recourses and scientific expertise to be generated, such as large-scale genomics or brain imaging data. When this is the case, one alternative strategy would be to use *cross-validation* in order to investigate the reproducibility of the results when limited to a single sample. Cross-validation techniques insure training and testing our model on different data within the sample (Yarkoni & Westfall, 2017).

In Study 1, the identified link between certain gene sets and depressive symptoms in a large sample of healthy young adults (N = 2'099) was replicated in an independent sample (N = 1'523). In Study 2, we used fMRI and behavioral data of a single sample of 1'410 healthy young adults. Although we technically lacked an independent replication sample in this study, due to the large sample size we were able to split the initial sample into three different samples of 645, 665 and 100 participants, respectively, while maintaining adequate statistical power for our analyses. We trained our prediction model on the first sample and tested it on the

second and third sample, respectively, insuring higher generalizability of our findings. For achieving the highest independency between our three samples, we created them by chronologically ordering the participants of the overall sample by date of study participation and then performing the sample split.

4.2 Study-specific considerations

While the need for replication of the results is a general requirement for increasing the validity of scientific research, many aspects of the robustness of findings are tightly related to the particular specificities of the study in question, such as the study aim and design, the nature and size of the datasets, the specific tools used for data analysis and the number of conducted tests. Therefore, below I will discuss some specific considerations regarding the robustness of findings in Study 1 and Study 2, respectively.

4.2.1 Statistical significance and multiple testing correction

In Study 1, we estimated the statistical significance of the association between depressive symptoms and a large number of predefined gene sets (*N* = 1'411) based on an *enrichment p-value* provided for each gene set. The enrichment p-value was calculated based on the observed number of genes associated with the phenotype, i.e., depressive symptoms, (above a given enrichment threshold) within the gene set, compared to the number of phenotype-associated genes expected by chance for a gene set of that size (Segre et al., 2010). However, because we repeated the enrichment test for each of the 1'411 gene sets, it was necessary to make a statistical

adjustment in order avoid “false-positive” results due to multiple testing (Goeman & Solari, 2014).

The classical type of adjustment for multiple testing based on the probability of at least one false discovery, i.e., *family-wise error rate (FWER)*, can be overly conservative, greatly reducing the power to detect true findings, particularly in the context of very large number of tests (Chen et al., 2010). Having over 1’400 tests in our discovery sample, we opted for the more lenient *false discovery rate (FDR)* type of multiple testing correction, based on the expected proportion of falsely rejected discoveries. Since in the replication sample we ran the analysis for only a few gene sets identified as significantly associated with depressive symptoms in the discovery sample, here we applied the more stringent FWER correction.

In order to identify gene sets implicated in depressive symptomatology, we have chosen the commonly applied statistical significance level of *0.05* (after multiple-testing adjustment). While having practical value, such thresholds for the assessment of statistical significance are arbitrary and should be taken with critical consideration (Amrhein & Greenland, 2018; Benjamin et al., 2018).

4.2.2 Imaging genetics

Findings from genetics and (gen)omics studies of complex behavioral traits can be further validated and extended by the addition of brain-level information (Bogdan et al., 2017; Papassotiropoulos & de Quervain, 2011). The research field of brain imaging genetics combines information regarding (epi)genetic variation and brain structure, function, connectivity or chemistry in order to contribute to the understanding of the impact of genetic and molecular differences on behavioral traits on neural level

(Bogdan et al., 2017). While the pioneering brain imaging genetics research conducted over two decades ago consisted of candidate gene studies of receptor ligand binding measured using positron emission tomography (Laruelle et al., 1998; Pohjalainen et al., 1998), today this research field includes studies using a variety of sophisticated (f)MRI and (epi)genetic measurements (Bogdan et al., 2017). For example, imaging genetics findings from our own research lab include specific memory-related genetic variation on single variant and pathway level, as well as epigenetic differences, associated with brain activation (de Quervain et al., 2012; Heck et al., 2014, 2015, 2017; Papassotiropoulos et al., 2013; Vukojevic et al., 2014), a genetic variant related to emotional arousal and white matter properties of the brain (Spalek et al., 2016) and an epigenetic signature associated with memory and neocortical thickness (Freytag et al., 2017).

In study 1 of this PhD thesis, after identifying two gene sets associated with depressive symptoms in two independent samples, we added a level of DTI data and were able to a) link depressive symptoms to white matter properties of two different brain tracts and b) associate those tracts with one of the depressive symptoms-related gene sets.

4.2.3 Stable and reproducible data-driven dimensionality reduction

As stated before, the aim of Study 2 was to estimate recognition memory performance based on the fMRI contrast of seeing old vs. new images while conducting the memory task. We have obtained brain-wide fMRI contrast parameters for over 56’000 voxels per participant. The large number of parameters can be problematic for our memory estimation due to a phenomenon known as *overfitting*. Overfitting occurs when the

model estimation is too closely tailored to the specific dataset and therefore may poorly generalize to new data (Yarkoni & Westfall, 2017).

To overcome this issue, one can reduce the voxel-level dataset to a smaller number of variables. Diverse *theory-driven* and *data-driven* approaches can be used for this purpose. While theory-driven approaches use models based on previous knowledge and/or specific hypotheses concerning the underlying mechanisms of the process in question, data-driven approaches are generally agnostic of such mechanisms (Huys et al., 2016). Therefore, by using a data-driven approach potential biases of prior findings can be avoided.

One data-driven method for dimensionality reduction, i.e., reduction of the number of variables, of a given dataset is independent component analysis (ICA). ICA produces a linear representation of non-Gaussian data, by decomposing them into components that are as statistically independent as possible, termed independent components (ICs) (Hyvarinen & Oja, 2000). ICA can be used to decompose a high-dimensional voxel-level dataset of brain structure or activation into a relatively small number of ICs, which may also be considered as potential independent brain networks (Smith et al., 2009; Vanasse et al., 2018).

The optimal number of ICs resulting from the ICA is a key user-defined parameter of this method and certain analytical steps can be taken for its estimation, such as assessing the components' *stability* and *reproducibility* (Franco et al., 2013; Kairov et al., 2017). Stability, i.e., robustness of the analysis within the initial sample, can be assessed by re-running the ICA multiple times in random subsets of the initial sample, i.e., resampling, and comparing the results across subsets. The ICA stability for a specific number of ICs increases with the similarity of those ICs across subsets. The components' reproducibility refers to the extent to which the dimensionality

reduction with the same number of ICs can be replicated in an independent sample (Franco et al., 2013).

In Study 2, we assessed the components' stability by comparing the ICA results across 100 different subsets of the initial, i.e., *training* sample, each of which contained 90% of the participants from the overall sample. We repeated this assessment for ICAs with different number of components (3-32). We then repeated the five ICAs with best stability in another sample of similar size, i.e., *replication sample*, in order to test their reproducibility. The most reproducible ICA was chosen for downstream analysis. By carefully choosing the number of ICs for ICA decomposition of our dataset based on their stability and reproducibility metrics, we ensured their robustness for estimation of behavior.

5 Original research papers

5.1. The NCAM1 gene set is linked to depressive symptoms and their brain structural correlates in healthy individuals

Journal of Psychiatric Research 91 (2017) 116–123

Contents lists available at ScienceDirect

Journal of Psychiatric Research

journal homepage: www.elsevier.com/locate/psychires

The NCAM1 gene set is linked to depressive symptoms and their brain structural correlates in healthy individuals

Jana Petrovska, MS [a, e, *], David Coynel, PhD [b, e], Matthias Fastenrath, PhD [b, e], Annette Milnik, PhD, MD [a, d, e], Bianca Auschra, MS [a, e], Tobias Egli, MS [a, e], Leo Gschwind, PhD [a, e], Francina Hartmann, PhD [a, e], Eva Loos, MS [b, e], Klara Sifalakis, PhD [b, e], Christian Vogler, PhD [a, d, e], Dominique J.-F. de Quervain, MD [b, d, e], Andreas Papassotiropoulos, MD [a, c, d, e], Angela Heck, PhD [a, d, e]

[a] University of Basel, Department of Psychology, Division of Molecular Neuroscience, Birmannsgasse 8, CH-4055 Basel, Switzerland
[b] University of Basel, Department of Psychology, Division of Cognitive Neuroscience, Birmannsgasse 8, CH-4055 Basel, Switzerland
[c] University of Basel, Department Biozentrum, Life Sciences Training Facility, Klingelbergstrasse 50, CH-4056 Basel, Switzerland
[d] University of Basel, Psychiatric University Clinics, Wilhelm Klein-Strasse 27, CH-4002 Basel, Switzerland
[e] University of Basel, Transfaculty Research Platform Molecular and Cognitive Neurosciences, Birmannsgasse 8, CH-4055 Basel, Switzerland

ARTICLE INFO

Article history:
Received 7 December 2016
Received in revised form
2 March 2017
Accepted 3 March 2017

Keywords:
NCAM1 Interactions
Depressive symptoms
MADRS
Gene set enrichment analysis
DTI
Healthy participants

ABSTRACT

Depressive symptoms exist on a continuum, the far end of which is found in depressive disorders. Utilizing the continuous spectrum of depressive symptoms may therefore contribute to the understanding of the biological underpinnings of depression. Gene set enrichment analysis (GSEA) is an important tool for the identification of gene groups linked to complex traits, and was applied in the present study on genome-wide association study (GWAS) data of depression scores and their brain-level structural correlates in healthy young individuals. On symptom level (i.e. depression scores), robust enrichment was identified for two gene sets: NCAM1 Interactions and Collagen Formation. Depression scores were also associated with decreased fractional anisotropy (FA) – a brain white matter property – within the forceps minor and the left superior temporal longitudinal fasciculus. Within each of these tracts, mean FA value of depression score-associated voxels was used as a phenotype in a subsequent GSEA. The NCAM1 Interactions gene set was significantly enriched in these tracts. By linking the NCAM1 Interactions gene set to depression scores and their structural brain correlates in healthy participants, the current study contributes to the understanding of the molecular underpinnings of depressive symptomatology.

1. Introduction

Depressive symptoms are continuously distributed in the general population, as supported by taxometric studies of large community samples (Hankin et al., 2005; Slade and Andrews, 2005). Depressive disorders are considered to represent the far end of this continuum (Ayuso-Mateos et al., 2010; Kendler and Gardner, 1998; Slade, 2007), and subthreshold depressive symptoms have been associated with the same risk factors as diagnosable depressive episodes worldwide (Ayuso-Mateos et al., 2010). Moreover, higher depressive symptoms have been associated with higher levels of psychosocial dysfunction and increased risk for Major Depressive Disorder (MDD) and substance use disorder in the general adult population (Lewinsohn et al., 2000).

Furthermore, while multiple brain-level structural changes have been implicated in MDD (LeWinn et al., 2014; Ota et al., 2015; Wu et al., 2011; Zuo et al., 2012), microstructural changes within various neuroanatomical tracts have also been associated with subthreshold depressive symptoms (Hayakawa et al., 2013; McIntosh et al., 2013; Sprengelmeyer et al., 2014). Therefore, utilizing the continuous spectrum of depressive symptoms may contribute to the understanding of the biological underpinnings of depression.

* Corresponding author. University of Basel, Department of Psychology, Division of Molecular Neuroscience, Birmannsgasse 8, CH-4055 Basel, Switzerland.
E-mail address: jana.petrovska@unibas.ch (J. Petrovska).

http://dx.doi.org/10.1016/j.jpsychires.2017.03.007
0022-3956/

Self-reported depressive symptoms are moderately heritable in healthy adults, with heritability estimates of 30–37% (Kendler et al., 1994; Sham et al., 2000), which approximately equals heritability estimates for MDD of 31–42% (Sullivan et al., 2000), rendering them a suitable phenotype for genetic studies.

Gene set enrichment analysis (GSEA) can be used to improve the detection and the explanatory power of the genetic basis of heritable traits (Wang et al., 2010). Importantly, GSEA is particularly suitable for the study of complex traits, which are characterized by small genetic effects of multiple genetic variants that contribute to the trait in question (Lohmueller et al., 2003), as demonstrated by previous studies (Heck et al., 2014, 2015; Lips et al., 2012; Nurnberger et al., 2014). Specifically, it tests whether multiple genes with modest associations with a given complex trait are enriched in specific biological processes. The objective of the current study was to dissect the biological basis of depression scores, measured as a continuous, quantitative phenotype in healthy participants, by applying GSEA to genome-wide association study (GWAS) data. Notably, the NETRIN1 signaling pathway was recently associated with MDD using a similar approach (Zeng et al., 2017). Furthermore, the Synaptic transmission pathway was associated with MDD and several immune-inflammatory pathways with depressive symptoms, respectively, using genome-wide expression data (Elovainio et al., 2015; Hori et al., 2016). Therefore, it was hypothesized that depression scores are related to particular gene sets in the current study. Replication was performed in an independent study, having the identical phenotype. Additionally, diffusion tensor imaging (DTI) data in individuals of the replication study were available. Decreases of fractional anisotropy (FA) have been previously reported in both MDD (LeWinn et al., 2014; Ota et al., 2015; Wu et al., 2011; Zuo et al., 2012) and subthreshold depressive symptoms (McIntosh et al., 2013; Sprengelmeyer et al., 2014). FA is a measure of the directional dependence of diffusion (Basser, 1995) and reflects white matter tracts properties such as fiber density, as well as coherence within a voxel (Beaulieu, 2002). To test the hypothesis of a link between depression scores and FA values in our sample of healthy young adults, we first identified brain structural correlates of the depression scores by correlating them with brain-wide FA measurements. To furthermore check if depressive symptoms and brain structural correlates of the depression scores share some genetic background, we ran a GSEA for each of the identified brain tracts, by extracting the mean FA values for depression score-associated voxels from the DTI analysis and using these as a phenotype in a subsequent GSEA.

2. Materials and methods

2.1. Studies

Discovery study (Basel_1): This study was conducted with 2099 cognitively healthy young adults from the general population, recruited in Basel, Switzerland, as part of an ongoing behavioral genetics study (data lock May 2015). Sample characteristics are presented in Table 1. Participants were free of medication and of any neurological and psychiatric conditions at the time of the study as assessed by standard questionnaires. All participants provided written informed consent prior to participation in the study. Data of the Montgomery Asberg Depression Rating Scale (MADRS) (Montgomery and Asberg, 1979), consisting of ten items rated on a scale from 1 to 6, were available for N = 1651 participants. The ratings were summed up to a single depression score (0–60) per participant, ranging from 0 to 46 in this sample, with a mean value (±SD) of 8.48 (±6.32). For comparison, mean MADRS score (±SD) of 23.4 (±13.2) has been reported for MDD patients (Muller et al., 2003). Score distributions for our participants are reported in Supplementary Fig. 1. The internal consistency was high (Cronbach's alpha = 0.83), and correlation between the self-reported MADRS and Beck Depression Inventory (Beck et al., 1996) was r = 0.62, and thus in line with prior reports comparing both instruments in both clinical and healthy samples (Carter et al., 2010; Kjaergaard et al., 2014; Wikberg et al., 2015).

Replication study (Basel_2): This study was conducted with 1523 cognitively healthy young adults from the general population, recruited in Basel, Switzerland, as part of an ongoing imaging genetics study (data lock May 2015). Sample characteristics are presented in Table 1. Participants were free of medication and of any neurological and psychiatric conditions at the time of the study as assessed by standard questionnaires. All participants provided written informed consent prior to participation in the study. 1135 participants completed the MADRS in this sample. MADRS scores ranged from 0 to 33 in this sample with a mean value (±SD) of 7.29 (±5.40). Score distributions are reported in Supplementary Fig. 2. Furthermore, a magnetic resonance imaging (MRI) scanning session was conducted including a picture recognition task, followed by an anatomical imaging sequence and a DTI sequence, conducted for 658 of the participants. Sample characteristics and MADRS scores distribution for the DTI subsample are provided in Table 1 and Supplementary Fig. 3, respectively. Additional information regarding the scanning procedure is provided in the Supplementary Materials.

We used sex and age-corrected depression scores for all analyses by regressing out the effects of sex and age in both studies.

The ethics committee of the Canton of Basel approved both protocols.

2.2. Array-based SNP genotyping

Array-based SNP genotyping was performed as described in the Genome-Wide Human SNP Nsp/Sty 6.0 User Guide (Affymetrix). Briefly, genomic DNA was digested with Nsp I and Sty I restriction enzymes and ligated to an enzyme-specific adaptor. Adaptor-ligated DNA fragments were subjected to polymerase chain reactions (PCR). PCR amplification products were combined and purified using Agencourt Magnetic Beads. The amplified DNA was fragmented, labeled and hybridized onto a Genome - Wide Human SNP 6.0 Array. The hybridized array was washed, stained and scanned. Generation of SNP calls and array quality control (QC) was performed. Contrast QC was chosen as the QC metric, using a default value ≥ 0.4. All samples passing the QC criteria were genotyped using the Birdseed (v2) algorithm. Mean Call Rate averaged >98.5%. Additional information is provided in the Supplementary Materials.

2.3. Brain imaging

2.3.1. Scanning procedure

Scanning was performed on a Siemens Magnetom Verio 3 T whole body MR unit equipped with a twelve-channel head coil. For a detailed description of the scanning procedure please refer to the Supplementary Materials.

Table 1
Sample descriptives.

Sample	N	N Females (%)	Age range (years)	Age mean
Basel_1	2099	1378 (65.6)	18–35	22.47
Basel_2	1523	939 (61.6)	18–35	22.37
Basel_2: DTI	658	393 (59.73)	18–35	22.36

2.3.2. DTI: preprocessing

After visual inspection, 38 participants were excluded due to corrupted T1-weighted images (movement or anatomical abnormalities). Furthermore, two participants were excluded due to excessive movement during the DTI acquisition. Complete datasets (behavior and imaging) were available for N = 658 participants. Diffusion-weighted images were analyzed using FSL (4.1.7). Images were co-registered to the reference unweighted volume (b = 0) using an affine transformation for correction of head motion and eddy current–induced image distortion.

2.3.3. DTI: FA statistical analysis

Voxel-wise statistical analysis of FA data was conducted using Tract-Based Spatial Statistics (TBSS 1.2) (Smith et al., 2006), part of the FMRIB Software Library (FSL) (Smith et al., 2004). Briefly, individual FA data were non-linearly warped to the standard space FA template (FMRIB58_FA) and projected onto the population mean FA skeleton. These data were used as input for voxel-wise between-subject statistics. GLM analyses, as implemented in the randomize tool (Winkler et al., 2014), were applied in search of negative voxel-wise FA associations with depression scores. Statistical significance was assessed through 5000 permutations and results were considered significant for $p < 0.05$, corrected for multiple comparisons across space using the 'two-dimensional' parameter settings with threshold-free cluster enhancement (Smith and Nichols, 2009), which avoids using an arbitrary threshold for the initial cluster-formation.

2.4. Statistical genetics analysis

2.4.1. GWAS

For the input for the GSEA (i.e., association statistics on a genome-wide level), a standard GWAS was performed on autosomal SNPs using the "–assoc" command with asymptotic (Wald test) significance values, as implemented in the PLINK software package (Purcell et al., 2007). SNPs with a genotype call-rate < 95%, minor allele frequency (MAF) < 1%, or a significant deviation from Hardy-Weinberg Equilibrium (HWE) ($p < 0.0001$) were excluded from the analysis.

2.4.2. Genetic heterogeneity

The genomic control inflation factor indicated no notable admixture in the discovery sample ($\lambda = 1.0017$) and the replication sample ($\lambda = 1.0000$), respectively. Q-Q plots are presented in Supplementary Figs. 4 and 5, for the discovery and the replication sample, respectively.

2.4.3. GSEA

GWAS-derived association statistics were entered in a GSEA. More in detail, SNPs were mapped onto genes and genes were assigned to gene sets. Information regarding pre-defined gene sets was obtained from the following databases: Gene Ontology (GO) (http://geneontology.org/), Kyoto Encyclopedia of Genes and Genomes (KEGG) (http://www.genome.jp/kegg/), BioCarta (http://www.biocarta.com/) and Reactome (http://www.reactome.org/). GSEA was conducted using the MAGENTA software package (Segrè et al., 2010). Gene boundaries were set to ±0 kb, thus capturing only SNPs within transcripts, in order to avoid known potential biases introduced by overlapping genes (Sedeno-Cortes and Pavlidis, 2014). Consequently, high-effect SNPs in regulatory regions may be missed. Gene set size was limited to 20 to 200 genes. 1411 gene sets met this criterion and an enrichment p-value was provided for each of them. The enrichment p-value is estimated based on the difference between the observed number of phenotype-associated genes above a given enrichment cutoff within the gene set and the number of phenotype-associated genes that is expected by chance for a gene set of the same size. In order to correct for multiple testing within a gene set, false discovery rate (FDR) correction with a 75th percentile cutoff was used, which is considered the optimal cutoff for GSEA of complex traits with multiple weak effects (Segrè et al., 2010). The FDR cutoff was computed jointly for all gene-set databases.

2.5. Workflow

2.5.1. GSEA for depression scores

Gene sets with $q_{75\%} < 0.05$ were identified for depression scores in the discovery sample. Significantly enriched gene sets in this sample were checked for association with depression scores in the replication sample. In case of significant enrichment, defined as $p < 0.05/N_{(GENE\ SETS)}$ in the replication sample, the gene set was considered to be within-phenotype replicated.

2.5.2. From tract-based statistics to GSEA

As a next step, DTI analysis was conducted to investigate the neural correlates of depression scores, by applying a GLM in search of voxel-wise FA associations. Age and sex were used as covariates in the analysis. Voxel-wise FA-depression associations derived from the DTI statistical analysis were localized to brain tracts using the JHU White-Matter Tractography Atlas (Hua et al., 2008). The proportion of significant voxels (corrected $p < 0.05$) belonging to each of the specific tracts was calculated. We focused on tracts containing a sizable portion (over 20%) of the overall significant voxels for further analyses. For each participant we extracted an average FA value for the depression score-associated voxels within each of the relevant tracts separately, and used them as phenotypes in a hypothesis-driven GSEA. More specifically, GWAS was run on the tract-based FA values and GSEA was applied to the genome-wide association data for these traits.

3. Results

3.1. GSEA for depression scores

Significant enrichment of depression score associations was identified on a multiple testing-corrected level for three gene sets: Collagen Formation (Reactome: REACT_120729), $q_{75\%} = 0.011$; NCAM1 Interactions (Reactome: REACT_18312), $q_{75\%} = 0.021$; Acute Myocardial Infarction (AMI) Pathway (BioCarta: h_amiPathway), $q_{75\%} = 0.034$. Furthermore, enrichments for the Collagen Formation and the NCAM1 Interactions gene sets were also significant ($p < 0.01$) in the replication sample (Collagen Formation $p = 9.90 \times 10^{-5}$; NCAM1 Interactions $p = 1.00 \times 10^{-4}$). FDR corrected ($q_{75\%}$) and nominal (p) GSEA values for each of these gene sets are reported in Table 2. Of note, including regions 110 kb upstream and 40 kb downstream of the gene in the GSEA did not significantly change the results (Supplementary Table 1).

Notably, there is a substantial genetic overlap between the NCAM1 Interactions and the Collagen Formation gene set ($p = 1.94 \times 10^{-40}$). Furthermore, the NCAM1 Interactions and the Collagen Formation gene set enrichments were due to collagen-related genes, respectively, as shown by a systematic overview of genes contributing to the gene set associations with depression scores, i.e., passing the enrichment cutoff in each sample (Table 3).

Of note, the genetic effects of the NCAM1 Interactions and the Collagen Formation gene sets on depression scores were significantly mediated by trait anxiety ($p < 0.001$). For more details regarding this analysis please refer to the Supplementary Information and Supplementary Figures 6 and 7. Major depressive disorder (MDD) and anxiety disorders share significant amount of

Table 2
Gene set associations with depression scores in A) Basel_1 and B) Basel_2.

Database	Gene Set	p	$q_{75\%}$	Gene set size	Observed genes above enrichment cutoff	Expected genes above enrichment cutoff
				2A		
REACTOME	Collagen Formation	1.00×10^{-4}	0.011	53	27	13
REACTOME	NCAM1 Interactions	3.00×10^{-4}	0.021	35	19	9
BIOCARTA	AMI Pathway	6.00×10^{-4}	0.034	15	10	4
				2B		
REACTOME	Collagen Formation	9.90×10^{-5}	0.030	53	26	13
REACTOME	NCAM1 Interactions	1.00×10^{-4}	0.025	35	19	9
BIOCARTA	AMI Pathway	0.016	0.44	15	8	4

p, uncorrected values; $q_{75\%}$, FDR corrected values.

Table 3
Genes contributing to the gene set association with depression scores, i.e., passing the enrichment cutoff.

Discovery sample: Basel_1		Replication sample: Basel_2	
Collagen Formation	NCAM1 Interactions	Collagen Formation	NCAM1 Interactions
ADAMTS14	*CACNA1I*	*ADAMTS3*	*CACNA1H*
ADAMTS2	*CACNB2*	*COL1A1*	*CACNA1I*
BMP1	*CACNB4*	*COL1A2*	*CACNA1S*
COL1A1	*CNTN2*	*COL3A1*	*CACNB1*
COL1A2	*COL1A1*	*COL4A1*	*COL1A1*
COL2A1	*COL1A2*	*COL4A2*	*COL1A2*
COL4A1	*COL2A1*	*COL4A3*	*COL3A1*
COL4A2	*COL4A1*	*COL5A1*	*COL4A1*
COL4A3	*COL4A2*	*COL6A2*	*COL4A2*
COL4A4	*COL4A3*	*COL6A3*	*COL4A3*
COL5A1	*COL4A4*	*COL8A1*	*COL5A1*
COL5A3	*COL5A1*	*COL9A2*	*COL6A2*
COL6A1	*COL6A1*	*COL11A1*	*COL6A3*
COL6A2	*COL6A2*	*COL13A1*	*COL9A2*
COL8A1	*GDNF*	*COL14A1*	*GDNF*
COL12A1	*GFRA2*	*COL15A1*	*NCAM1*
COL13A1	*NRTN*	*COL19A1*	*NCAN*
COL15A1	*ST8SIA2*	*COL21A1*	*ST8SIA2*
COL22A1	*ST8SIA4*	*COL22A1*	*ST8SIA4*
COL27A1	-	*COL23A1*	-
COL28A1	-	*COL25A1*	-
GLT25D2	-	*COL27A1*	-
LEPREL1	-	*COL28A1*	-
PPIB	-	*LEPREL1*	-
SERPINH1	-	*PCOLCE2*	-
TLL1	-	*TLL2*	-
TLL2	-	-	-

Genes contributing to the gene set association with depression scores, i.e., passing the enrichment cutoff, are listed for each sample, for the Collagen Formation gene set and the NCAM1 Interactions gene set, respectively. Overlapping genes between the two gene sets per sample are marked in gray color.

genetic etiology (Kendler et al., 2003) and these results suggest that depression and anxiety may also have overlapping genetic bases at symptom/trait level in healthy participants.

The AMI gene set did not exceed the significance threshold in the replication sample ($p = 0.016$). GSEA p-values of the remaining gene sets that were nominally associated with depression scores ($p < 0.05$) are provided in Supplementary Tables 2A and 2B, for the discovery and the replication sample, respectively.

Of note, no SNP reached genome wide significance ($p < 5 \times 10^{-8}$) in the GWAS of depression scores in the discovery sample and the replication sample, respectively, demonstrating the usefulness of GSEA to detect associations of weaker effect sizes. The GWAS p-values for the best SNP of each gene passing the enrichment cutoff in the GSEA are provided in Supplementary Table 3 and Supplementary Table 4 for the NCAM1 Interactions and the Collagen Formation gene set, respectively.

3.2. GSEA for MDD

As a next step, we investigated whether the NCAM1 Interactions and the Collagen Formation gene sets are associated with MDD diagnosis, by applying the GSEA to publically available summary statistics of a large MDD case-control GWAS (https://www.med.unc.edu/pgc/results-and-downloads) (Ripke et al., 2013). While we identified nominally significant enrichment for the Collagen Formation gene set in this sample ($p = 0.013$), the depression association with the NCAM1 Interactions gene set did not extend to MDD patients ($p = 0.13$). Of note, the MDD analysis was conducted using case-control data. However, it has been previously demonstrated that the use of continuous measurements, rather than clinical cut-offs, can substantially improve the power for detection of genetic variants associated with polygenic traits (van der Sluis et al., 2013).

3.3. DTI results: FA associations with depression scores

We found whole-brain significant negative associations between FA and depression scores, as illustrated in Fig. 1. FA reductions have been associated with subclinical depressive symptoms in two previous studies (Hayakawa et al., 2014;

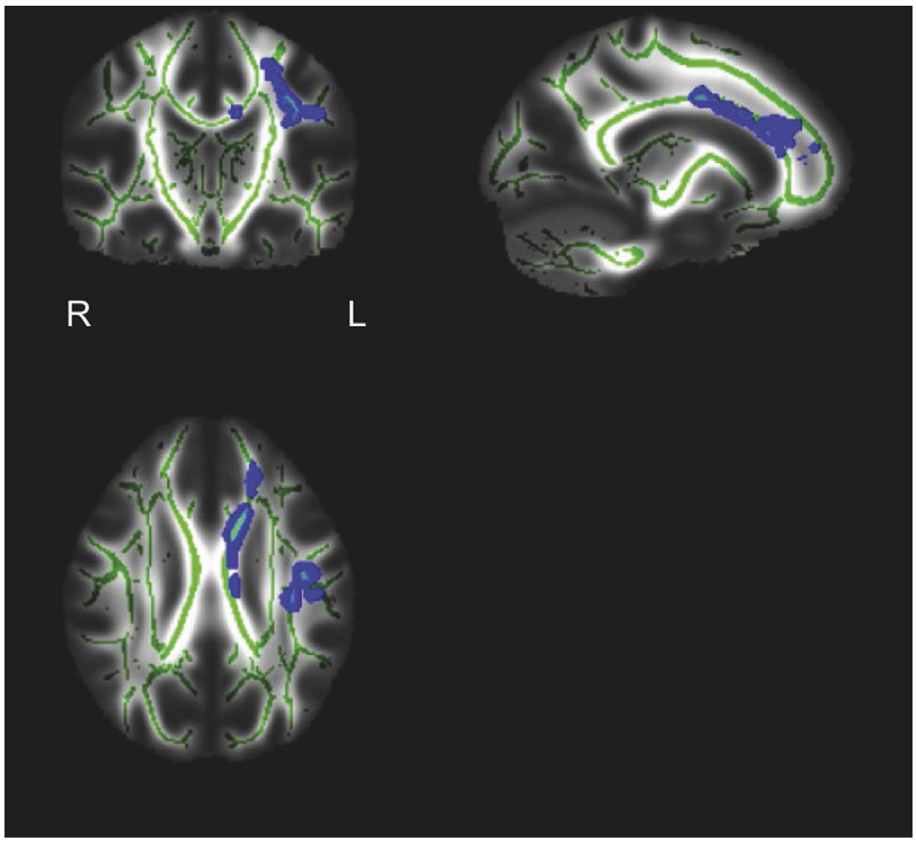

Fig. 1. Association between FA data and depression scores. Associations are presented using color-coded, multiple testing corrected t values within a display range of 0.95:1 (corresponding to $p < 0.05$). The mean FA image of the Basel_2 sample is presented in coronal (upper left), sagittal (upper right) and axial (lower left) view. The mean FA skeleton, overlaid on the mean FA image, is presented in green color. Negative associations are presented in blue color. Abbreviations: FA, Fractional Anisotropy; L, left; R, right. (For interpretation of the references to colour in this figure legend, the reader is referred to the web version of this article.)

McIntosh et al., 2013).

The JHU White-Matter Tractography Atlas was used for tract identification. The proportion of significant voxels allocated to a particular tract, as well as the proportion of significant voxels among all the voxels within each tract is provided in Table 4. The majority of significantly associated voxels was localized within the forceps minor (FM) (21.86%) and the left superior longitudinal fasciculus (SLF) (34.08%), mainly confined to its temporal part (tSLF) (24.38%). FA decreases within these regions have been previously associated with MDD (LeWinn et al., 2014; Ota et al., 2015; Wu et al., 2011; Zuo et al., 2012).

3.4. Hypothesis-driven GSEA of depression score-associated FA within three brain tracts

Average FA values for the voxels significantly associated with depression scores were calculated for the forceps minor, the left SLF and the left tSLF, respectively. To test if there is a shared genetic basis between depression scores and the respective brain tracts, we ran a separate GSEA for each brain tract. The GSEAs showed significant enrichment for the NCAM1 Interactions gene set on a nominal level (FM: $p = 0.016$; SLF: $p = 0.033$; tSLF: $p = 0.007$), and no association with the Collagen Formation gene set (see Table 5). An overview of the remaining significantly enriched gene sets is provided in Supplementary Table 5, Supplementary Table 6 and Supplementary Table 7, for the FM, the left SLF and the left tSLF, respectively.

We further investigated whether the enrichment of the NCAM1 Interactions gene set for each DTI phenotype is solely dependent on depression scores. The respective FA values were corrected for depression scores using linear regression analysis, and the GSEA was re-run. Removing the depression-related variance reduced the NCAM1 Interactions FA association for each DTI-derived phenotype (FM: $p = 0.14$; SLF: $p = 0.080$; tSLF: $p = 0.016$), suggesting that these associations may be partly mediated by depression scores.

4. Discussion

This study identified two gene sets related to self-reported depression scores in healthy participants. By applying a GSEA approach, robust associations were identified for the Collagen Formation and the NCAM1 Interactions gene sets, respectively.

As a next step, a DTI analysis was conducted in search of brain structural correlates of depressive symptom scores, resulting in the identification of depression score-associated FA reductions, localized mainly in the forceps minor and the left SLF. Although based on depression score differences in healthy participants, our findings are in line with previously reported FA decrease in the SLF and corpus callosum in individuals diagnosed with MDD (LeWinn et al., 2014; Ota et al., 2015; Wu et al., 2011; Zuo et al., 2012), bipolar disorder (Saricicek et al., 2016), generalized anxiety disorder (Wang et al., 2016) and autism spectrum disorders (Fitzgerald et al., 2016). Additionally, subclinical depressive symptoms have been associated with widespread FA decrease in healthy female participants, including corpus callosum and the right anterior cingulum (Hayakawa et al., 2014), and FA decrease in the bilateral uncinate fasciculus in healthy individuals over 70 years of age (McIntosh et al., 2013). An FA decrease was also detected in a small fraction

Table 4
Proportion of depression scores-associated voxels per brain tract.

Tract name	Overall associated voxels %	Tract's associated voxels %
Anterior_thalamic_radiation_L	5.05	1.68
Anterior_thalamic_radiation_R	0.48	0.18
Cingulum_(cingulate_gyrus)_L	3.28	5.05
Cingulum_(cingulate_gyrus)_R	0	0
Cingulum_(hippocampus)_L	0	0
Cingulum_(hippocampus)_R	0	0
Corticospinal_tract_L	0	0
Corticospinal_tract_R	0	0
Forceps_major	0	0
Forceps_minor	21.86	6.01
Inferior_fronto-occipital_fasciculus_L	0.48	0.13
Inferior_fronto-occipital_fasciculus_R	2.05	0.51
Inferior_longitudinal_fasciculus_L	0	0
Inferior_longitudinal_fasciculus_R	0	0
Superior_longitudinal_fasciculus_L	34.08	10.74
Superior_longitudinal_fasciculus_R	0	0
Superior_longitudinal_fasciculus_(temporal_part)_L	24.38	14.63
Superior_longitudinal_fasciculus_(temporal_part)_R	0	0
Uncinate_fasciculus_L	0	0
Uncinate_fasciculus_R	1.30	1.97

Overall associated voxels %: Proportion (in percent) of all significant voxels belonging to the specific tract; Tract's associated voxels %: the proportion (in percent) of significant voxels, among all the voxels of the particular tract; Abbreviations: L, left; R, right.

Table 5
Gene set associations with DTI-derived phenotypes.

DTI phenotype	Database	Gene Set	p value	Gene set size	Genes above enrichment cutoff
Forceps Minor	REACTOME	Collagen Formation	0.15	53	14
Forceps Minor	REACTOME	NCAM1 Interactions	0.016	35	12
Left SLF	REACTOME	Collagen Formation	0.093	53	16
Left SLF	REACTOME	NCAM1 Interactions	0.033	35	13
Left tSLF	REACTOME	Collagen Formation	0.093	53	16
Left tSLF	REACTOME	NCAM1 Interactions	0.007	35	15

of the right uncinate fasciculus in the current study (Table 4).

Moreover, in order to further validate our initial genetic findings, DTI-derived measurements of depression score-associated microstructural properties within the forceps minor and the left (temporal) SLF were subjected to a hypothesis-driven GSEA. The NCAM1 Interactions gene set was significantly associated with each of the three DTI phenotypes, additionally pointing to its possible involvement in depression-relevant biological pathways.

Genes constituting the neural cell adhesion molecule (NCAM1) Interactions gene set are implicated in neural development and synaptic plasticity (Nielsen et al., 2010; Rutishauser, 2008; Walmod et al., 2004) and code for both intracellular components, e.g. subunits of voltage-gated calcium channels, and molecules of the extracellular matrix, most prominently collagen components (coded by 17 out of the 39 genes comprising this gene set), associated with NCAM activity.

Noteworthy, Collagen Formation, a gene set with substantial genetic overlap with NCAM1 Interactions ($p = 1.94 \times 10^{-40}$), was also associated with depression scores in this study (Table 2). Ten out of the 17 genes shared by these gene sets contributed to the association with depression scores in the discovery and the replication sample, respectively (Table 3).

NCAM has been investigated in the context of depression, due to its modulatory role in intracellular cascades and brain plasticity (Wainwright and Galea, 2013). NCAM deficits and resulting changes in neural plasticity have been associated with an increase of depression-like behavior and reduced efficacy of common antidepressants in animal models (Aonurm-Helm et al., 2008; Jürgenson et al., 2012; Wainwright et al., 2015). Additionally, genetic variants within or near *NCAM1* have been associated with suicidal behavior (Sokolowski et al., 2016), cannabis use and MDD (Hodgson et al., 2017), as well as other disorders, such as bipolar disorder, (Arai et al., 2004), schizophrenia (Zhang et al., 2014) and autism (Marui et al., 2009). According to the references listed above, one may assume *NCAM1* as a general vulnerability factor for neurodevelopmental and psychiatric disorders. Moreover, collagens have a notable impact on NCAM downstream activity (Monzo et al., 2013). Our genetic association data are in line with these biological observations.

Furthermore, the NCAM1 Interactions gene set was associated with DTI correlates of depression scores. NCAM-derived polysialic acid has been implicated in axonal development, myelination and path finding (Rutishauser, 2008), all of which can impact the microstructural properties of brain tracts and therefore be reflected by the DTI (FA) measurement. Moreover, as regressing out the depression-related variance reduced the association between the NCAM1 Interactions gene set and each DTI-derived phenotype, the respective associations are likely to be at least partly mediated by depression scores.

By linking the NCAM1 Interactions gene set to depression scores and their structural brain correlates in healthy participants, the current study contributes to the understanding of the molecular underpinnings of depressive symptomatology.

Funding

This work was funded by the Swiss National Science Foundation (Sinergia grant CRSI33_130080 to D.Q. and A.P., individual grant 320030_159740 to D.Q.), and by the European Community's Seventh Framework Programme (FP7/2007–2013) under grant agreement #602450 (IMAGEMEND).

Appendix A. Supplementary data

Supplementary data related to this article can be found at http://dx.doi.org/10.1016/j.jpsychires.2017.03.007.

References

Aonurm-Helm, A., Jurgenson, M., Zharkovsky, T., Sonn, K., Berezin, V., Bock, E., Zharkovsky, A., 2008. Depression-like behaviour in neural cell adhesion molecule (NCAM)-deficient mice and its reversal by an NCAM-derived peptide, FGL. Eur. J. Neurosci. 28 (8), 1618–1628.

Arai, M., Itokawa, M., Yamada, K., Toyota, T., Arai, M., Haga, S., Ujike, H., Sora, I., Ikeda, K., Yoshikawa, T., 2004. Association of neural cell adhesion molecule 1 gene polymorphisms with bipolar affective disorder in Japanese individuals. Biol. Psychiatry 55 (8), 804–810.

Ayuso-Mateos, J.L., Nuevo, R., Verdes, E., Naidoo, N., Chatterji, S., 2010. From depressive symptoms to depressive disorders: the relevance of thresholds. Br. J. Psychiatry 196 (5), 365–371.

Basser, P.J., 1995. Inferring microstructural features and the physiological state of tissues from diffusion-weighted images. NMR Biomed. 8 (7), 333–344.

Beaulieu, C., 2002. The basis of anisotropic water diffusion in the nervous system–a technical review. NMR Biomed. 15 (7–8), 435–455.

Beck, A.T., Steer, R.A., Brown, G.K., 1996. Beck depression inventory-II. San. Ant. TX, 78204–72498.

Carter, J.D., Frampton, C.M., Mulder, R.T., Luty, S.E., Joyce, P.R., 2010. The relationship of demographic, clinical, cognitive and personality variables to the discrepancy between self and clinician rated depression. J. Affect. Disord. 124 (1–2), 202–206.

Elovainio, M., Taipale, T., Seppala, I., Mononen, N., Raitoharju, E., Jokela, M., Pulkki-Raback, L., Illig, T., Waldenberger, M., Hakulinen, C., Hintsa, T., Kivimaki, M., Kahonen, M., Keltikangas-Jarvinen, L., Raitakari, O., Lehtimaki, T., 2015. Activated immune-inflammatory pathways are associated with long-standing depressive symptoms: evidence from gene-set enrichment analyses in the young finns study. J. Psychiatr. Res. 71, 120–125.

Fitzgerald, J., Gallagher, L., McGrath, J., 2016. Widespread disrupted white matter microstructure in autism spectrum disorders. J. Autism Dev. Disord. 1–11.

Hankin, B.L., Fraley, R.C., Lahey, B.B., Waldman, I.D., 2005. Is depression best viewed as a continuum or discrete category? A taxometric analysis of childhood and adolescent depression in a population-based sample. J. Abnorm. Psychol. 114 (1), 96–110.

Hayakawa, Y.K., Sasaki, H., Takao, H., Hayashi, N., Kunimatsu, A., Ohtomo, K., Aoki, S., 2014. Depressive symptoms and neuroanatomical structures in community-dwelling women: a combined voxel-based morphometry and diffusion tensor imaging study with tract-based spatial statistics. NeuroImage: Clinical 4, 481–487.

Hayakawa, Y.K., Sasaki, H., Takao, H., Mori, H., Hayashi, N., Kunimatsu, A., Aoki, S., Ohtomo, K., 2013. Structural brain abnormalities in women with subclinical depression, as revealed by voxel-based morphometry and diffusion tensor imaging. J. Affect. Disord. 144 (3), 263–268.

Heck, A., Fastenrath, M., Ackermann, S., Auschra, B., Bickel, H., Coynel, D., Gschwind, L., Jessen, F., Kaduszkiewicz, H., Maier, W., 2014. Converging genetic and functional brain imaging evidence links neuronal excitability to working memory, psychiatric disease, and brain activity. Neuron 81 (5), 1203–1213.

Heck, A., Fastenrath, M., Coynel, D., Auschra, B., Bickel, H., Freytag, V., Gschwind, L., Hartmann, F., Jessen, F., Kaduszkiewicz, H., Maier, W., Milnik, A., Pentzek, M., Riedel-Heller, S.G., Spalek, K., Vogler, C., Wagner, M., Weyerer, S., Wolfsgruber, S., de Quervain, D.J., Papassotiropoulos, A., 2015. Genetic analysis of association between calcium signaling and hippocampal activation, memory performance in the young and old, and risk for sporadic alzheimer disease. JAMA Psychiatry 72 (10), 1029–1036.

Hodgson, K., Almasy, L., Knowles, E.E., Kent Jr., J.W., Curran, J.E., Dyer, T.D., Goring, H.H., Olvera, R.L., Woolsey, M.D., Duggirala, R., Fox, P.T., Blangero, J., Glahn, D.C., 2017. The genetic basis of the comorbidity between cannabis use and major depression. Addiction 112 (1), 113–123.

Hori, H., Sasayama, D., Teraishi, T., Yamamoto, N., Nakamura, S., Ota, M., Hattori, K., Kim, Y., Higuchi, T., Kunugi, H., 2016. Blood-based gene expression signatures of medication-free outpatients with major depressive disorder: integrative genome-wide and candidate gene analyses. Sci. Rep. 6, 18776.

Hua, K., Zhang, J., Wakana, S., Jiang, H., Li, X., Reich, D.S., Calabresi, P.A., Pekar, J.J., van Zijl, P.C., Mori, S., 2008. Tract probability maps in stereotaxic spaces: analyses of white matter anatomy and tract-specific quantification. Neuroimage 39 (1), 336–347.

Jürgenson, M., Aonurm-Helm, A., Zharkovsky, A., 2012. Partial reduction in neural cell adhesion molecule (NCAM) in heterozygous mice induces depression-related behaviour without cognitive impairment. Brain Res. 1447, 106–118.

Kendler, K.S., Gardner Jr., C.O., 1998. Boundaries of major depression: an evaluation of DSM-IV criteria. Am. J. Psychiatry 155 (2), 172–177.

Kendler, K.S., Prescott, C.A., Myers, J., Neale, M.C., 2003. The structure of genetic and environmental risk factors for common psychiatric and substance use disorders in men and women. Archives General Psychiatry 60 (9), 929–937.

Kendler, K.S., Walters, E.E., Truett, K.R., Heath, A.C., Neale, M.C., Martin, N.G., Eaves, L.J., 1994. Sources of individual differences in depressive symptoms: analysis of two samples of twins and their families. Am. J. Psychiatry 151 (11), 1605–1614.

Kjaergaard, M., Arfwedson Wang, C.E., Waterloo, K., Jorde, R., 2014. A study of the psychometric properties of the Beck depression inventory-II, the Montgomery and Asberg depression rating scale, and the hospital anxiety and depression scale in a sample from a healthy population. Scand. J. Psychol. 55 (1), 83–89.

LeWinn, K.Z., Connolly, C.G., Wu, J., Drahos, M., Hoeft, F., Ho, T.C., Simmons, A.N., Yang, T.T., 2014. White matter correlates of adolescent depression: structural evidence for frontolimbic disconnectivity. J. Am. Acad. Child Adolesc. Psychiatry 53 (8), 899–909 e897.

Lewinsohn, P.M., Solomon, A., Seeley, J.R., Zeiss, A., 2000. Clinical implications of "subthreshold" depressive symptoms. J. Abnorm Psychol. 109 (2), 345–351.

Lips, E.S., Cornelisse, L.N., Toonen, R.F., Min, J.L., Hultman, C., Holmans, P.A., O'Donovan, M.C., Purcell, S., Smit, A., Verhage, M., 2012. Functional gene group analysis identifies synaptic gene groups as risk factor for schizophrenia. Mol. Psychiatry 17 (10), 996–1006.

Lohmueller, K.E., Pearce, C.L., Pike, M., Lander, E.S., Hirschhorn, J.N., 2003. Meta-analysis of genetic association studies supports a contribution of common variants to susceptibility to common disease. Nat. Genet. 33 (2), 177–182.

Marui, T., Funatogawa, I., Koishi, S., Yamamoto, K., Matsumoto, H., Hashimoto, O., Nanba, E., Nishida, H., Sugiyama, T., Kasai, K., Watanabe, K., Kano, Y., Sasaki, T., Kato, N., 2009. Association of the neuronal cell adhesion molecule (NRCAM) gene variants with autism. Int. J. Neuropsychopharmacol. 12 (1), 1–10.

McIntosh, A., Bastin, M., Luciano, M., Maniega, S.M., Hernández, M.d.C.V., Royle, N., Hall, J., Murray, C., Lawrie, S., Starr, J., 2013. Neuroticism, depressive symptoms and white-matter integrity in the Lothian Birth Cohort 1936. Psychol. Med. 43 (06), 1197–1206.

Montgomery, S.A., Asberg, M., 1979. A New Depression Scale Designed to Be Sensitive to Change. Brit. J. Psychiat. 134 (4), 382–389.

Monzo, H.J., Park, T.I., Dieriks, B.V., Jansson, D., Faull, R.L., Dragunow, M., Curtis, M.A., 2013. Insulin and IGF1 modulate turnover of polysialylated neural cell adhesion molecule (PSA–NCAM) in a process involving specific extracellular matrix components. J. Neurochem. 126 (6), 758–770.

Muller, M.J., Himmerich, H., Kienzle, B., Szegedi, A., 2003. Differentiating moderate and severe depression using the Montgomery-Asberg depression rating scale (MADRS). J. Affect. Disord. 77 (3), 255–260.

Nielsen, J., Kulahin, N., Walmod, P.S., 2010. Extracellular Protein Interactions Mediated by the Neural Cell Adhesion Molecule, NCAM: Heterophilic Interactions between NCAM and Cell Adhesion Molecules, Extracellular Matrix Proteins, and Viruses, Structure and Function of the Neural Cell Adhesion Molecule NCAM. Adv. Exp. Med. Biol. 663, 23–53.

Nurnberger, J.I., Koller, D.L., Jung, J., Edenberg, H.J., Foroud, T., Guella, I., Vawter, M.P., Kelsoe, J.R., 2014. Identification of pathways for bipolar disorder: a meta-analysis. JAMA Psychiatry 71 (6), 657–664.

Ota, M., Noda, T., Sato, N., Hattori, K., Hori, H., Sasayama, D., Teraishi, T., Nagashima, A., Obu, S., Higuchi, T., 2015. White matter abnormalities in major depressive disorder with melancholic and atypical features: a diffusion tensor imaging study. Psychiatry Clin. Neurosci. 69 (6), 360–368.

Purcell, S., Neale, B., Todd-Brown, K., Thomas, L., Ferreira, M.A., Bender, D., Maller, J., Sklar, P., De Bakker, P.I., Daly, M.J., 2007. PLINK: a tool set for whole-genome association and population-based linkage analyses. Am. J. Hum. Genet. 81 (3), 559–575.

Ripke, S., Wray, N.R., Lewis, C.M., Hamilton, S.P., Weissman, M.M., Breen, G., Byrne, E.M., Blackwood, D.H., Boomsma, D.I., Cichon, S., Heath, A.C., Holsboer, F., Lucae, S., Madden, P.A., Martin, N.G., McGuffin, P., Muglia, P., Noethen, M.M., Penninx, B.P., Pergadia, M.L., Potash, J.B., Rietschel, M., Lin, D., Muller-Myhsok, B., Shi, J., Steinberg, S., Grabe, H.J., Lichtenstein, P., Magnusson, P., Perlis, R.H., Preisig, M., Smoller, J.W., Stefansson, K., Uher, R., Kutalik, Z., Tansey, K.E., Teumer, A., Viktorin, A., Barnes, M.R., Bettecken, T., Binder, E.B., Breuer, R., Castro, V.M., Churchill, S.E., Coryell, W.H., Craddock, N., Craig, I.W., Czamara, D., De Geus, E.J., Degenhardt, F., Farmer, A.E., Fava, M., Frank, J., Gainer, V.S., Gallagher, P.J., Gordon, S.D., Goryachev, S., Gross, M., Guipponi, M., Henders, A.K., Herms, S., Hickie, I.B., Hoefels, S., Hoogendijk, W., Hottenga, J.J., Iosifescu, D.V., Ising, M., Jones, I., Jones, L., Jung-Ying, T., Knowles, J.A., Kohane, I.S., Kohli, M.A., Korszun, A., Landen, M., Lawson, W.B., Lewis, G., Macintyre, D., Maier, W., Mattheisen, M., McGrath, P.J., McIntosh, A., McLean, A., Middeldorp, C.M., Middleton, L., Montgomery, G.M., Murphy, S.N., Nauck, M., Nolen, W.A., Nyholt, D.R., O'Donovan, M., Oskarsson, H., Pedersen, N., Scheftner, W.A., Schulz, A., Schulze, T.G., Shyn, S.I., Sigurdsson, E., Slager, S.L., Smit, J.H., Stefansson, H., Steffens, M., Thorgeirsson, T., Tozzi, F., Treutlein, J., Uhr, M., van den Oord, E.J., Van Grootheest, G., Volzke, H., Weilburg, J.B., Willemsen, G., Zitman, F.G., Neale, B., Daly, M., Levinson, D.F., Sullivan, P.F., 2013. A mega-analysis of genome-wide association studies for major depressive disorder. Mol. Psychiatry 18 (4), 497–511.

Rutishauser, U., 2008. Polysialic acid in the plasticity of the developing and adult vertebrate nervous system. Nat. Rev. Neurosci. 9 (1), 26–35.

Saricicek, A., Zorlu, N., Yalin, N., Hidiroglu, C., Cavusoglu, B., Ceylan, D., Ada, E., Tunca, Z., Ozerdem, A., 2016. Abnormal white matter integrity as a structural endophenotype for bipolar disorder. Psychol. Med. 46 (7), 1547–1558.

Sedeno-Cortes, A.E., Pavlidis, P., 2014. Pitfalls in the application of gene-set analysis to genetics studies. Trends Genet. 30 (12), 513–514.

Segrè, A.V., Groop, L., Mootha, V.K., Daly, M.J., Altshuler, D., DIAGRAM Consortium, MAGIC Investigators, 2010. Common inherited variation in mitochondrial genes is not enriched for associations with type 2 diabetes or related glycemic traits. PLoS Genet. 6 (8), e1001058.

Sham, P., Sterne, A., Purcell, S., Cherny, S., Webster, M., Rijsdijk, F., Asherson, P.,

Ball, D., Craig, I., Eley, T., 2000. GENESiS: creating a composite index of the vulnerability to anxiety and depression in a community-based sample of siblings. Twin Res. 3 (04), 316–322.
Slade, T., 2007. Taxometric investigation of depression: evidence of consistent latent structure across clinical and community samples. Aust. N. Z. J. Psychiatry 41 (5), 403–410.
Slade, T., Andrews, G., 2005. Latent structure of depression in a community sample: a taxometric analysis. Psychol. Med. 35 (04), 489–497.
Smith, S.M., Jenkinson, M., Johansen-Berg, H., Rueckert, D., Nichols, T.E., Mackay, C.E., Watkins, K.E., Ciccarelli, O., Cader, M.Z., Matthews, P.M., 2006. Tract-based spatial statistics: voxelwise analysis of multi-subject diffusion data. Neuroimage 31 (4), 1487–1505.
Smith, S.M., Jenkinson, M., Woolrich, M.W., Beckmann, C.F., Behrens, T.E., Johansen-Berg, H., Bannister, P.R., De Luca, M., Drobnjak, I., Flitney, D.E., 2004. Advances in functional and structural MR image analysis and implementation as FSL. Neuroimage 23, 208–219.
Smith, S.M., Nichols, T.E., 2009. Threshold-free cluster enhancement: addressing problems of smoothing, threshold dependence and localisation in cluster inference. Neuroimage 44 (1), 83–98.
Sokolowski, M., Wasserman, J., Wasserman, D., 2016. Polygenic associations of neurodevelopmental genes in suicide attempt. Mol. Psychiatry 21 (10), 1381–1390.
Sprengelmeyer, R., Orth, M., Müller, H.-P., Wolf, R., Grön, G., Depping, M., Kassubek, J., Justo, D., Rees, E., Haider, S., 2014. The neuroanatomy of subthreshold depressive symptoms in Huntington's disease: a combined diffusion tensor imaging (DTI) and voxel-based morphometry (VBM) study. Psychol. Med. 44 (09), 1867–1878.
Sullivan, P.F., Neale, M.C., Kendler, K.S., 2000. Genetic epidemiology of major depression: review and meta-analysis. Am. J. Psychiatry 157 (10), 1552–1562.
van der Sluis, S., Posthuma, D., Nivard, M.G., Verhage, M., Dolan, C.V., 2013. Power in GWAS: lifting the curse of the clinical cut-off. Mol. Psychiatry 18 (1), 2–3.
Wainwright, S.R., Barha, C.K., Hamson, D.K., Epp, J.R., Chow, C., Lieblich, S.E., Rutishauser, U., Galea, L.A., 2016. Enzymatic depletion of the polysialic acid moiety associated with the neural cell adhesion molecule inhibits antidepressant efficacy. Neuropsychopharmacology 41 (6), 1670–1680.
Wainwright, S.R., Galea, L.A., 2013. The neural plasticity theory of depression: assessing the roles of adult neurogenesis and PSA-NCAM within the hippocampus. Neural Plast. 2013.
Walmod, P.S., Kolkova, K., Berezin, V., Bock, E., 2004. Zippers make signals: NCAM-mediated molecular interactions and signal transduction. Neurochem. Res. 29 (11), 2015–2035.
Wang, K., Li, M., Hakonarson, H., 2010. Analysing biological pathways in genome-wide association studies. Nat. Rev. Genet. 11 (12), 843–854.
Wang, W., Qian, S., Liu, K., Li, B., Li, M., Xin, K., Sun, G., 2016. Reduced white matter integrity and its correlation with clinical symptom in first-episode, treatment-naive generalized anxiety disorder. Behav. Brain Res. 314, 159–164.
Wikberg, C., Nejati, S., Larsson, M.E., Petersson, E.L., Westman, J., Ariai, N., Kivi, M., Eriksson, M., Eggertsen, R., Hange, D., Baigi, A., Bjorkelund, C., 2015. Comparison between the montgomery-asberg depression rating scale-self and the Beck depression inventory II in primary care. Prim. Care Companion CNS Disord. 17 (3).
Winkler, A.M., Ridgway, G.R., Webster, M.A., Smith, S.M., Nichols, T.E., 2014. Permutation inference for the general linear model. Neuroimage 92, 381–397.
Wu, F., Tang, Y., Xu, K., Kong, L., Sun, W., Wang, F., Kong, D., Li, Y., Liu, Y., 2011. Whiter matter abnormalities in medication-naive subjects with a single short-duration episode of major depressive disorder. Psychiatry Res. Neuroimaging 191 (1), 80–83.
Zeng, Y., Navarro, P., Fernandez-Pujals, A.M., Hall, L.S., Clarke, T.K., Thomson, P.A., Smith, B.H., Hocking, L.J., Padmanabhan, S., Hayward, C., MacIntyre, D.J., Wray, N.R., Deary, I.J., Porteous, D.J., Haley, C.S., McIntosh, A.M., 2017. A combined pathway and regional heritability analysis indicates NETRIN1 pathway is associated with major depressive disorder. Biol. Psychiatry 81 (4), 336–346.
Zhang, W., Xiao, M.S., Ji, S., Tang, J., Xu, L., Li, X., Li, M., Wang, H.Z., Jiang, H.Y., Zhang, D.F., Wang, J., Zhang, S., Xu, X.F., Yu, L., Zheng, P., Chen, X., Yao, Y.G., 2014. Promoter variant rs2301228 on the neural cell adhesion molecule 1 gene confers risk of schizophrenia in Han Chinese. Schizophrenia Res. 160 (1), 88–96.
Zuo, N., Fang, J., Lv, X., Zhou, Y., Hong, Y., Li, T., Tong, H., Wang, X., Wang, W., Jiang, T., 2012. White matter abnormalities in major depression: a tract-based spatial statistics and rumination study. PloS One 7 (5), e37561.

Supplementary Information for

The NCAM1 gene set is linked to depressive symptoms and their brain structural correlates in healthy individuals

Jana Petrovska, MS, David Coynel, PhD, Matthias Fastenrath, PhD, Annette Milnik, PhD, MD, Bianca Auschra, MS, Tobias Egli, MS, Leo Gschwind, PhD, Francina Hartmann, PhD, Eva Loos, MS, Klara Spalek, PhD, Christian Vogler, PhD, Dominique F. de Quervain, MD, Andreas Papassotiropoulos, MD, Angela Heck, PhD

The PDF file includes:

Materials and Methods

Array-based SNP genotyping

Array-based SNP genotyping was performed as described in the Genome-Wide Human SNP Nsp/Sty 6.0 User Guide (Affymetrix). Briefly, genomic DNA concentration was determined and adjusted to 50 ng/µl in water. 250 ng of DNA was digested with 10 units of Nsp I and Sty I restriction enzymes for 2hr at 37°C. Enzyme-specific adaptor oligonucleotides were ligated onto the digested ends with T4 DNA Ligase for 3hr at 16°C. After adjustment to 100µl with water, 10µl of the diluted ligation reactions were subjected to polymerase chain reactions (PCR) of 100µl (three for Sty-digested products and four for Nsp). Reactions were then verified to migrate at an average size between 200-to 1,100 bps using 2% TBE gel electrophoresis. PCR amplification products were combined and purified using Agencourt Magnetic Beads (Beckman Coulter). 4-5µg/µl of purified PCR products was obtained on average for each sample. The amplified DNA was then fragmented, labeled and hybridized onto a Genome- Wide Human SNP 6.0 Array, using the SNP Nsp/Sty 5.0/6.0 Assay Kit (Affymetrix). The hybridized array was washed, stained and scanned. Generation of SNP calls and array quality control (QC) were performed. Contrast QC was chosen as the QC metric, using a default value of ≥ 0.4. All samples passing the QC criteria were genotyped using the Birdseed (v2) algorithm. Mean Call Rate for all samples (i.e., individuals) averaged >98.5% and ranged from 95.1% to 99.7%. Thus, no individual with a SNP call rate below 95% was included.

Scanning procedure

Scanning was performed on a Siemens Magnetom Verio 3 T whole body MR unit equipped with a twelve-channel head coil. The scanning session consisted of 20 min. long picture recognition task (not reported), followed by an anatomical and a diffusion imaging sequence (10min. each).

Sequence description:

Anatomical: Three-dimensional, high-resolution T1-weighted images were acquired with magnetization prepared rapid gradient echo (MPRAGE) sequence. Acquisition parameters: repetition time (TR)=2000 ms; echo time (TE)=3.37 ms; inversion time (TI)=1000 ms; flip angle=8°; 176 sagittal slices; field of view (FOV)=256 mm; voxel size = 1 x 1 x 1 mm^3.

DTI: Diffusion volumes were acquired using a singe-shot EPI sequence, and consisted of 64 diffusion-weighted volumes with b=900s/mm^2 and one unweighted volume (b=0). Acquisition parameters: TR=9s; TE=82ms; FOV=320 mm; GRAPPA R=2.0; voxel size = 2.5 x 2.5 x 2.5mm^3.

Mediation analyses

Trait anxiety was measured with the trait subscale of the State-Trait Anxiety Inventory (STAI) (Spielberg et al., 1970). In both samples depression scores and trait anxiety were significantly associated, showing large effect sizes (Discovery Sample $r = 0.57$, $p < 10e\text{-}16$, Replication Sample $r = 0.65$, $p < 10e\text{-}16$). Hence, we were interested in whether the association between the multilocus genetic scores on depression might at least partially be mediated by trait anxiety. For doing so, we conducted mediation analyses as described in (Baron and Kenny, 1986; Shrout and Bolger, 2002), separately for the NCAM1 Interactions and the Collagen Formation gene sets and for both samples. To control for confounding effects of sex and age, we regressed out their effects from the behavioral phenotypes. We used the MBESS-package in R to retrieve empirical p-values for the indirect effect (10'000 iterations; confidence-interval 99.9%).

For both genetic scores the indirect effect of trait anxiety was significant (discovery sample: NCAM1 $r = 0.078$, $p < 0.001$; Collagen formation $r = 0.094$, $p < 0.001$; replication sample: NCAM1 $r = 0.122$, $p < 0.001$; Collagen formation $r = 0.122$, $p < 0.001$).

Supplementary Figures

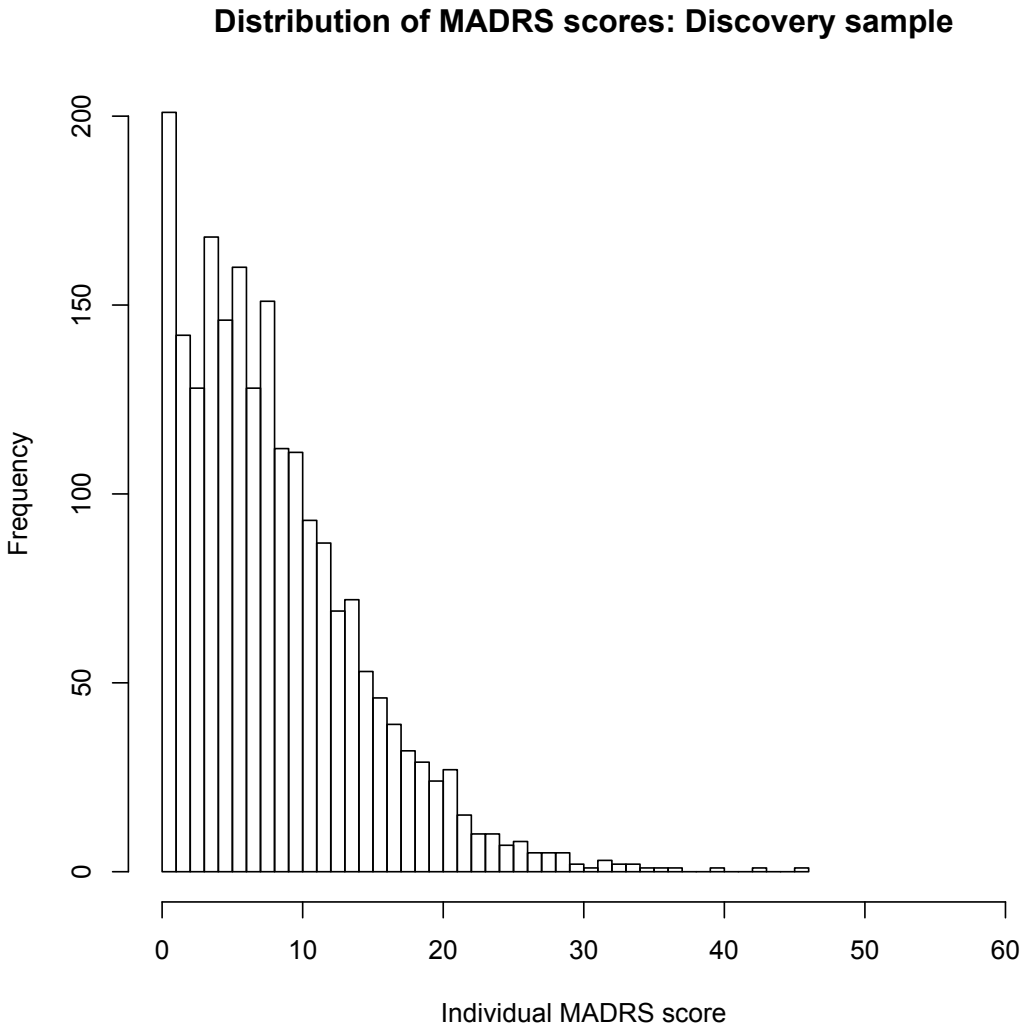

Supplementary Figure 1 A visual representation of the distribution of depression scores in the discovery sample (N=1651)

Abbreviations: MADRS, Montgomery Asberg Depression Rating Scale

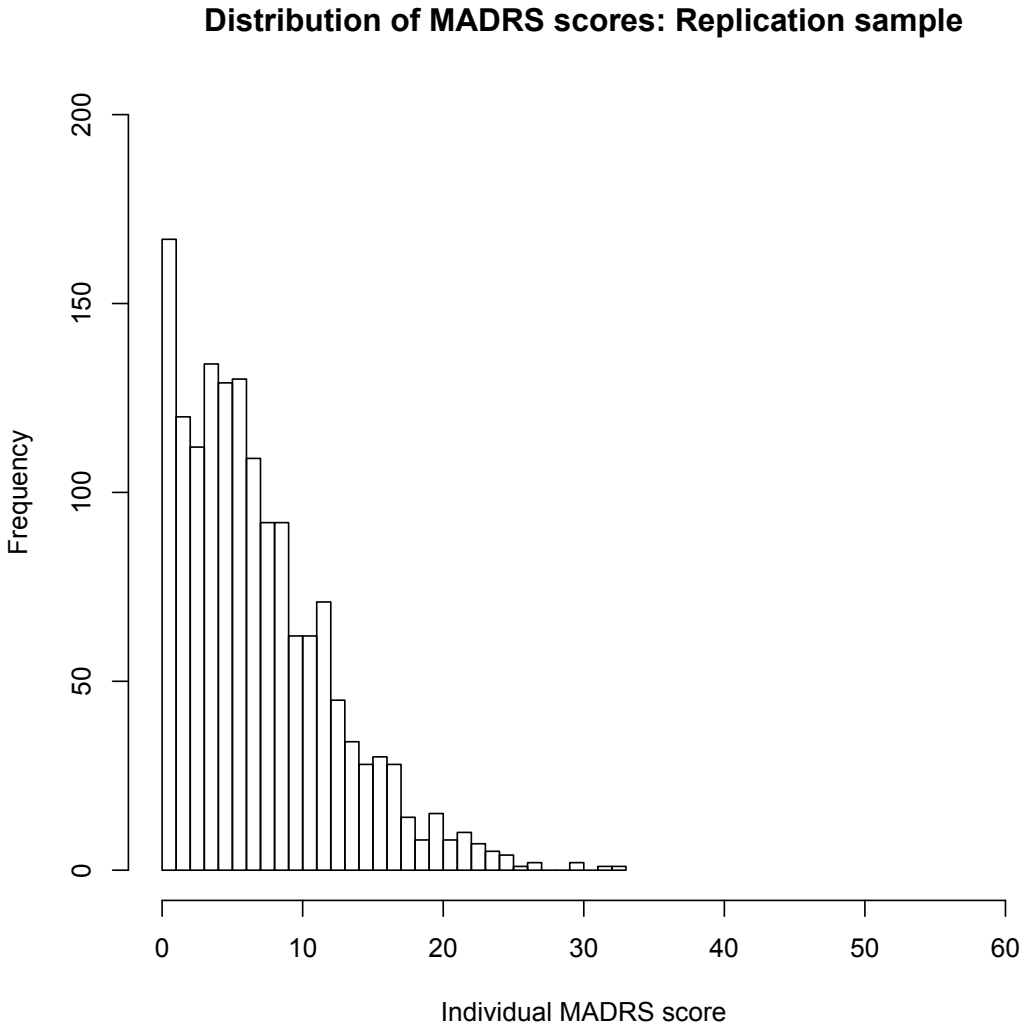

Supplementary Figure 2 A visual representation of the distribution of depression scores in the replication sample (N=1135)

Abbreviations: MADRS, Montgomery Asberg Depression Rating Scale

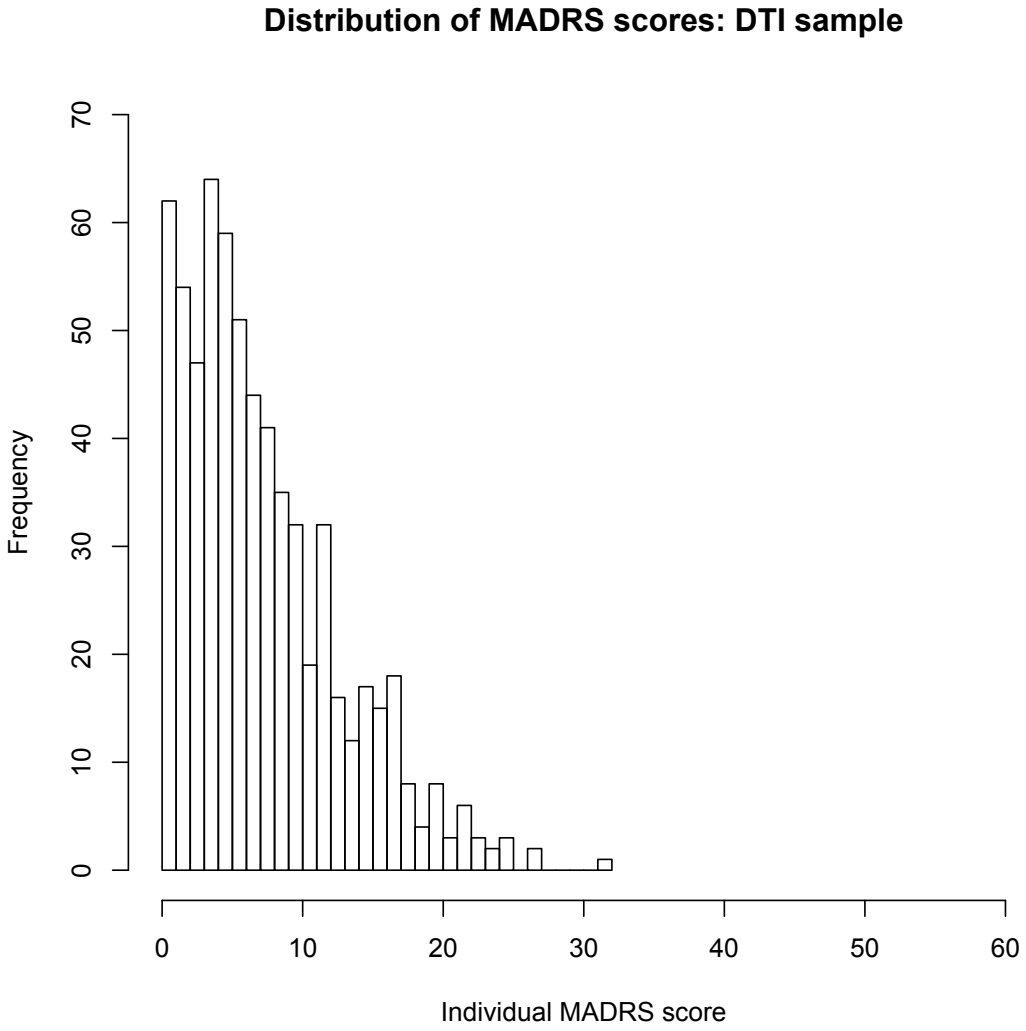

Supplementary Figure 3 A visual representation of the distribution of depression scores in the DTI subsample of the replication sample (N=658)

Abbreviations: MADRS, Montgomery Asberg Depression Rating Scale

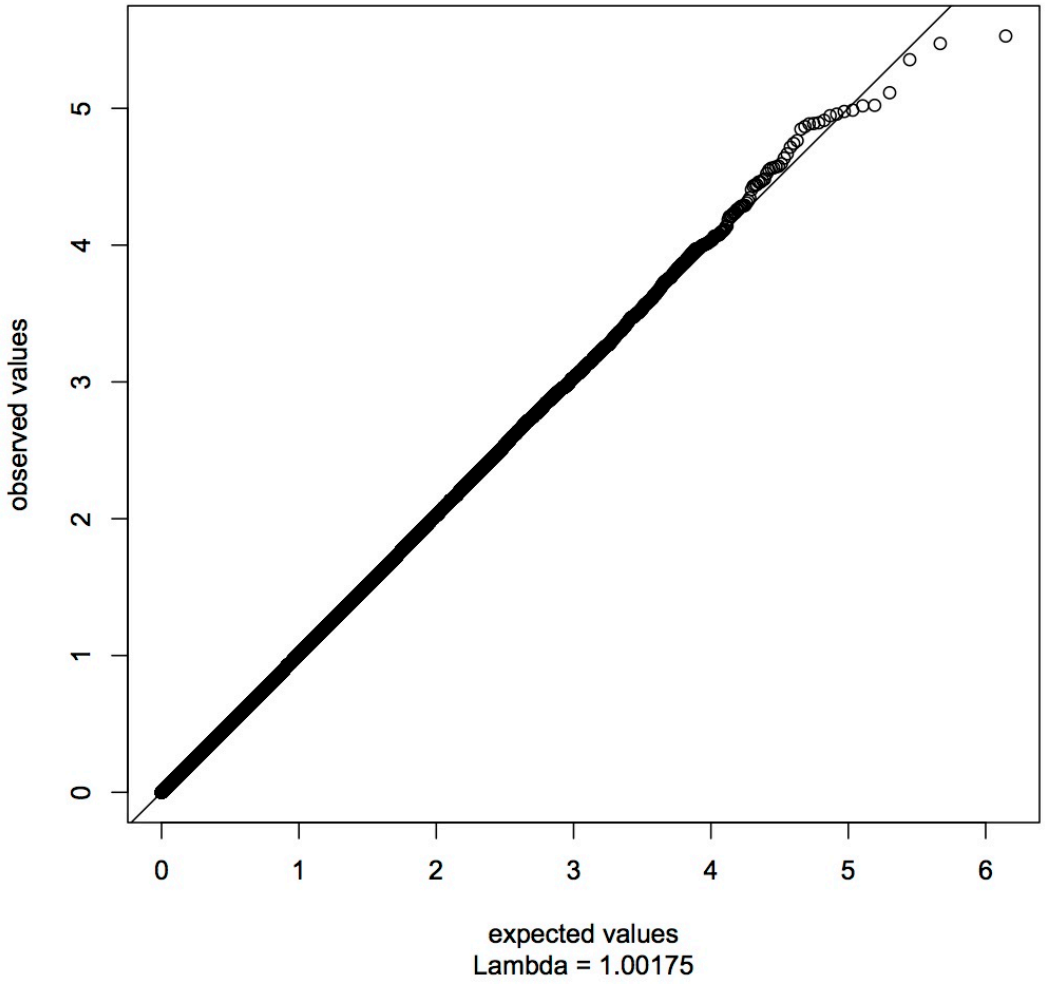

Supplementary Figure 4 Quantile-quantile plot for genetic association in the discovery sample

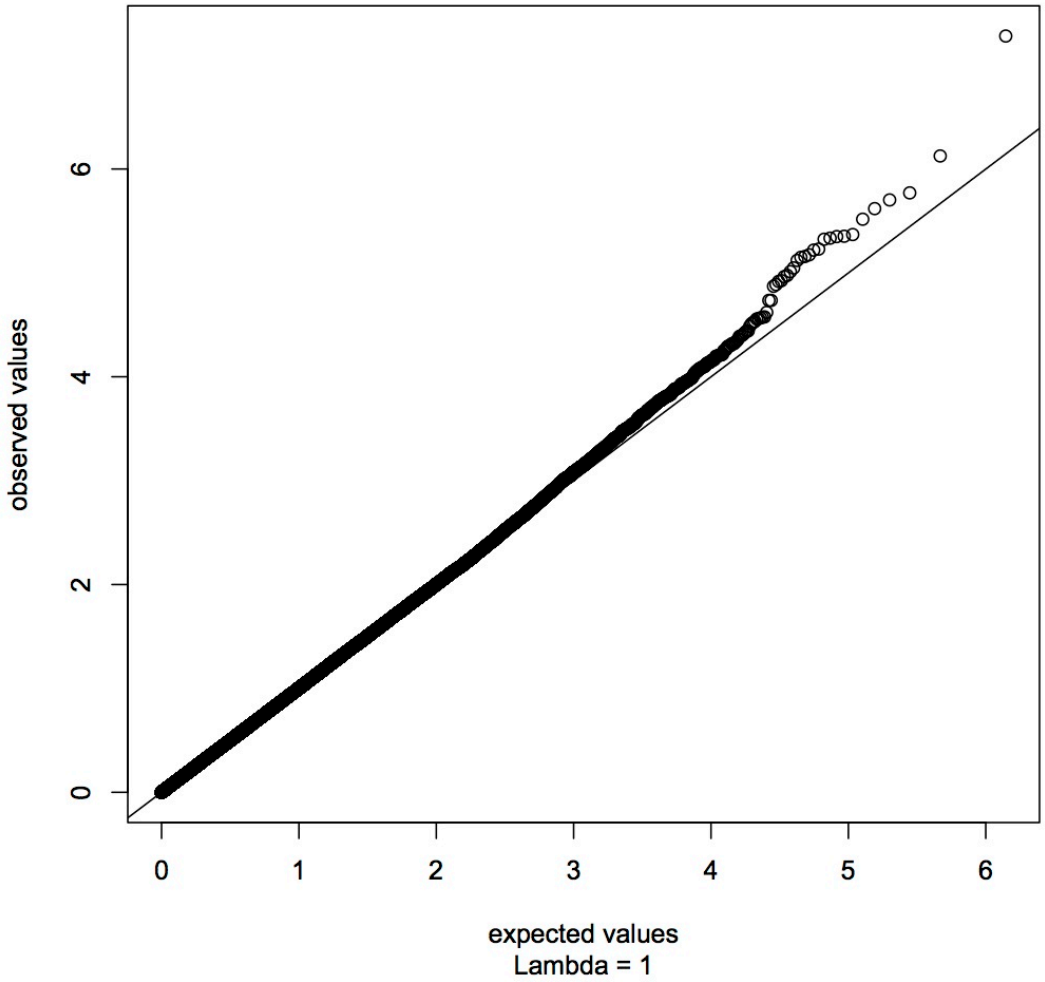

Supplementary Figure 5 Quantile-quantile plot for genetic association in the replication sample

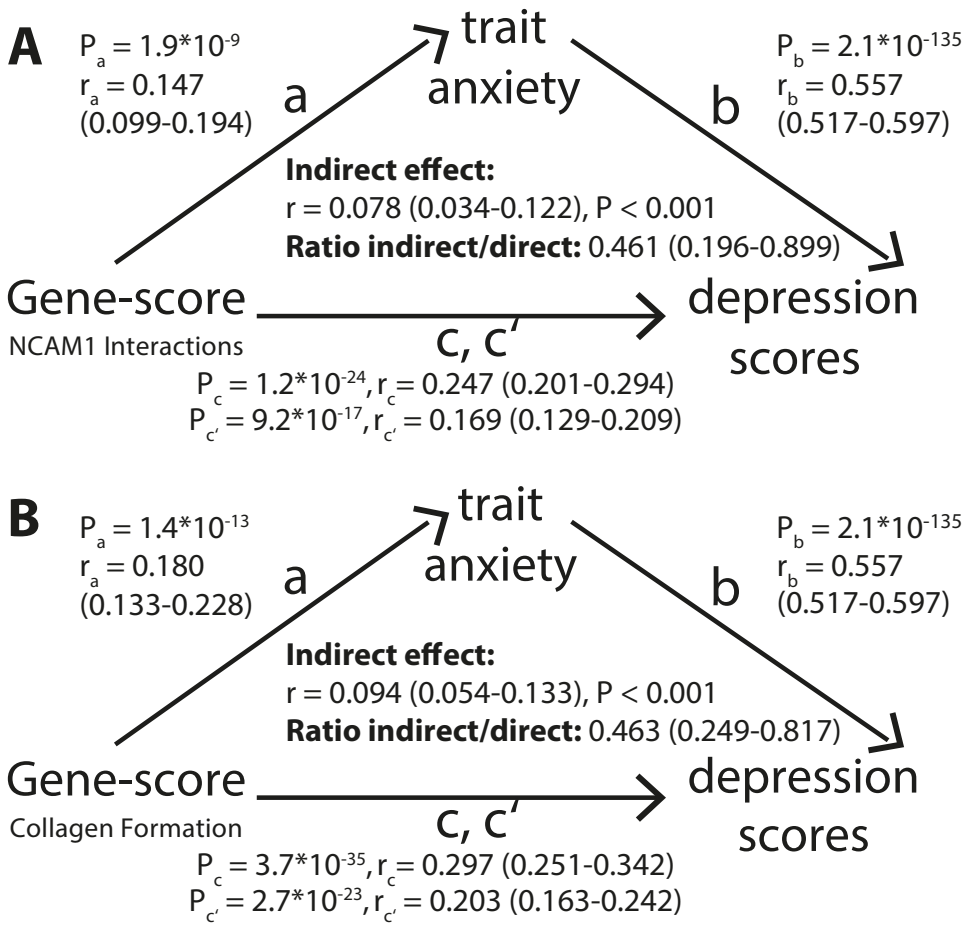

Supplementary Figure 6 Visual representation of the results from the mediation analyses, testing if trait anxiety mediates the association between gene-scores and depression scores for A) the NCAM1 Interactions B) Collagen Formation gene set, in the discovery sample

Path (a) represents the effect of gene-score on trait anxiety, path (b) the effect of trait anxiety on depression scores, path (c) the effect of the gene-scores on depression scores, and path (c') the effect of gene-score on depression scores while controlling for the indirect effect of trait anxiety. The indirect effect is computed by multiplying the effects of (a) and (b). Parameters (r) show the association strength (+/- 99.9% confidence interval). Ratio indirect/direct represents the strength of mediation ((a x b)/c'). Parameters (P) show the significance for each path.

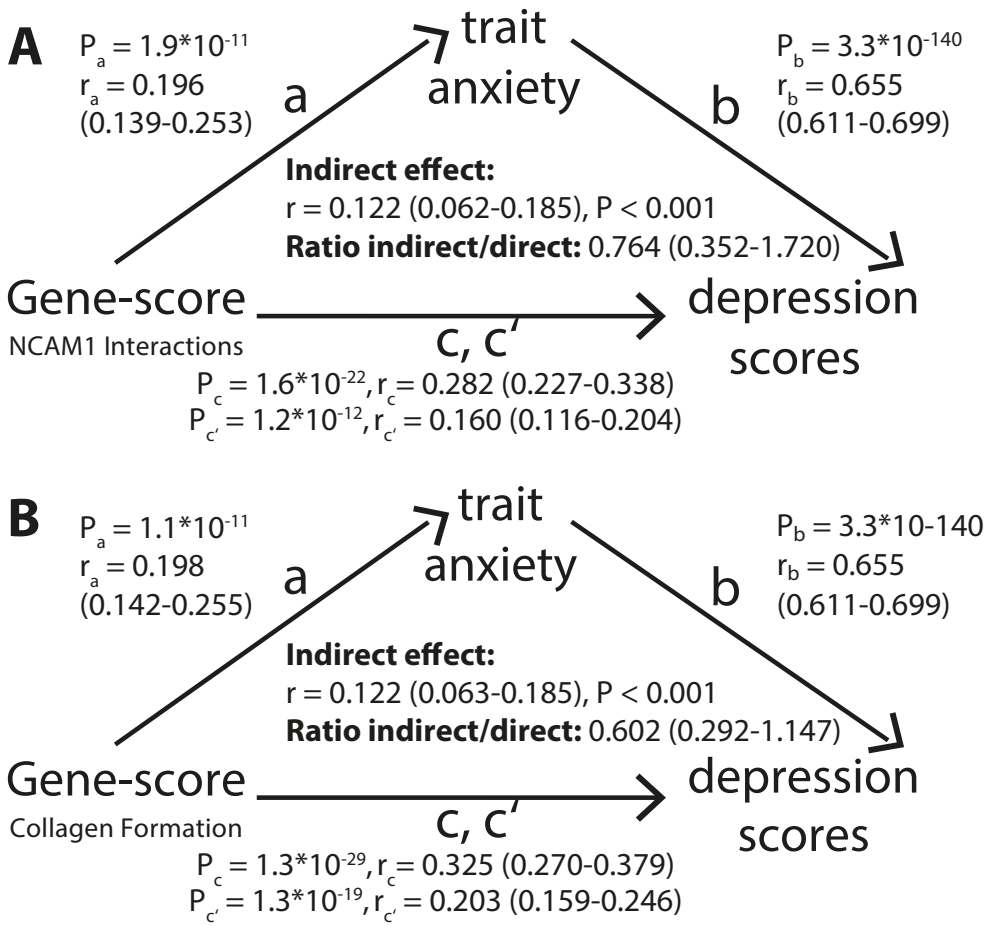

Supplementary Figure 7 Visual representation of the results from the mediation analyses, testing if trait anxiety mediates the association between gene-scores and depression scores for A) the NCAM1 Interactions B) Collagen Formation gene set, in the replication sample

Path (a) represents the effect of gene-score on trait anxiety, path (b) the effect of trait anxiety on depression scores, path (c) the effect of the gene-scores on depression scores, and path (c') the effect of gene-score on depression scores while controlling for the indirect effect of trait anxiety. The indirect effect is computed by multiplying the effects of (a) and (b). Parameters (r) show the association strength (+/- 99.9% confidence interval). Ratio indirect/direct represents the strength of mediation ((a x b)/c'). Parameters (P) show the significance for each path.

Supplementary Tables

Supplementary Table 1 Gene set associations with depression scores, with 110kb upstream of the gene start site and 40kb downstream of the gene end site included

Sample	Gene Set	p value	$q_{75\%}$	Gene set size	Observed genes above enrichment cutoff	Expected genes above enrichment cutoff
Basel_1	Collagen Formation	2.0×10^{-4}	0.040	53	26	13
Basel_1	NCAM1 Interactions	1.0×10^{-4}	0.024	35	19	9
Basel_2	Collagen Formation	1.0×10^{-4}	0.014	53	27	13
Basel_2	NCAM1 Interactions	0.001	0.064	35	18	9

Supplementary Table 2 Gene set associations with depression scores A) in the discovery sample (Basel_1); B) in the replication sample (Basel_2) (only gene sets with $p < 0.05$ are listed)

Supplementary Table 2A

Data base	Gene set	p	$q_{75\%}$
REACTOME	**REACTOME_COLLAGEN_FORMATION**	**1.00E-04**	**1.06E-02**
REACTOME	**REACTOME_NCAM1_INTERACTIONS**	**3.00E-04**	**2.12E-02**
REACTOME	REACTOME_ION_CHANNEL_TRANSPORT	3.00E-04	5.15E-02
BIOCARTA	**BIOCARTA_AMI_PATHWAY**	**6.00E-04**	**3.44E-02**
GO	INTEGRIN_BINDING	8.00E-04	3.25E-01
GO	AMINE_TRANSMEMBRANE_TRANSPORTER_ACTIVITY	9.00E-04	2.47E-01
REACTOME	REACTOME_SIGNALING_BY_PDGF	1.30E-03	7.51E-02
REACTOME	REACTOME_NCAM_SIGNALING_FOR_NEURITE_OUT_GROWTH	1.40E-03	9.85E-02
KEGG	KEGG_OOCYTE_MEIOSIS	2.30E-03	3.69E-01
REACTOME	REACTOME_RNA_POL_I_TRANSCRIPTION_TERMINATION	2.50E-03	8.86E-02
BIOCARTA	BIOCARTA_INTRINSIC_PATHWAY	2.90E-03	6.90E-02
REACTOME	REACTOME_DAG_AND_IP3_SIGNALING	2.90E-03	1.10E-01
GO	AMINO_ACID_TRANSMEMBRANE_TRANSPORTER_ACTIVITY	3.10E-03	4.08E-01
REACTOME	REACTOME_ION_TRANSPORT_BY_P_TYPE_ATPASES	3.30E-03	1.07E-01
REACTOME	REACTOME_EXTRACELLULAR_MATRIX_ORGANIZATION	3.40E-03	1.32E-01
GO	NEURON_DEVELOPMENT	3.40E-03	4.40E-01
REACTOME	REACTOME_TRANSPORT_OF_INORGANIC_CATIONS_ANIONS_AND_AMINO_ACIDS_OLIGOPEPTIDES	3.50E-03	1.24E-01
GO	POSITIVE_REGULATION_OF_NUCLEOBASENUCLEOSIDENUCLEOTIDE_AND_NUCLEIC_ACID	4.50E-03	3.78E-01
GO	POSITIVE_REGULATION_OF_TRANSCRIPTION	4.50E-03	4.26E-01
GO	CARBOXYLIC_ACID_TRANSMEMBRANE_TRANSPORTER_ACTIVITY	5.40E-03	4.18E-01
REACTOME	REACTOME_ABC_FAMILY_PROTEINS_MEDIATED_TRANSPORT	5.60E-03	1.24E-01
KEGG	KEGG_COMPLEMENT_AND_COAGULATION_CASCADES	6.00E-03	3.61E-01
GO	POSITIVE_REGULATION_OF_TRANSCRIPTIONDNA_DEPENDENT	6.20E-03	3.54E-01
GO	NEURITE_DEVELOPMENT	6.20E-03	3.81E-01
KEGG	KEGG_CALCIUM_SIGNALING_PATHWAY	6.40E-03	2.78E-01
KEGG	KEGG_AXON_GUIDANCE	6.90E-03	1.79E-01
GO	ATPASE_ACTIVITY_COUPLED_TO_MOVEMENT_OF_SUBSTANCES	6.90E-03	3.85E-01
REACTOME	REACTOME_SIGNALING_BY_ROBO_RECEPTOR	7.20E-03	1.26E-01
GO	ORGANIC_ACID_TRANSMEMBRANE_TRANSPORTER_ACTIVITY	7.40E-03	3.83E-01
REACTOME	REACTOME_RNA_POL_I_TRANSCRIPTION_INITIATION	7.50E-03	1.31E-01
GO	ACTIVE_TRANSMEMBRANE_TRANSPORTER_ACTIVITY	7.70E-03	3.87E-01
GO	PROTEIN_TYROSINE_KINASE_ACTIVITY	7.80E-03	3.68E-01
GO	POSITIVE_REGULATION_OF_TRANSCRIPTION_FROM_RNA_POLYMERASE_II_PROMOTER	7.90E-03	3.91E-01
REACTOME	REACTOME_GABA_RECEPTOR_ACTIVATION	8.10E-03	1.48E-01
REACTOME	REACTOME_AMINO_ACID_TRANSPORT_ACROSS_THE_PLASMA_MEMBRANE	8.60E-03	1.30E-01
KEGG	KEGG_ECM_RECEPTOR_INTERACTION	8.80E-03	2.18E-01
GO	HYDROLASE_ACTIVITY_ACTING_ON_ACID_ANHYDRIDESCATALYZING_TRANSMEMBRANE_MOVEME	1.06E-02	3.33E-01
GO	AMINE_TRANSPORT	1.15E-02	3.31E-01
REACTOME	REACTOME_AMINO_ACID_AND_OLIGOPEPTIDE_SLC_TRANSPORTERS	1.17E-02	1.87E-01
GO	WOUND_HEALING	1.20E-02	3.27E-01
GO	PRIMARY_ACTIVE_TRANSMEMBRANE_TRANSPORTER_ACTIVITY	1.24E-02	3.60E-01
GO	POSITIVE_REGULATION_OF_RNA_METABOLIC_PROCESS	1.39E-02	3.58E-01
GO	COFACTOR_BINDING	1.43E-02	3.44E-01
KEGG	KEGG_ABC_TRANSPORTERS	1.48E-02	2.66E-01
GO	ACTIN_FILAMENT_BINDING	1.48E-02	3.20E-01
REACTOME	REACTOME_CIRCADIAN_REPRESSION_OF_EXPRESSION_BY_REV_ERBA	1.67E-02	2.12E-01
BIOCARTA	BIOCARTA_PPARA_PATHWAY	1.67E-02	3.81E-01
GO	POSITIVE_REGULATION_OF_TRANSPORT	1.69E-02	3.50E-01
REACTOME	REACTOME_CA_DEPENDENT_EVENTS	1.81E-02	2.04E-01
GO	KINETOCHORE	1.91E-02	3.53E-01
REACTOME	REACTOME_PHOSPHOLIPASE_C_MEDIATED_CASCADE	2.02E-02	2.56E-01
REACTOME	REACTOME_FORMATION_OF_FIBRIN_CLOT_CLOTTING_CASCADE	2.06E-02	2.33E-01
REACTOME	REACTOME_TRANSMISSION_ACROSS_CHEMICAL_SYNAPSES	2.12E-02	3.22E-01
GO	REGULATION_OF_SECRETION	2.14E-02	4.45E-01
GO	PROTEIN_COMPLEX_BINDING	2.25E-02	4.79E-01
REACTOME	REACTOME_EFFECTS_OF_PIP2_HYDROLYSIS	2.27E-02	2.42E-01
REACTOME	REACTOME_PHOSPHORYLATION_OF_THE_APC_C	2.37E-02	2.36E-01
GO	TRANSMEMBRANE_RECEPTOR_PROTEIN_KINASE_ACTIVITY	2.45E-02	4.81E-01
KEGG	KEGG_GLYCOSPHINGOLIPID_BIOSYNTHESIS_LACTO_AND_NEOLACTO_SERIES	2.66E-02	3.65E-01
GO	LIGAND_DEPENDENT_NUCLEAR_RECEPTOR_ACTIVITY	2.75E-02	4.83E-01
GO	DI___TRI_VALENT_INORGANIC_CATION_TRANSPORT	2.84E-02	4.97E-01

KEGG	KEGG_MELANOGENESIS	2.90E-02	4.44E-01
REACTOME	REACTOME_INTEGRIN_CELL_SURFACE_INTERACTIONS	2.98E-02	3.87E-01
REACTOME	REACTOME_DOWNSTREAM_SIGNAL_TRANSDUCTION	3.01E-02	3.86E-01
REACTOME	REACTOME_NEUROTRANSMITTER_RECEPTOR_BINDING_AND_DOWNSTREAM_TRANSMISSION	3.10E-02	3.84E-01
GO	EXTRINSIC_TO_MEMBRANE	3.10E-02	4.89E-01
GO	PEPTIDYL_AMINO_ACID_MODIFICATION	3.12E-02	5.74E-01
REACTOME	REACTOME_MITOTIC_PROMETAPHASE	3.13E-02	3.99E-01
GO	TRANSMEMBRANE_RECEPTOR_PROTEIN_TYROSINE_KINASE_ACTIVITY	3.29E-02	5.56E-01
KEGG	KEGG_GLIOMA	3.31E-02	4.95E-01
REACTOME	REACTOME_TRANSPORT_OF_GLUCOSE_AND_OTHER_SUGARS_BILE_SALTS_AND_ORGANIC_ACIDS	3.34E-02	3.91E-01
GO	METAL_ION_TRANSMEMBRANE_TRANSPORTER_ACTIVITY	3.41E-02	5.37E-01
GO	NEURON_DIFFERENTIATION	3.49E-02	5.54E-01
GO	PROTEIN_N_TERMINUS_BINDING	3.50E-02	6.05E-01
REACTOME	REACTOME_RORA_ACTIVATES_CIRCADIAN_EXPRESSION	3.67E-02	3.46E-01
GO	CELL_PROJECTION	3.78E-02	5.99E-01
KEGG	KEGG_DILATED_CARDIOMYOPATHY	3.91E-02	4.78E-01
GO	CALCIUM_ION_TRANSPORT	3.93E-02	5.84E-01
GO	CALCIUM_CHANNEL_ACTIVITY	4.11E-02	5.62E-01
GO	AMINO_ACID_TRANSPORT	4.13E-02	5.70E-01
GO	ADHERENS_JUNCTION	4.17E-02	5.88E-01
GO	AXONOGENESIS	4.22E-02	5.42E-01
GO	ATPASE_ACTIVITY_COUPLED	4.31E-02	5.72E-01
BIOCARTA	BIOCARTA_PGC1A_PATHWAY	4.31E-02	6.38E-01
KEGG	KEGG_PROGESTERONE_MEDIATED_OOCYTE_MATURATION	4.36E-02	4.68E-01
REACTOME	REACTOME_NETRIN1_SIGNALING	4.46E-02	3.88E-01
GO	MEMBRANE_ORGANIZATION_AND_BIOGENESIS	4.47E-02	5.75E-01
REACTOME	REACTOME_COMPLEMENT_CASCADE	4.51E-02	3.74E-01
REACTOME	REACTOME_NUCLEAR_RECEPTOR_TRANSCRIPTION_PATHWAY	4.52E-02	3.98E-01
KEGG	KEGG_ARRHYTHMOGENIC_RIGHT_VENTRICULAR_CARDIOMYOPATHY_ARVC	4.54E-02	4.48E-01
REACTOME	REACTOME_LIPID_DIGESTION_MOBILIZATION_AND_TRANSPORT	4.70E-02	3.97E-01
GO	PERINUCLEAR_REGION_OF_CYTOPLASM	4.74E-02	5.76E-01
GO	CALCIUM_ION_BINDING	4.81E-02	5.80E-01

Supplementary Table 2B

Data base	Gene set	p	$q_{75\%}$
KEGG	KEGG_ECM_RECEPTOR_INTERACTION	9.90E-05	1.00E-04
REACTOME	**REACTOME_COLLAGEN_FORMATION**	**9.90E-05**	**3.03E-02**
REACTOME	**REACTOME_NCAM1_INTERACTIONS**	**1.00E-04**	**2.48E-02**
GO	GLYCOSAMINOGLYCAN_BINDING	1.00E-04	6.81E-02
GO	POLYSACCHARIDE_BINDING	1.00E-04	9.92E-02
REACTOME	REACTOME_NCAM_SIGNALING_FOR_NEURITE_OUT_GROWTH	3.00E-04	5.38E-02
REACTOME	REACTOME_L1CAM_INTERACTIONS	5.00E-04	2.96E-02
REACTOME	REACTOME_INTEGRIN_CELL_SURFACE_INTERACTIONS	6.00E-04	4.61E-02
REACTOME	REACTOME_CELL_SURFACE_INTERACTIONS_AT_THE_VASCULAR_WALL	1.40E-03	7.63E-02
GO	HEMOSTASIS	1.50E-03	1.70E-01
GO	PATTERN_BINDING	1.60E-03	1.69E-01
GO	PROTEIN_OLIGOMERIZATION	2.80E-03	1.86E-01
GO	GUANYL_NUCLEOTIDE_EXCHANGE_FACTOR_ACTIVITY	2.90E-03	1.91E-01
GO	HEPARIN_BINDING	3.10E-03	1.92E-01
GO	BLOOD_COAGULATION	3.20E-03	1.66E-01
KEGG	KEGG_AMINO_SUGAR_AND_NUCLEOTIDE_SUGAR_METABOLISM	3.90E-03	1.43E-01
GO	PROTEIN_COMPLEX_ASSEMBLY	4.50E-03	2.59E-01
GO	COAGULATION	4.60E-03	2.12E-01
GO	CELL_CORTEX_PART	4.60E-03	2.13E-01
GO	COLLAGEN	6.30E-03	2.21E-01
BIOCARTA	BIOCARTA_ECM_PATHWAY	6.40E-03	3.63E-01
GO	POTASSIUM_CHANNEL_ACTIVITY	6.60E-03	2.57E-01
KEGG	KEGG_GLYCOSAMINOGLYCAN_BIOSYNTHESIS_CHONDROITIN_SULFATE	6.90E-03	1.75E-01
REACTOME	REACTOME_APOPTOTIC_EXECUTION_PHASE	6.90E-03	2.27E-01
REACTOME	REACTOME_TRIGLYCERIDE_BIOSYNTHESIS	7.20E-03	2.13E-01
REACTOME	REACTOME_SIGNALING_BY_RHO_GTPASES	7.60E-03	2.15E-01
GO	METAL_ION_TRANSMEMBRANE_TRANSPORTER_ACTIVITY	7.60E-03	3.63E-01
REACTOME	REACTOME_PHOSPHOLIPID_METABOLISM	8.30E-03	2.23E-01
REACTOME	REACTOME_APOPTOTIC_CLEAVAGE_OF_CELLULAR_PROTEINS	8.40E-03	1.97E-01
REACTOME	REACTOME_INTERFERON_GAMMA_SIGNALING	8.40E-03	2.07E-01
GO	CORTICAL_CYTOSKELETON	8.50E-03	2.68E-01
GO	PROTEINACEOUS_EXTRACELLULAR_MATRIX	8.70E-03	3.47E-01
REACTOME	REACTOME_CHONDROITIN_SULFATE_BIOSYNTHESIS	9.10E-03	1.96E-01
GO	EXTRACELLULAR_MATRIX	9.30E-03	3.73E-01
REACTOME	REACTOME_NRAGE_SIGNALS_DEATH_THROUGH_JNK	1.10E-02	2.13E-01
REACTOME	REACTOME_CHONDROITIN_SULFATE_DERMATAN_SULFATE_METABOLISM	1.17E-02	2.28E-01
KEGG	KEGG_SMALL_CELL_LUNG_CANCER	1.17E-02	3.57E-01
GO	REGULATION_OF_BODY_FLUID_LEVELS	1.27E-02	3.52E-01
REACTOME	REACTOME_G_ALPHA_Z_SIGNALLING_EVENTS	1.30E-02	2.26E-01
REACTOME	REACTOME_EXTRACELLULAR_MATRIX_ORGANIZATION	1.31E-02	2.37E-01
GO	SKELETAL_DEVELOPMENT	1.39E-02	3.90E-01
REACTOME	REACTOME_CELL_DEATH_SIGNALLING_VIA_NRAGE_NRIF_AND_NADE	1.47E-02	2.41E-01
GO	EXTRACELLULAR_MATRIX_PART	1.49E-02	4.03E-01
BIOCARTA	BIOCARTA_KERATINOCYTE_PATHWAY	1.50E-02	2.57E-01
REACTOME	REACTOME_ABC_FAMILY_PROTEINS_MEDIATED_TRANSPORT	1.53E-02	2.24E-01
BIOCARTA	BIOCARTA_MYOSIN_PATHWAY	1.53E-02	3.09E-01
BIOCARTA	BIOCARTA_PAR1_PATHWAY	1.57E-02	2.08E-01
REACTOME	REACTOME_PURINE_METABOLISM	1.59E-02	2.32E-01
BIOCARTA	BIOCARTA_AMI_PATHWAY	1.62E-02	4.42E-01
GO	CARBOHYDRATE_BINDING	1.65E-02	4.45E-01
KEGG	KEGG_ABC_TRANSPORTERS	1.80E-02	3.68E-01
REACTOME	REACTOME_P75_NTR_RECEPTOR_MEDIATED_SIGNALLING	1.94E-02	2.86E-01
GO	PROTEIN_HOMOOLIGOMERIZATION	1.96E-02	3.92E-01
KEGG	KEGG_TIGHT_JUNCTION	1.99E-02	4.41E-01
REACTOME	REACTOME_INTEGRATION_OF_ENERGY_METABOLISM	2.05E-02	2.85E-01
REACTOME	REACTOME_SPHINGOLIPID_METABOLISM	2.08E-02	2.74E-01
GO	MEMBRANE_LIPID_METABOLIC_PROCESS	2.12E-02	5.71E-01
GO	SUBSTRATE_SPECIFIC_CHANNEL_ACTIVITY	2.23E-02	5.89E-01
KEGG	KEGG_WNT_SIGNALING_PATHWAY	2.32E-02	4.66E-01
REACTOME	REACTOME_SEMAPHORIN_INTERACTIONS	2.40E-02	3.21E-01
REACTOME	REACTOME_GLYCOSAMINOGLYCAN_METABOLISM	2.58E-02	3.17E-01
REACTOME	REACTOME_GLYCEROPHOSPHOLIPID_BIOSYNTHESIS	2.62E-02	3.27E-01
GO	ION_TRANSPORT	2.64E-02	6.41E-01
GO	CATION_CHANNEL_ACTIVITY	2.67E-02	6.26E-01
GO	CARBOHYDRATE_BIOSYNTHETIC_PROCESS	2.71E-02	5.62E-01
GO	LIPID_TRANSPORTER_ACTIVITY	2.73E-02	5.05E-01
KEGG	KEGG_VASCULAR_SMOOTH_MUSCLE_CONTRACTION	2.78E-02	4.37E-01
GO	CELL_MIGRATION	2.78E-02	6.18E-01
REACTOME	REACTOME_GLUCOSE_METABOLISM	2.98E-02	3.14E-01
GO	CATION_TRANSPORT	3.03E-02	6.14E-01
GO	ALCOHOL_METABOLIC_PROCESS	3.18E-02	6.46E-01
GO	ACTIN_CYTOSKELETON	3.42E-02	6.06E-01

KEGG	KEGG_LONG_TERM_DEPRESSION	3.43E-02	4.60E-01
REACTOME	REACTOME_POTASSIUM_CHANNELS	3.47E-02	3.41E-01
GO	PHOSPHOLIPID_METABOLIC_PROCESS	3.55E-02	6.23E-01
GO	METAL_ION_TRANSPORT	3.67E-02	6.11E-01
GO	GUANYL_NUCLEOTIDE_BINDING	3.76E-02	6.49E-01
GO	ACTIVE_TRANSMEMBRANE_TRANSPORTER_ACTIVITY	3.77E-02	6.12E-01
BIOCARTA	BIOCARTA_BAD_PATHWAY	3.87E-02	3.76E-01
GO	INORGANIC_CATION_TRANSMEMBRANE_TRANSPORTER_ACTIVITY	3.89E-02	6.11E-01
GO	DIGESTION	3.89E-02	6.35E-01
BIOCARTA	BIOCARTA_INTRINSIC_PATHWAY	3.94E-02	3.72E-01
REACTOME	REACTOME_PTM_GAMMA_CARBOXYLATION_HYPUSINE_FORMATION_AND_ARYLSULFATASE	3.96E-02	3.11E-01
KEGG	KEGG_DILATED_CARDIOMYOPATHY	3.98E-02	4.65E-01
REACTOME	REACTOME_GLYCOSPHINGOLIPID_METABOLISM	4.03E-02	3.44E-01
REACTOME	REACTOME_REGULATION_OF_INSULIN_SECRETION_BY_GLUCAGON_LIKE_PEPTIDE1	4.03E-02	3.51E-01
GO	ION_CHANNEL_ACTIVITY	4.08E-02	6.66E-01
REACTOME	REACTOME_CHOLESTEROL_BIOSYNTHESIS	4.20E-02	3.28E-01
REACTOME	REACTOME_INSULIN_SYNTHESIS_AND_PROCESSING	4.21E-02	3.01E-01
GO	WOUND_HEALING	4.31E-02	6.11E-01
REACTOME	REACTOME_G_ALPHA1213_SIGNALLING_EVENTS	4.36E-02	3.83E-01
GO	CYTOSKELETAL_PROTEIN_BINDING	4.61E-02	6.97E-01
GO	AMINE_TRANSMEMBRANE_TRANSPORTER_ACTIVITY	4.69E-02	6.08E-01
REACTOME	REACTOME_KERATAN_SULFATE_KERATIN_METABOLISM	4.83E-02	3.85E-01
GO	EXTRACELLULAR_MATRIX_STRUCTURAL_CONSTITUENT	4.94E-02	6.56E-01
KEGG	KEGG_ADHERENS_JUNCTION	4.96E-02	4.32E-01

Supplementary Table 3 GWAS p-values for the most significant i.e. best SNP of each gene in the NCAM1 Interactions gene set A) in the discovery sample (Basel_1); B) in the replication sample (Basel_2)

Supplementary Table 3A

Gene	Gene p-value	Best SNP	Best SNP p-value
COL6A1	1.79E-02	rs2776407	6.36E-03
COL4A1	4.41E-02	rs11069830	3.80E-03
COL6A2	4.47E-02	rs4819203	1.02E-02
COL4A3	4.75E-02	rs4263106	4.55E-03
CNTN2	6.78E-02	rs12117194	1.49E-02
COL4A4	8.09E-02	rs1317770	8.38E-03
COL4A2	8.64E-02	rs9515203	4.66E-03
CACNB4	8.90E-02	rs16830513	4.45E-03
GFRA2	9.14E-02	rs4073433	1.54E-02
CACNA1I	9.18E-02	rs3788562	1.36E-02
COL1A1	9.78E-02	rs2696245	2.52E-02
COL2A1	1.31E-01	rs740024	3.13E-02
ST8SIA2	1.59E-01	rs8037133	2.93E-02
GDNF	1.74E-01	rs7731209	4.41E-02
CACNB2	1.82E-01	rs1106380	3.54E-03
COL5A1	1.93E-01	rs7044151	1.66E-02
ST8SIA4	2.25E-01	rs17724833	4.52E-02
NRTN	2.35E-01	rs3763046	5.98E-02
COL1A2	2.35E-01	rs10046552	5.68E-02
COL5A2	3.35E-01	rs10166301	5.90E-02
COL3A1	3.78E-01	rs3736487	1.06E-01
COL6A3	3.99E-01	rs3790990	8.63E-02
NCAN	3.99E-01	rs1064395	1.28E-01
CACNA1S	4.19E-01	rs3820421	8.81E-02
NCAM1	4.81E-01	rs644668	3.50E-02
CACNA1H	5.00E-01	rs11859240	1.55E-01
COL9A1	5.73E-01	rs9294863	1.51E-01
GFRA1	5.94E-01	rs17668282	9.40E-02
CACNB1	6.20E-01	rs17633541	2.48E-01
CACNA1G	6.60E-01	rs4794166	2.52E-01
COL9A3	7.40E-01	rs6010757	3.60E-01
COL9A2	7.44E-01	rs2281399	3.68E-01
GFRA4	7.61E-01	rs616749	3.68E-01
PRNP	8.25E-01	rs6107516	5.05E-01
AGRN	9.32E-01	rs2465136	7.70E-01
CACNB3	NaN	NaN	NaN
PSPN	NaN	NaN	NaN
ARTN	NaN	NaN	NaN

Supplementary Table 3B

Gene	Gene p-value	Best SNP	Best SNP p-value
COL4A3	4.84E-03	rs7608142	6.26E-04
ST8SIA4	1.16E-02	rs3909452	2.86E-03
ST8SIA2	3.89E-02	rs3784722	7.45E-03
COL4A1	5.10E-02	rs7987982	4.81E-03
CACNA1S	6.09E-02	rs12405259	9.37E-03
NCAM1	6.63E-02	rs17114760	2.21E-03
COL6A3	6.80E-02	rs4663723	1.15E-02
CACNA1H	8.16E-02	rs11859240	1.96E-02
CACNB1	8.60E-02	rs16537	2.34E-02
COL4A2	9.11E-02	rs331592	5.22E-03
COL6A2	9.83E-02	rs9978055	2.41E-02
COL9A2	1.01E-01	rs2076696	2.67E-02
NCAN	1.33E-01	rs11672216	3.79E-02
COL5A1	1.51E-01	rs3922982	1.34E-02
COL1A2	1.56E-01	rs2023729	3.64E-02
CACNA1I	1.77E-01	rs136855	3.08E-02
COL1A1	2.15E-01	rs2075555	6.35E-02
COL3A1	2.28E-01	rs12693525	5.97E-02
GDNF	2.56E-01	rs2910797	7.20E-02
COL9A1	3.13E-01	rs604896	5.98E-02
COL4A4	3.65E-01	rs16823258	5.81E-02
COL2A1	4.41E-01	rs12811832	1.40E-01
COL9A3	4.42E-01	rs4809261	1.49E-01
GFRA1	4.57E-01	rs10885864	5.82E-02
CACNB2	4.68E-01	rs10828308	1.99E-02
CNTN2	5.51E-01	rs4951163	1.81E-01
PRNP	6.73E-01	rs7274758	3.25E-01
CACNA1G	7.31E-01	rs198542	3.21E-01
GFRA4	7.48E-01	rs616749	3.50E-01
CACNB4	7.60E-01	rs2344734	1.54E-01
AGRN	7.70E-01	rs2465136	4.33E-01
GFRA2	7.87E-01	rs4073433	3.37E-01
COL6A1	8.62E-01	rs9978314	5.92E-01
COL5A2	9.29E-01	rs7419288	5.60E-01
NRTN	9.71E-01	rs3763046	9.20E-01
CACNB3	NaN	NaN	NaN
PSPN	NaN	NaN	NaN
ARTN	NaN	NaN	NaN

Supplementary Table 4 GWAS p-values for the most significant i.e. best SNP of each gene in the Collagen Formation gene set A) in the discovery sample (Basel_1); B) in the replication sample (Basel_2)

Supplementary Table 4A

Gene	Gene p-value	Best SNP	Best SNP p-value
COL27A1	6.09E-03	rs1468010	5.81E-04
COL15A1	1.16E-02	rs4743299	1.58E-03
COL6A1	1.79E-02	rs2776407	6.36E-03
COL8A1	2.33E-02	rs12107500	2.54E-03
TLL2	2.66E-02	rs10882801	2.74E-03
ADAMTS14	3.56E-02	rs10999487	5.00E-03
COL4A1	4.41E-02	rs11069830	3.80E-03
COL6A2	4.47E-02	rs4819203	1.02E-02
COL5A3	4.60E-02	rs16996952	1.05E-02
COL4A3	4.75E-02	rs4263106	4.55E-03
GLT25D2	7.29E-02	rs10752928	9.97E-03
COL12A1	7.39E-02	rs11966644	1.03E-02
COL4A4	8.09E-02	rs1317770	8.38E-03
COL4A2	8.64E-02	rs9515203	4.66E-03
BMP1	9.75E-02	rs3857979	2.18E-02
COL1A1	9.78E-02	rs2696245	2.52E-02
COL28A1	1.23E-01	rs1294627	1.15E-02
SERPINH1	1.25E-01	rs646474	3.18E-02
COL2A1	1.31E-01	rs740024	3.13E-02
LEPREL1	1.43E-01	rs16865025	1.50E-02
COL22A1	1.84E-01	rs10106218	6.47E-03
COL5A1	1.93E-01	rs7044151	1.66E-02
PPIB	1.96E-01	rs7177371	5.65E-02
ADAMTS2	2.10E-01	rs1530499	1.37E-02
TLL1	2.20E-01	rs17505658	1.81E-02
COL1A2	2.35E-01	rs10046552	5.68E-02
COL13A1	2.42E-01	rs10999049	2.44E-02
PLOD2	2.84E-01	rs3804664	6.26E-02
PLOD3	2.85E-01	rs7802724	9.48E-02
PCOLCE2	3.29E-01	rs9841007	7.53E-02
COL5A2	3.35E-01	rs10166301	5.90E-02
COL3A1	3.78E-01	rs3736487	1.06E-01
COL6A3	3.99E-01	rs3790990	8.63E-02
P4HB	4.23E-01	rs2070871	1.55E-01
COL25A1	4.38E-01	rs2198329	1.04E-02
COL21A1	4.46E-01	rs742497	6.60E-02
COL14A1	5.22E-01	rs10505377	6.58E-02
COL16A1	5.34E-01	rs11584199	1.72E-01
COL23A1	5.34E-01	rs6600941	3.36E-02
COL17A1	5.49E-01	rs17821926	1.79E-01

LEPREL2	5.65E-01	rs4963513	2.13E-01
COL9A1	5.73E-01	rs9294863	1.51E-01
COL24A1	6.01E-01	rs17408298	3.08E-02
PLOD1	6.85E-01	rs2336381	3.08E-01
COL19A1	6.93E-01	rs12190849	7.50E-02
COL9A3	7.40E-01	rs6010757	3.60E-01
COL9A2	7.44E-01	rs2281399	3.68E-01
COL11A1	7.45E-01	rs2045819	1.62E-01
ADAMTS3	7.52E-01	rs16847841	1.38E-01
CRTAP	8.13E-01	rs12054462	4.44E-01
COL7A1	8.29E-01	rs2228561	4.97E-01
GLT25D1	8.76E-01	rs10418441	5.96E-01
COL10A1	9.35E-01	rs1059277	7.61E-01
COL4A6	NaN	NaN	NaN
COL8A2	NaN	NaN	NaN
PCOLCE	NaN	NaN	NaN

Supplementary Table 4B

Gene	Gene p-value	Best SNP	Best SNP p-value
COL4A3	4.84E-03	rs7608142	6.26E-04
TLL2	1.27E-02	rs3789950	1.55E-03
COL19A1	1.68E-02	rs3806039	4.28E-04
COL8A1	3.54E-02	rs17777478	4.32E-03
COL22A1	3.66E-02	rs10096258	9.95E-04
COL4A1	5.10E-02	rs7987982	4.81E-03
COL6A3	6.80E-02	rs4663723	1.15E-02
COL4A2	9.11E-02	rs331592	5.22E-03
COL6A2	9.83E-02	rs9978055	2.41E-02
COL9A2	1.01E-01	rs2076696	2.67E-02
PCOLCE2	1.19E-01	rs7642969	2.39E-02
COL15A1	1.23E-01	rs3780621	1.76E-02
COL27A1	1.34E-01	rs7023208	1.35E-02
COL28A1	1.48E-01	rs7789187	1.56E-02
COL25A1	1.49E-01	rs17039914	1.82E-03
COL5A1	1.51E-01	rs3922982	1.34E-02
COL1A2	1.56E-01	rs2023729	3.64E-02
COL23A1	1.77E-01	rs2913787	5.45E-03
LEPREL1	1.80E-01	rs710551	2.15E-02
COL11A1	2.08E-01	rs12728397	1.81E-02
COL21A1	2.09E-01	rs17219382	2.36E-02
ADAMTS3	2.11E-01	rs10518102	1.41E-02
COL1A1	2.15E-01	rs2075555	6.35E-02
COL14A1	2.26E-01	rs7842055	1.85E-02
COL3A1	2.28E-01	rs12693525	5.97E-02
COL13A1	2.28E-01	rs1227753	2.34E-02
PPIB	2.76E-01	rs41434449	7.86E-02
PLOD2	2.87E-01	rs10935606	6.82E-02
COL9A1	3.13E-01	rs604896	5.98E-02
COL4A4	3.65E-01	rs16823258	5.81E-02
ADAMTS14	3.80E-01	rs7081273	7.56E-02
ADAMTS2	3.94E-01	rs751546	3.80E-02
COL5A3	4.30E-01	rs3745597	1.29E-01
PLOD1	4.39E-01	rs2336381	1.52E-01
COL2A1	4.41E-01	rs12811832	1.40E-01
COL9A3	4.42E-01	rs4809261	1.49E-01
COL24A1	4.72E-01	rs861933	1.88E-02
BMP1	4.98E-01	rs4072420	1.62E-01
GLT25D2	5.01E-01	rs2148675	1.15E-01
LEPREL2	5.83E-01	rs4963513	2.32E-01
COL16A1	5.95E-01	rs16834652	2.11E-01
COL17A1	6.02E-01	rs2181833	2.13E-01
COL12A1	6.38E-01	rs240724	1.88E-01
CRTAP	6.55E-01	rs4074415	2.81E-01

COL10A1	7.25E-01	rs1059277	3.62E-01
SERPINH1	7.83E-01	rs585821	4.05E-01
TLL1	8.10E-01	rs2292082	2.21E-01
GLT25D1	8.25E-01	rs10418441	5.09E-01
COL6A1	8.62E-01	rs9978314	5.92E-01
PLOD3	8.68E-01	rs7802724	6.11E-01
P4HB	9.18E-01	rs2070871	7.38E-01
COL5A2	9.29E-01	rs7419288	5.60E-01
COL7A1	9.54E-01	rs2228561	8.64E-01
COL4A6	NaN	NaN	NaN
COL8A2	NaN	NaN	NaN
PCOLCE	NaN	NaN	NaN

Supplementary Table 5 Gene set associations with the mean FA value of the depression-associated voxels within the forceps minor (only gene sets with p < 0.05 are listed)

Data base	Gene set	p	$q_{75\%}$
REACTOME	REACTOME_SIGNALING_BY_HIPPO	1.00E-04	4.60E-03
GO	LAMELLIPODIUM	5.00E-04	7.42E-02
GO	CELL_PROJECTION_BIOGENESIS	2.10E-03	2.97E-01
KEGG	KEGG_WNT_SIGNALING_PATHWAY	2.30E-03	3.57E-01
GO	RECEPTOR_COMPLEX	2.80E-03	6.17E-01
GO	DNA_HELICASE_ACTIVITY	4.30E-03	4.95E-01
GO	LEADING_EDGE	5.70E-03	6.23E-01
KEGG	KEGG_ABC_TRANSPORTERS	6.70E-03	2.95E-01
REACTOME	REACTOME_NEUROTRANSMITTER_RECEPTOR_BINDING_AND_DOWNSTREAM_TRANSMISSION	7.10E-03	8.10E-01
KEGG	KEGG_PANCREATIC_CANCER	7.50E-03	2.67E-01
REACTOME	REACTOME_PHOSPHOLIPID_METABOLISM	7.70E-03	7.56E-01
GO	BLOOD_COAGULATION	7.80E-03	5.58E-01
KEGG	KEGG_LONG_TERM_DEPRESSION	8.40E-03	2.09E-01
KEGG	KEGG_ECM_RECEPTOR_INTERACTION	8.50E-03	2.29E-01
GO	HEMATOPOIETIN_INTERFERON_CLASSD200_DOMAIN_CYTOKINE_RECEPTOR_ACTIVITY	8.80E-03	5.44E-01
REACTOME	REACTOME_ACTIVATION_OF_THE_PRE_REPLICATIVE_COMPLEX	9.00E-03	9.73E-01
KEGG	KEGG_RENAL_CELL_CARCINOMA	1.07E-02	2.02E-01
GO	COAGULATION	1.13E-02	6.75E-01
REACTOME	REACTOME_G2_M_CHECKPOINTS	1.20E-02	6.28E-01
KEGG	KEGG_COLORECTAL_CANCER	1.26E-02	2.10E-01
BIOCARTA	BIOCARTA_SPPA_PATHWAY	1.27E-02	7.30E-01
REACTOME	REACTOME_ABC_FAMILY_PROTEINS_MEDIATED_TRANSPORT	1.30E-02	5.17E-01
GO	ER_GOLGI_INTERMEDIATE_COMPARTMENT	1.35E-02	6.22E-01
GO	CELL_PROJECTION	1.49E-02	8.54E-01
REACTOME	REACTOME_APOPTOTIC_EXECUTION_PHASE	1.51E-02	4.79E-01
KEGG	KEGG_VASCULAR_SMOOTH_MUSCLE_CONTRACTION	1.52E-02	2.73E-01
REACTOME	REACTOME_SPHINGOLIPID_DE_NOVO_BIOSYNTHESIS	1.62E-02	5.93E-01
REACTOME	**REACTOME_NCAM1_INTERACTIONS**	**1.65E-02**	**4.43E-01**
GO	PROTEIN_HOMODIMERIZATION_ACTIVITY	1.76E-02	8.63E-01
REACTOME	REACTOME_NCAM_SIGNALING_FOR_NEURITE_OUT_GROWTH	1.91E-02	4.22E-01
REACTOME	REACTOME_INHIBITION_OF_VOLTAGE_GATED_CA2_CHANNELS_VIA_GBETA_GAMMA_SUBUNITS	2.00E-02	4.63E-01
GO	BONE_REMODELING	2.04E-02	7.96E-01
GO	TISSUE_REMODELING	2.06E-02	8.74E-01
REACTOME	REACTOME_NITRIC_OXIDE_STIMULATES_GUANYLATE_CYCLASE	2.07E-02	3.93E-01
GO	TRANSFERASE_ACTIVITY_TRANSFERRING_ACYL_GROUPS	2.15E-02	8.80E-01
REACTOME	REACTOME_YAP1_AND_WWTR1_TAZ_STIMULATED_GENE_EXPRESSION	2.21E-02	4.28E-01
REACTOME	REACTOME_ACYL_CHAIN_REMODELLING_OF_PC	2.31E-02	3.99E-01
KEGG	KEGG_PROSTATE_CANCER	2.33E-02	3.45E-01
GO	REGULATION_OF_BODY_FLUID_LEVELS	2.39E-02	8.30E-01
REACTOME	REACTOME_SPHINGOLIPID_METABOLISM	2.47E-02	4.37E-01
GO	PHOSPHOLIPID_BINDING	2.61E-02	7.91E-01
GO	HEMOSTASIS	2.71E-02	7.61E-01
REACTOME	REACTOME_ACTIVATION_OF_ATR_IN_RESPONSE_TO_REPLICATION_STRESS	2.72E-02	4.44E-01
BIOCARTA	BIOCARTA_MET_PATHWAY	2.72E-02	5.10E-01
BIOCARTA	BIOCARTA_DEATH_PATHWAY	2.76E-02	6.36E-01
GO	TRANSFERASE_ACTIVITY_TRANSFERRING_GLYCOSYL_GROUPS	2.84E-02	7.87E-01
KEGG	KEGG_VIRAL_MYOCARDITIS	2.85E-02	3.52E-01
GO	CELL_SUBSTRATE_ADHESION	2.85E-02	7.35E-01
GO	CATION_TRANSPORT	2.85E-02	7.87E-01
BIOCARTA	BIOCARTA_CERAMIDE_PATHWAY	2.89E-02	7.93E-01
REACTOME	REACTOME_ACTIVATED_TLR4_SIGNALLING	2.93E-02	4.84E-01
GO	POSITIVE_REGULATION_OF_CELL_DIFFERENTIATION	2.96E-02	8.24E-01
GO	HELICASE_ACTIVITY	2.97E-02	7.40E-01
REACTOME	REACTOME_DOUBLE_STRAND_BREAK_REPAIR	2.98E-02	4.43E-01
KEGG	KEGG_AXON_GUIDANCE	3.00E-02	4.02E-01
GO	RUFFLE	3.05E-02	7.27E-01
REACTOME	REACTOME_TRANSPORT_OF_GLUCOSE_AND_OTHER_SUGARS_BILE_SALTS_AND_ORGANIC_ACID	3.29E-02	4.59E-01
GO	RECEPTOR_SIGNALING_PROTEIN_ACTIVITY	3.31E-02	7.92E-01
GO	ATPASE_ACTIVITY	3.47E-02	7.80E-01
GO	RECEPTOR_SIGNALING_PROTEIN_SERINE_THREONINE_KINASE_ACTIVITY	3.87E-02	8.50E-01

REACTOME	REACTOME_INWARDLY_RECTIFYING_K_CHANNELS	3.89E-02	4.78E-01
REACTOME	REACTOME_MYD88_MAL_CASCADE_INITIATED_ON_PLASMA_MEMBRANE	3.90E-02	5.27E-01
GO	ENDOPLASMIC_RETICULUM_PART	4.11E-02	7.78E-01
BIOCARTA	BIOCARTA_IL12_PATHWAY	4.12E-02	4.76E-01
GO	WOUND_HEALING	4.16E-02	8.08E-01
REACTOME	REACTOME_METAL_ION_SLC_TRANSPORTERS	4.19E-02	5.03E-01
REACTOME	REACTOME_RESPONSE_TO_ELEVATED_PLATELET_CYTOSOLIC_CA2_	4.21E-02	5.18E-01
REACTOME	REACTOME_ACYL_CHAIN_REMODELLING_OF_PE	4.25E-02	5.05E-01
KEGG	KEGG_P53_SIGNALING_PATHWAY	4.41E-02	3.70E-01
GO	HUMORAL_IMMUNE_RESPONSE	4.42E-02	8.16E-01
KEGG	KEGG_APOPTOSIS	4.56E-02	3.95E-01
GO	NUCLEAR_ENVELOPE_ENDOPLASMIC_RETICULUM_NETWORK	4.58E-02	7.31E-01
GO	AMINE_TRANSMEMBRANE_TRANSPORTER_ACTIVITY	4.65E-02	7.99E-01
GO	CELL_MATRIX_ADHESION	4.70E-02	7.04E-01
GO	ACTIN_BINDING	4.76E-02	7.35E-01
KEGG	KEGG_ACUTE_MYELOID_LEUKEMIA	4.95E-02	3.68E-01
BIOCARTA	BIOCARTA_FCER1_PATHWAY	4.98E-02	5.63E-01

Supplementary Table 6 Gene set associations with the mean FA value of the depression-associated voxels within the left Superior Longitudinal Fasciculus (SLF) (only gene sets with $p < 0.05$ are listed)

Data base	Gene set	p	$q_{75\%}$
BIOCARTA	BIOCARTA_HDAC_PATHWAY	1.00E-04	4.55E-03
BIOCARTA	BIOCARTA_MEF2D_PATHWAY	1.00E-04	4.90E-03
KEGG	KEGG_ARRHYTHMOGENIC_RIGHT_VENTRICULAR_CARDIOMYOPATHY_ARVC	1.00E-04	3.04E-02
REACTOME	REACTOME_CHONDROITIN_SULFATE_BIOSYNTHESIS	2.00E-04	4.67E-02
KEGG	KEGG_DILATED_CARDIOMYOPATHY	3.00E-04	2.07E-02
GO	ACTIVE_TRANSMEMBRANE_TRANSPORTER_ACTIVITY	3.00E-04	1.94E-01
KEGG	KEGG_LINOLEIC_ACID_METABOLISM	4.00E-04	1.56E-02
REACTOME	REACTOME_AMINE_COMPOUND_SLC_TRANSPORTERS	6.00E-04	9.72E-02
GO	TRANSFORMING_GROWTH_FACTOR_BETA_RECEPTOR_SIGNALING_PATHWAY	8.00E-04	2.89E-01
KEGG	KEGG_B_CELL_RECEPTOR_SIGNALING_PATHWAY	1.00E-03	2.86E-02
REACTOME	REACTOME_TRANSMISSION_ACROSS_CHEMICAL_SYNAPSES	1.50E-03	1.26E-01
KEGG	KEGG_ALDOSTERONE_REGULATED_SODIUM_REABSORPTION	1.90E-03	2.64E-02
GO	ATPASE_ACTIVITY_COUPLED_TO_MOVEMENT_OF_SUBSTANCES	1.90E-03	2.73E-01
KEGG	KEGG_WNT_SIGNALING_PATHWAY	2.10E-03	4.85E-02
REACTOME	REACTOME_GLYCOSAMINOGLYCAN_METABOLISM	2.10E-03	1.38E-01
REACTOME	REACTOME_NUCLEOTIDE_BINDING_DOMAIN_LEUCINE_RICH_REPEAT_CONTAINING_RECEPTOR_	2.40E-03	1.86E-01
BIOCARTA	BIOCARTA_FCER1_PATHWAY	2.50E-03	6.95E-02
REACTOME	REACTOME_HEPARAN_SULFATE_HEPARIN_HS_GAG_METABOLISM	2.70E-03	1.72E-01
GO	AMINE_TRANSMEMBRANE_TRANSPORTER_ACTIVITY	2.80E-03	3.33E-01
GO	PROTEIN_IMPORT	3.10E-03	3.02E-01
BIOCARTA	BIOCARTA_VIP_PATHWAY	3.30E-03	5.36E-02
KEGG	KEGG_THYROID_CANCER	3.70E-03	4.58E-02
KEGG	KEGG_LONG_TERM_DEPRESSION	4.10E-03	6.36E-02
GO	HYDROLASE_ACTIVITY_ACTING_ON_ACID_ANHYDRIDESCATALYZING_TRANSMEMBRANE_MOVEM	4.10E-03	2.81E-01
REACTOME	REACTOME_GABA_RECEPTOR_ACTIVATION	4.20E-03	1.33E-01
REACTOME	REACTOME_CHONDROITIN_SULFATE_DERMATAN_SULFATE_METABOLISM	4.30E-03	1.41E-01
GO	HUMORAL_IMMUNE_RESPONSE	4.50E-03	2.84E-01
REACTOME	REACTOME_ION_CHANNEL_TRANSPORT	4.80E-03	1.36E-01
REACTOME	REACTOME_NEUROTRANSMITTER_RECEPTOR_BINDING_AND_DOWNSTREAM_TRANSMISSION	4.80E-03	1.62E-01
BIOCARTA	BIOCARTA_NDKDYNAMIN_PATHWAY	5.40E-03	5.32E-02
KEGG	KEGG_T_CELL_RECEPTOR_SIGNALING_PATHWAY	5.50E-03	7.66E-02
GO	PRIMARY_ACTIVE_TRANSMEMBRANE_TRANSPORTER_ACTIVITY	5.50E-03	3.24E-01
KEGG	KEGG_HYPERTROPHIC_CARDIOMYOPATHY_HCM	5.70E-03	6.46E-02
GO	REGULATION_OF_ANGIOGENESIS	7.20E-03	3.32E-01
REACTOME	REACTOME_GABA_B_RECEPTOR_ACTIVATION	7.90E-03	1.87E-01
GO	METAL_ION_TRANSMEMBRANE_TRANSPORTER_ACTIVITY	7.90E-03	4.70E-01
KEGG	KEGG_LONG_TERM_POTENTIATION	8.10E-03	8.16E-02
GO	PROTEOGLYCAN_METABOLIC_PROCESS	8.40E-03	3.31E-01
KEGG	KEGG_MELANOGENESIS	8.50E-03	8.15E-02
REACTOME	REACTOME_CLASS_B_2_SECRETIN_FAMILY_RECEPTORS	9.00E-03	2.23E-01
GO	POSITIVE_REGULATION_OF_HYDROLASE_ACTIVITY	9.20E-03	4.24E-01
GO	ION_CHANNEL_ACTIVITY	9.30E-03	4.36E-01
GO	SUBSTRATE_SPECIFIC_CHANNEL_ACTIVITY	9.40E-03	4.87E-01
KEGG	KEGG_ECM_RECEPTOR_INTERACTION	1.00E-02	8.26E-02
BIOCARTA	BIOCARTA_GPCR_PATHWAY	1.12E-02	1.08E-01
GO	CATION_CHANNEL_ACTIVITY	1.13E-02	4.58E-01
BIOCARTA	BIOCARTA_GCR_PATHWAY	1.14E-02	1.12E-01
REACTOME	REACTOME_OPIOID_SIGNALLING	1.24E-02	2.69E-01
GO	CARBOXYLIC_ACID_METABOLIC_PROCESS	1.24E-02	4.58E-01
REACTOME	REACTOME_RESPONSE_TO_ELEVATED_PLATELET_CYTOSOLIC_CA2_	1.25E-02	2.54E-01
GO	PROTEIN_IMPORT_INTO_NUCLEUS	1.27E-02	4.33E-01
GO	ACTIN_CYTOSKELETON	1.39E-02	4.38E-01
GO	PROTEIN_SECRETION	1.41E-02	4.71E-01
GO	TRANSMEMBRANE_RECEPTOR_PROTEIN_SERINE_THREONINE_KINASE_SIGNALING_PATHWAY	1.47E-02	4.25E-01
KEGG	KEGG_CARDIAC_MUSCLE_CONTRACTION	1.54E-02	1.19E-01
BIOCARTA	BIOCARTA_BCR_PATHWAY	1.55E-02	1.24E-01
REACTOME	REACTOME_NOD1_2_SIGNALING_PATHWAY	1.59E-02	2.61E-01
GO	ORGANIC_ACID_METABOLIC_PROCESS	1.63E-02	4.45E-01
REACTOME	REACTOME_IL1_SIGNALING	1.69E-02	2.53E-01
GO	GATED_CHANNEL_ACTIVITY	1.74E-02	4.37E-01

GO	REGULATION_OF_HYDROLASE_ACTIVITY	1.79E-02	4.46E-01
KEGG	KEGG_NATURAL_KILLER_CELL_MEDIATED_CYTOTOXICITY	1.85E-02	1.60E-01
BIOCARTA	BIOCARTA_CALCINEURIN_PATHWAY	1.86E-02	1.21E-01
GO	WOUND_HEALING	1.93E-02	4.54E-01
GO	CYSTEINE_TYPE_PEPTIDASE_ACTIVITY	1.95E-02	4.70E-01
GO	NEGATIVE_REGULATION_OF_CELL_PROLIFERATION	1.98E-02	4.24E-01
REACTOME	REACTOME_TRANS_GOLGI_NETWORK_VESICLE_BUDDING	2.01E-02	2.58E-01
GO	NUCLEAR_IMPORT	2.03E-02	4.49E-01
GO	REGULATION_OF_SECRETION	2.09E-02	4.54E-01
KEGG	KEGG_AXON_GUIDANCE	2.10E-02	1.71E-01
REACTOME	REACTOME_A_TETRASACCHARIDE_LINKER_SEQUENCE_IS_REQUIRED_FOR_GAG_SYNTHESIS	2.12E-02	2.40E-01
REACTOME	REACTOME_ACTIVATION_OF_KAINATE_RECEPTORS_UPON_GLUTAMATE_BINDING	2.19E-02	2.70E-01
REACTOME	REACTOME_INHIBITION_OF_VOLTAGE_GATED_CA2_CHANNELS_VIA_GBETA_GAMMA_SUBUNITS	2.20E-02	2.47E-01
BIOCARTA	BIOCARTA_TCR_PATHWAY	2.24E-02	1.82E-01
REACTOME	REACTOME_L1CAM_INTERACTIONS	2.24E-02	3.16E-01
GO	VOLTAGE_GATED_POTASSIUM_CHANNEL_COMPLEX	2.43E-02	4.34E-01
KEGG	KEGG_APOPTOSIS	2.45E-02	1.67E-01
KEGG	KEGG_HEDGEHOG_SIGNALING_PATHWAY	2.47E-02	1.80E-01
GO	POTASSIUM_ION_TRANSPORT	2.51E-02	4.23E-01
KEGG	KEGG_VASCULAR_SMOOTH_MUSCLE_CONTRACTION	2.55E-02	1.77E-01
REACTOME	REACTOME_GOLGI_ASSOCIATED_VESICLE_BIOGENESIS	2.75E-02	3.14E-01
GO	NITROGEN_COMPOUND_BIOSYNTHETIC_PROCESS	2.76E-02	4.39E-01
GO	PROTEIN_DOMAIN_SPECIFIC_BINDING	2.78E-02	4.50E-01
GO	ION_TRANSPORT	2.79E-02	4.68E-01
KEGG	KEGG_CALCIUM_SIGNALING_PATHWAY	2.82E-02	1.90E-01
BIOCARTA	BIOCARTA_IL1R_PATHWAY	2.86E-02	1.70E-01
GO	LIPID_TRANSPORT	2.87E-02	4.31E-01
GO	CARBOHYDRATE_BIOSYNTHETIC_PROCESS	2.97E-02	4.39E-01
REACTOME	REACTOME_ION_TRANSPORT_BY_P_TYPE_ATPASES	3.00E-02	3.21E-01
GO	POTASSIUM_CHANNEL_ACTIVITY	3.09E-02	4.60E-01
GO	POSITIVE_REGULATION_OF_CASPASE_ACTIVITY	3.10E-02	4.26E-01
GO	LIPASE_ACTIVITY	3.12E-02	4.47E-01
REACTOME	REACTOME_PLC_BETA_MEDIATED_EVENTS	3.17E-02	3.77E-01
REACTOME	**REACTOME_NCAM1_INTERACTIONS**	**3.33E-02**	**3.87E-01**
REACTOME	REACTOME_SIGNALING_BY_ILS	3.73E-02	4.46E-01
GO	KINASE_INHIBITOR_ACTIVITY	3.74E-02	4.32E-01
GO	AMINE_METABOLIC_PROCESS	3.74E-02	5.07E-01
GO	NITROGEN_COMPOUND_METABOLIC_PROCESS	3.76E-02	5.05E-01
BIOCARTA	BIOCARTA_NOS1_PATHWAY	3.90E-02	1.94E-01
KEGG	KEGG_O_GLYCAN_BIOSYNTHESIS	3.92E-02	1.90E-01
GO	SULFUR_METABOLIC_PROCESS	3.97E-02	4.97E-01
BIOCARTA	BIOCARTA_FMLP_PATHWAY	4.02E-02	1.95E-01
GO	RECEPTOR_COMPLEX	4.07E-02	4.84E-01
REACTOME	REACTOME_HS_GAG_BIOSYNTHESIS	4.11E-02	3.92E-01
KEGG	KEGG_GNRH_SIGNALING_PATHWAY	4.13E-02	2.32E-01
GO	DAMAGED_DNA_BINDING	4.14E-02	4.54E-01
GO	METAL_ION_TRANSPORT	4.23E-02	5.33E-01
BIOCARTA	BIOCARTA_PGC1A_PATHWAY	4.25E-02	2.01E-01
GO	BLOOD_COAGULATION	4.83E-02	5.10E-01
KEGG	KEGG_ALZHEIMERS_DISEASE	4.97E-02	2.78E-01
GO	RESPONSE_TO_WOUNDING	4.97E-02	5.74E-01

Supplementary Table 7 Gene set associations with the mean FA value of the depression-associated voxels within the left temporal Superior Longitudinal Fasciculus (tSLF) (only gene sets with $p < 0.05$ are listed)

Data base	Gene set	p	$q_{75\%)}$
KEGG	KEGG_DILATED_CARDIOMYOPATHY	9.90E-05	2.50E-03
REACTOME	REACTOME_CHONDROITIN_SULFATE_BIOSYNTHESIS	9.90E-05	3.80E-03
KEGG	KEGG_ARRHYTHMOGENIC_RIGHT_VENTRICULAR_CARDIOMYOPATHY_ARVC	9.90E-05	4.00E-03
GO	VOLTAGE_GATED_CATION_CHANNEL_ACTIVITY	5.00E-04	2.20E-01
GO	METAL_ION_TRANSMEMBRANE_TRANSPORTER_ACTIVITY	6.00E-04	1.20E-01
GO	GATED_CHANNEL_ACTIVITY	7.00E-04	1.12E-01
GO	HUMORAL_IMMUNE_RESPONSE	7.00E-04	1.59E-01
KEGG	KEGG_ECM_RECEPTOR_INTERACTION	8.00E-04	5.68E-02
GO	POTASSIUM_ION_TRANSPORT	8.00E-04	3.83E-01
KEGG	KEGG_HYPERTROPHIC_CARDIOMYOPATHY_HCM	1.10E-03	1.98E-02
GO	CATION_CHANNEL_ACTIVITY	1.20E-03	1.05E-01
REACTOME	REACTOME_TRANS_GOLGI_NETWORK_VESICLE_BUDDING	1.20E-03	1.70E-01
REACTOME	REACTOME_GOLGI_ASSOCIATED_VESICLE_BIOGENESIS	1.40E-03	1.09E-01
REACTOME	REACTOME_CHONDROITIN_SULFATE_DERMATAN_SULFATE_METABOLISM	1.40E-03	1.16E-01
GO	SUBSTRATE_SPECIFIC_CHANNEL_ACTIVITY	2.00E-03	1.49E-01
GO	POTASSIUM_CHANNEL_ACTIVITY	2.10E-03	1.51E-01
GO	VOLTAGE_GATED_CHANNEL_ACTIVITY	2.50E-03	1.60E-01
KEGG	KEGG_LINOLEIC_ACID_METABOLISM	3.10E-03	4.71E-02
GO	VOLTAGE_GATED_POTASSIUM_CHANNEL_ACTIVITY	3.30E-03	1.63E-01
GO	NEGATIVE_REGULATION_OF_CELL_PROLIFERATION	3.60E-03	1.66E-01
GO	CYSTEINE_TYPE_PEPTIDASE_ACTIVITY	3.70E-03	1.49E-01
GO	ION_CHANNEL_ACTIVITY	3.80E-03	1.46E-01
REACTOME	REACTOME_GLYCOSAMINOGLYCAN_METABOLISM	3.90E-03	2.38E-01
GO	TRANSFORMING_GROWTH_FACTOR_BETA_RECEPTOR_SIGNALING_PATHWAY	4.10E-03	1.48E-01
GO	VOLTAGE_GATED_POTASSIUM_CHANNEL_COMPLEX	4.20E-03	1.47E-01
REACTOME	REACTOME_L1CAM_INTERACTIONS	4.20E-03	2.07E-01
GO	NUCLEOTIDE_EXCISION_REPAIR	5.30E-03	1.53E-01
REACTOME	REACTOME_RESPONSE_TO_ELEVATED_PLATELET_CYTOSOLIC_CA2_	5.80E-03	2.28E-01
REACTOME	REACTOME_POTASSIUM_CHANNELS	6.10E-03	2.07E-01
GO	ATPASE_ACTIVITY_COUPLED_TO_MOVEMENT_OF_SUBSTANCES	6.30E-03	1.64E-01
REACTOME	**REACTOME_NCAM1_INTERACTIONS**	**6.70E-03**	**2.59E-01**
GO	APOPTOTIC_PROGRAM	6.80E-03	1.91E-01
GO	MONOVALENT_INORGANIC_CATION_TRANSPORT	6.90E-03	1.81E-01
KEGG	KEGG_GLYCOSAMINOGLYCAN_BIOSYNTHESIS_CHONDROITIN_SULFATE	7.40E-03	8.94E-02
KEGG	KEGG_CARDIAC_MUSCLE_CONTRACTION	7.50E-03	1.01E-01
KEGG	KEGG_CALCIUM_SIGNALING_PATHWAY	7.60E-03	1.18E-01
REACTOME	REACTOME_TRANSMISSION_ACROSS_CHEMICAL_SYNAPSES	8.20E-03	2.46E-01
REACTOME	REACTOME_GABA_B_RECEPTOR_ACTIVATION	8.40E-03	2.00E-01
GO	HYDROLASE_ACTIVITY_ACTING_ON_ACID_ANHYDRIDESCATALYZING_TRANSMEMBRANE_MOVEME	8.50E-03	2.10E-01
REACTOME	REACTOME_GABA_RECEPTOR_ACTIVATION	8.60E-03	2.32E-01
GO	POSITIVE_REGULATION_OF_HYDROLASE_ACTIVITY	8.80E-03	2.05E-01
GO	LIPID_TRANSPORT	9.00E-03	1.86E-01
BIOCARTA	BIOCARTA_HDAC_PATHWAY	9.40E-03	5.80E-01
GO	ACTIN_CYTOSKELETON	9.50E-03	2.43E-01
GO	REGULATION_OF_MAPKKK_CASCADE	1.06E-02	1.90E-01
KEGG	KEGG_ALDOSTERONE_REGULATED_SODIUM_REABSORPTION	1.15E-02	1.34E-01
REACTOME	REACTOME_NEUROTRANSMITTER_RECEPTOR_BINDING_AND_DOWNSTREAM_TRANSMISSION_IN_	1.18E-02	2.90E-01
GO	ACTIVE_TRANSMEMBRANE_TRANSPORTER_ACTIVITY	1.18E-02	2.99E-01
REACTOME	REACTOME_HEPARAN_SULFATE_HEPARIN_HS_GAG_METABOLISM	1.43E-02	3.00E-01
GO	PRIMARY_ACTIVE_TRANSMEMBRANE_TRANSPORTER_ACTIVITY	1.59E-02	2.83E-01
GO	LIPASE_ACTIVITY	1.62E-02	2.89E-01
GO	PROTEIN_KINASE_BINDING	1.75E-02	3.32E-01
GO	REGULATION_OF_HYDROLASE_ACTIVITY	1.77E-02	3.69E-01
REACTOME	REACTOME_INHIBITION_OF_VOLTAGE_GATED_CA2_CHANNELS_VIA_GBETA_GAMMA_SUBUNITS	1.86E-02	3.08E-01
REACTOME	REACTOME_SMOOTH_MUSCLE_CONTRACTION	1.94E-02	2.85E-01
REACTOME	REACTOME_APOPTOTIC_CLEAVAGE_OF_CELLULAR_PROTEINS	2.11E-02	3.35E-01
GO	POSITIVE_REGULATION_OF_CATALYTIC_ACTIVITY	2.12E-02	4.44E-01
BIOCARTA	BIOCARTA_P38MAPK_PATHWAY	2.15E-02	7.84E-01
GO	METAL_ION_TRANSPORT	2.25E-02	4.57E-01
GO	REGULATION_OF_ANGIOGENESIS	2.37E-02	3.75E-01

REACTOME	REACTOME_INTEGRIN_CELL_SURFACE_INTERACTIONS	2.60E-02	4.33E-01
GO	SYNAPTIC_TRANSMISSION	2.64E-02	4.74E-01
GO	CARBOXYLIC_ACID_METABOLIC_PROCESS	2.75E-02	4.93E-01
GO	NITROGEN_COMPOUND_BIOSYNTHETIC_PROCESS	2.82E-02	3.67E-01
KEGG	KEGG_MELANOGENESIS	2.85E-02	3.03E-01
GO	PROTEOGLYCAN_METABOLIC_PROCESS	2.85E-02	3.84E-01
KEGG	KEGG_ALANINE_ASPARTATE_AND_GLUTAMATE_METABOLISM	2.89E-02	2.67E-01
KEGG	KEGG_HEMATOPOIETIC_CELL_LINEAGE	2.99E-02	2.92E-01
GO	NITROGEN_COMPOUND_METABOLIC_PROCESS	3.04E-02	4.98E-01
REACTOME	REACTOME_APOPTOTIC_EXECUTION_PHASE	3.06E-02	4.18E-01
BIOCARTA	BIOCARTA_IL1R_PATHWAY	3.06E-02	6.98E-01
REACTOME	REACTOME_AMINE_COMPOUND_SLC_TRANSPORTERS	3.08E-02	4.11E-01
KEGG	KEGG_THYROID_CANCER	3.10E-02	2.91E-01
REACTOME	REACTOME_SIGNALING_BY_RHO_GTPASES	3.11E-02	4.58E-01
GO	KINASE_BINDING	3.20E-02	4.87E-01
KEGG	KEGG_ALZHEIMERS_DISEASE	3.21E-02	2.79E-01
REACTOME	REACTOME_NUCLEOTIDE_BINDING_DOMAIN_LEUCINE_RICH_REPEAT_CONTAINING_RECEPTOR_NL	3.39E-02	4.54E-01
REACTOME	REACTOME_MUSCLE_CONTRACTION	3.41E-02	4.37E-01
GO	AMINE_METABOLIC_PROCESS	3.48E-02	4.99E-01
GO	PHOSPHOLIPASE_ACTIVITY	3.50E-02	4.76E-01
GO	ATPASE_ACTIVITY	3.50E-02	4.87E-01
GO	CELL_JUNCTION	3.55E-02	4.84E-01
KEGG	KEGG_WNT_SIGNALING_PATHWAY	3.63E-02	3.01E-01
GO	ORGANIC_ACID_METABOLIC_PROCESS	3.84E-02	5.22E-01
GO	CARBOXYLESTERASE_ACTIVITY	3.88E-02	4.95E-01
GO	KINASE_INHIBITOR_ACTIVITY	3.92E-02	4.47E-01
BIOCARTA	BIOCARTA_PGC1A_PATHWAY	3.97E-02	5.07E-01
GO	TRANSMEMBRANE_RECEPTOR_PROTEIN_SERINE_THREONINE_KINASE_SIGNALING_PATHWAY	4.01E-02	4.82E-01
BIOCARTA	BIOCARTA_GCR_PATHWAY	4.03E-02	5.86E-01
REACTOME	REACTOME_INWARDLY_RECTIFYING_K_CHANNELS	4.18E-02	4.38E-01
GO	CONTRACTILE_FIBER_PART	4.19E-02	4.68E-01
BIOCARTA	BIOCARTA_VIP_PATHWAY	4.24E-02	4.27E-01
KEGG	KEGG_O_GLYCAN_BIOSYNTHESIS	4.43E-02	2.96E-01
GO	POSITIVE_REGULATION_OF_TRANSCRIPTION_FROM_RNA_POLYMERASE_II_PROMOTER	4.61E-02	4.95E-01
GO	AMINE_TRANSMEMBRANE_TRANSPORTER_ACTIVITY	4.63E-02	5.05E-01
GO	PEPTIDASE_ACTIVITY	4.72E-02	5.36E-01

Supplementary references

Baron, R.M., Kenny, D.A., 1986. The moderator-mediator variable distinction in social psychological research: conceptual, strategic, and statistical considerations. J. Pers. Soc. Psychol. **51**(6), 1173-1182.
Shrout, P.E., Bolger, N., 2002. Mediation in experimental and nonexperimental studies: new procedures and recommendations. Psychological Methods **7**(4), 422-445.
Spielberg, C., Gorsuch, R., Lushene, R., 1970. Manual for the state-trait anxiety inventory (self-evaluation questionnaire).

5.2 Recognition memory performance can be estimated based on few specific brain networks

Recognition memory performance can be estimated based on few specific brain networks

Authors:

Jana Petrovska[1,3,*], Eva Loos[2,3] , David Coynel[2,3], Tobias Egli[1,3], Andreas Papassotiropoulos[1,3,4,5], Dominique J.-F. de Quervain[2,3,4], Annette Milnik[1,3,4,*]

Affiliations:

1 Division of Molecular Neuroscience, Department of Psychology, University of Basel, CH-4055 Basel, Switzerland
2 Division of Cognitive Neuroscience, Department of Psychology, University of Basel, CH-4055 Basel, Switzerland
3 Transfaculty Research Platform Molecular and Cognitive Neurosciences, University of Basel, CH-4055 Basel, Switzerland
4 Psychiatric University Clinics, University of Basel, CH-4055 Basel, Switzerland
5 Department Biozentrum, Life Sciences Training Facility, University of Basel, CH-4056 Basel, Switzerland

***Corresponding authors**

Jana Petrovska and Annette Milnik

University of Basel, Divisions of Molecular Neuroscience

Birmannsgasse 8, CH-4009 Basel

Phone: + 41 61 267 0226

jana.petrovska@unibas.ch; annette.milnik@unibas.ch

Abstract

Background

Recognition memory is an essential ability for functioning in everyday life. Establishing robust brain networks linked to recognition memory performance can help in understanding the neural basis of recognition memory and thus contribute to the research on this key, basic ability.

Methods

We analysed behavioural and whole-brain fMRI data from 1'410 healthy young adults during a picture-recognition task. Using independent component analysis (ICA), we decomposed the fMRI contrast for previously seen vs. new (old-new) pictures into few networks of brain activity in two independent samples (training sample: *N* = 645, replication sample: *N* = 665). Next, we investigated the relationship between the identified brain networks and interindividual differences in recognition memory performance by conducting prediction analysis. We estimated predication accuracy in a third independent sample (test sample: *N* = 100).

Results

We identified 12 robust and replicable brain networks by applying ICA to the old-new fMRI contrast. Based on these networks we estimated recognition memory performance with high accuracy (*r* = 0.5).

Conclusion

Given the high prediction accuracy, the identified brain networks may be considered as potential biomarkers of recognition memory performance in healthy young adults and can be further investigated in the context of health and disease.

Introduction

Recognition memory describes the ability to judge whether an object or event has been previously encountered [1]. This ability is essential for functioning in everyday life and has an important role in shaping one's future behaviour and decision making [2, 3]. Thus, recognition memory paradigms are widely used in empirical research on human cognition in both health and disease [4-6]. Identifying brain activity related to recognition memory performance would contribute to the research on this key, basic ability.

Based on fMRI studies using task-based contrasts recognition memory has been linked to activation in multiple brain regions, such as the (para)hippocampus and perirhinal cortex in the medial temporal lobe, parts of the prefrontal cortex (PFC), the thalamus and the parietal cortex [7-15] These contrast-based analyses allow the identification of regions that are in general more (or less) active during a task or in a specific condition, however, they do not enable making inferences about interindividual differences in the behavioural outcome. For recognition memory, it has been additionally shown that brain activation of specific regions of interest (ROIs) within a core recollection network, including the medial PFC and the right hippocampus, is also associated with interindividual differences in task performance [16].

Instead of solely using task-based contrasts and ROIs approaches to investigate the link between brain activation and behaviour, more sophisticated network-level analyses can be used not only to identify large-scale brain networks but also to investigate their impact on individual differences in task performance [17, 18]. These analyses identify brain networks as the joint co-dependent activity of different parts of the brain [17]. It has already been shown that wide-spread functional brain networks are recruited by diverse behavioural tasks, as well as during rest [19-21]. Additionally, recent studies have linked

network-level brain activation to memory-related behavioural outcomes, including working memory performance, emotional memory and recollection speed of a context memory [22-24].

Utilizing a network-level approach instead of standard contrasts or ROI-approaches may therefore lead to a more comprehensive picture of the neural bases of recognition memory and their impact on memory performance differences. Therefore, we applied a whole-brain, data-driven approach to identify recognition memory-related brain networks and investigated their relationship with interindividual differences in recognition memory task performance. We used fMRI data from 1'410 healthy young adults who had performed a picture-recognition task in the scanner. The large number of participants allowed us to identify robust and replicable brain networks. Additionally, it enabled us to perform prediction analysis instead of simple association analysis, which allows higher generalizability of our results [25, 26].

Results

During a picture-recognition task, participants were shown 72 previously seen (old) and 72 new pictures and rated each of them as remembered (recollection), familiar (familiarity), or new (novelty). We analysed participants' brain activity when looking at old in comparison to new pictures (fMRI contrast old-new). For the behavioural data, we also compared the recognition memory performance of old and new pictures, by calculating false-alarm corrected performance scores separately for familiarity (familiarity rating of old – familiarity rating of new pictures) and for recollection (remembering rating of old – remembering rating of new pictures). We then calculated the overall recognition memory

performance as the sum of false-alarm corrected familiarity ratings and false-alarm corrected recollection ratings.

To achieve a robust estimation of networks of brain activation and of model fit when predicting the behavioural outcome, we divided the full sample into three independent samples for the following analyses (training sample: N = 645, replication sample: N = 665 and test sample: N = 100). The training and replication samples were used to determine the optimal number of brain networks that can be robustly identified, whereas the test sample was used to achieve unbiased estimates for the prediction accuracy.

Behavioural results

The mean recognition memory performance of our overall sample was 61.36 (SD = 7.70). Descriptive statistics for recognition memory performance scores in the training, replication and test sample separately are reported in Table 1. Recognition memory performance was significantly associated with participants' sex and age (t_{sex} = 2.48, p_{sex} = 0.013; t_{age} = -2.55, p_{age} = 0.011). Therefore, all subsequent analyses using behavioural data were corrected for sex and age.

Descriptive statistics for familiarity and recollection scores separately, as well as the separate ratings for old and new pictures, are reported in Suppl. Table 1. Additional information regarding the contribution of old and new picture ratings to the familiarity and recollection scores is provided in the Supplementary Material and Suppl. Figure 1. Of note, familiarity and recollection scores were negatively correlated (r = -0.76, $p < 2.2 \times 10^{-16}$).

Identification of stable and reproducible brain networks by using ICA decomposition

In order to decompose the old-new fMRI contrast estimates into few brain networks we conducted independent component analysis (ICA). ICA is an unbiased, data-driven method which reduces the dimensionality of the data to a lower number of statistically independent components (ICs, also termed brain networks throughout the following text) [27]. We determined the optimal number of ICs using a resampling procedure in the training sample and using independent validation in the replication sample. Specifically, we randomly selected 90% of the participants 100 times from the training sample and repeatedly performed IC decomposition with a varying number of ICs (26 different ICA solutions: ICA_3 … ICA_{32}, see Method section). The stability per number of ICs is depicted in Figure 1A. For each of the 5 most stable solutions (5, 10, 12, 14 and 15 ICs) we then performed IC decomposition in the entire training and the entire replication sample, respectively. The training and replication sample were of similar sample size (training $N = 645$; replication $N = 665$), which ensured comparable power in both samples for the estimation of the ICs. Based on the similarity of the voxel loadings between training and replication sample we determined the number of ICs that could be successfully replicated in an independent sample. We quantified the reproducibility per ICA solution as the average similarity (r^2 between voxel loadings) of matched vs. unmatched ICs between the training and the replication sample (see Method section), resulting in a reproducibility of 0.69, 0.47, 0.70, 0.58 and 0.54, for ICA_5, ICA_{10}, ICA_{12}, ICA_{14} and ICA_{15}, respectively (Suppl. Figure 2 and 3). As the solution comprising 12 ICs was most accurately reproduced in the replication sample (Figure 1B), we used this IC decomposition for the subsequent analyses (also see Figure 2, Suppl. Table 2, Suppl. Figure 4 and Suppl. Figure 5).

Prediction of recognition memory performance based on brain activation

We investigated if we could predict a participant's recognition memory performance based on the brain activation strength in these 12 ICs. Since the ICs represent co-activation networks resulting from the decomposition of the old-new contrast, the participants' brain activation strength per IC shows the contribution of each participant to the group-level network. In the training sample, we built a linear model (LM) including the recognition memory performace scores as outcome variable and the participants' activation of the 12 ICs as predictors. We then applied the beta weights from this model to the brain activation of the 12 ICs in the replication sample. With this procedure, we could successfully predict recognition memory performance with high accuracy ($r = 0.47$, $p < 2.2 \times 10^{-16}$; Figure 3A). Importantly, in this analysis the ICs activation was independently estimated in the two samples.

While having an independent estimation of ICs activation in the replication sample provides a robust estimate of our prediction model, it does not allow for the prediction model to be applied to a single participant. In order to assess if our prediction model can also be applied to single-participant level, we conducted an additional analysis. Namely, we projected the voxel loadings from the ICs derived from the larger training sample (N=645) onto the fMRI data of the smaller test sample (N=100). We then applied the beta weights of the training sample onto these projected ICs to predict the memory performance in the test sample. Again, we were able to predict the memory performance with a high accuracy ($r = 0.50$, $p = 1.29 \times 10^{-07}$; Figure 3B).

Prediction of familiarity and recollection separately based on brain activation

Familiarity-based and recollection-based recognition memory are often considered as separate constructs [1, 4]. Therefore, we repeated the prediction analyses for familiarity-

based and recollection-based recognition memory, separately, using the identical procedure. We were able to predict both familiarity and recollection with high accuracy (replication sample: familiarity: $r = 0.69$, $p < 2.2 \times 10^{-16}$, recollection: $r = 0.50$, $p < 2.2 \times 10^{-16}$; test sample: familiarity: $r = 0.68$, $p = 7.13 \times 10^{-15}$, recollection: $r = 0.45$, $p = 2.07 \times 10^{-06}$, Suppl. Figure 6).

Discussion

The aim of the current study was to estimate the recognition memory performance of healthy young individuals based on their fMRI activation patterns in a few robust brain networks. Therefore, we analysed the fMRI signal of a picture-recognition memory task and deconstructed the task-based contrast "old – new pictures" into 12 brain networks using ICA. Importantly, we confirmed the robustness of this IC estimation by using an independent replication sample. Based on the activation in these 12 brain networks we could predict recognition memory performance with high accuracy in a third independent sample. These results reveal the close relationship between the fMRI activation pattern when processing old compared to new pictures and the corresponding memory-related behavioural outcome.

Focusing on few robust networks and their relation to the behavioral outcome improves data reproducibility and interpretability, which is important especially in the context of basic clinical-related research [28, 29]. Given the stability of the IC estimation confirmed in two independent samples and the high prediction accuracy estimated in a third independent sample, the identified brain networks may be considered as potential imaging biomarkers of recognition memory performance in healthy young adults.

Of note, based on our 12 brain networks we could also estimate with high accuracy recollection-based recognition memory performance and familiarity-based recognition memory performance, when taken as separate constructs. Familiarity is typically defined as having a general sense of knowing an object or event while recollection is defined as remembering specific details associated with the recognised object or event [1, 4]. An alternative view is that familiarity and recollection are not distinct processes but rather describe differences in memory strength [30]. Further investigation of potential differences in network-level brain activation between familiarity-based and recollection-based memory performance is beyond the scope of this paper.

Recognition memory has an important role in our everyday life and aids efficient decision making [3]. Deficits in recognition memory performance have been associated with healthy aging, mild cognitive impairment and Alzheimer's disease, as well as schizophrenia [5, 6, 31]. Thus, the here identified networks have potential relevance in the context of both health and neuropathology.

In conclusion, we identified 12 robust functional brain networks, based on which we successfully predicted recognition memory performance. Given the high prediction accuracy, the identified brain networks may be considered as potential biomarkers of recognition memory performance in healthy young adults and can be further investigated in health and disease.

Materials and Methods

Study design

Healthy young adults took part in a large-scale, single-centre fMRI study in Basel, Switzerland, conducted between 2008 and 2015. The study has been described elsewhere [22, 32, 33]. Participants were free of any medication other than oral contraceptives and of any neurological and psychiatric illness at the time of the study. All participants provided written informed consent prior to study participation. The study protocol was approved by the ethics committee of the Cantons of Basel-Stadt and Basel-Landschaft.

Description of picture encoding and picture recognition task

1'446 participants were shown 72 meaningful pictures of positive, negative and neutral valence (24 per emotional valence category), and 24 scrambled pictures. Two additional neutral pictures were presented at the beginning and two at the end of the picture-encoding task, in order to account for potential primacy and recency effects. Each picture was presented for 2.5 s in a quasi-randomised order (no more than four consecutive pictures per category). A 500 ms fixation-cross appeared before each picture presentation. Each picture was rated on two separate three-point Likert scales, measuring subjective arousal and valence of positive, negative and neutral pictures and form and size of scrambled pictures. Ratings were given via button presses with three fingers of the participant's preferred hand.

The picture recognition task took place approximately 80 minutes after the picture encoding task. Participants were presented with the 72 old pictures shown in the encoding task and a set of new pictures comprising again 72 meaningful pictures with positive,

negative and neutral valence (24 per emotional valence category). Pictures were presented in a quasi-randomised order (no more than 4 consecutive pictures per category). A 500 ms fixation-cross appeared before each picture presentation. Participants rated each picture as remembered, familiar or new on a three-point Likert scale within 3 s after picture presentation via button presses with three fingers of their preferred hand.

For the encoding and the picture recognition task we used pictures from the International Affective Picture System (IAPS) [34]. The neutral pictures were additionally complemented by in-house standardised pictures to equate for visual complexity and content of the stimuli.

Subsampling

In order to obtain independent samples needed for the subsequent analyses (building of independent brain networks and prediction analysis), we divided our full sample of *N* = 1'446 participants with complete behavioural data in three samples. We created two equally sized samples (*N* = 673 participants) and an additional sample of *N* = 100 participants, referred to as training, replication and test sample throughout the paper. The samples were created by chronologically ordering the participants of the overall sample and then performing the sample split.

(f)MRI data acquisition, preprocessing and first-level analysis

Siemens Magnetom Verio 3 T whole-body MR unit equipped with a twelve-channel head coil was used for scanning. (f)MRI data acquisition, preprocessing and the construction of a population-based anatomical probabilistic atlas have been described elsewhere [22] and are also reported in the Supplementary Information. Preprocessing and first-level analysis of the

fMRI data was performed using the software SPM8 (Statistical Parametric Mapping, Wellcome Trust Centre for Neuroimaging; http://www.fil.ion.ucl.ac.uk/spm/) in MATLAB R2012b (MathWorks) using a standard fMRI pipeline.

Brain activation during presentation of old (presented during the encoding task) and new (not previously presented) pictures during the recognition task was separately estimated per participant.

The difference between the old and the new picture parameter estimates was calculated for each participant and voxel (first-level analysis for old-new contrast). Performance measurements were not included in the analysis.

fMRI second-level analysis

All further analyses were conducted with the statistical software R (3.4.2; RRID:SCR_001905). The old-new contrast parameters were included in a second-level group analysis. Only participants with complete fMRI data and behavioral data (training sample: *N* = 648; replication sample: *N* = 665; test sample: *N* = 100) were included. Additionally, we removed participants with missing values for > 10% of voxels (*N* = 3 in the training sample) and voxels with any missing values (*N* = 14'458). The final sample included 1'410 participants (training sample: *N* = 645; replication sample: *N* = 665; test sample: *N* = 100) and 56'764 voxels.

We regressed out the effects of age and sex from the voxel signal separately for the training and the replication sample and used the scaled residuals in all subsequent analyses. Scanner-related confounding variables (gradient coils and software changes) were present in the training sample and were also regressed out. To achieve independence on participant level in the test sample for the prediction analysis, we corrected for sex and age by applying

the sex and age beta values derived from the training sample to the test sample. Scaling was also based on the parameter derived from the training sample.

Identification of independent brain networks using ICA decomposition

We used ICA in order to decompose the whole-brain fMRI signal into a set of voxel-wise independent components. ICA is a dimensionality reduction method used for linear representation of non-Gaussian data by decomposing them into components that are as statistically independent as possible [27]. We applied ICA to a matrix X (old-new contrast parameters), comprising m observations (participants) and n variables (voxels). ICA estimates a matrix of k x n latent sources S that underlie the variables, while holding the source estimates (voxel loadings) as independent from each other as possible. Therefore, by applying ICA decomposition to old-new contrast parameters (a matrix with participants as rows and voxels as columns) our voxel loadings describe statistically independent latent sources that underlie the contrast estimates. Additionally, ICA provides a matrix of m x k mixing coefficients A (participants scores) for each independent component. The mixing coefficients of each component represent the component's activity strength, per participant [35]. Participants with high contrast estimates in voxels that load highly onto a particular component in a positive direction are assigned elevated scores for that component by this method. Therefore, we interpret the participants' scores as a measure of coactivation in the voxels that load onto the component.

Determining the optimal number of components

The number of independent components is a key ICA parameter, and there are several methods for its optimisation, such as estimation of component stability and reproducibility

for ICA solutions with N number of components (ICA_N) [36, 37], described in the following section.

ICA decomposition stability assessment

As a first step for identifying the optimal number of components for decomposition of the old-new fMRI contrast, we investigate the stability of decomposing the voxel signal into *N* = 3:24, 26, 28, 30 and 32 ICs (26 different ICA solutions: ICA_3 … ICA_{32}).

Procedure: 1) We used a resampling method with 100 repetitions and 90% of randomly selected participants from the training sample, producing 100 similar, but non-identical subsamples, in order to prevent overfitting. 2) For each of the 26 ICA solutions: a) We performed ICA on each of the 100 subsamples, using the fastICA algorithm (R-package "fastICA"; [27]); b) We calculated the stability of each IC by applying Pearson's correlation to its voxel loadings across subsamples. As the direction of IC estimates is arbitrary, we squared the correlation coefficients to adjust for directionality (r^2); c) ICA solution stability was calculated as the mean stability of its ICs.

ICA decomposition reproducibility assessment

As a second step for identifying the optimal number of components, we investigated the reproducibility of the five most stable ICA solutions: ICA_5, ICA_{10}, ICA_{12}, ICA_{14} and ICA_{15} between the training and the replication sample. For each ICA solution, we 1) conducted ICA with the complete training and replication sample, respectively (no subsampling), 2) created a correlation matrix by calculating Pearson's correlations between the voxel loadings per IC across samples. As the direction of IC estimates is arbitrary, we squared the correlation coefficients to adjust for directionality (r^2). Since the order of components derived from ICA

is arbitrary, we reordered the replication sample ICs, so that each IC matches its corresponding training sample IC ($r^2 \geq 0.6$). Furthermore, as the direction of IC estimates is also arbitrary, we recoded IC estimates (voxels loadings and participants scores, respectively), so that estimates have the same direction in the training and replication sample and voxels with the highest absolute loadings have positive loadings.

From the correlation matrix for each ICA solution we estimated the average correlation coefficient on the diagonal, i.e., for matched ICs (X) and off the diagonal, i.e., for unmatched ICs (Y), across samples. We used mean(r^2_X) – mean(r^2_Y) as a reproducibility metric. The most reproducible ICA solution was used for all subsequent analyses.

Recognition memory prediction

We built our prediction model based on the training sample (N = 645). Specifically, we performed multiple linear regression using the participants IC scores from all 12 ICs as predictors and recognition memory performance as the outcome variable.

We first estimated the model fit based on independently estimated ICs in the replication sample (N=665). We applied the regression weights of the predictive model to the participants IC scores from the 12 replication sample ICs.

Next, we estimated the model fit in the test sample (N = 100). Since ICA was not applied to the test sample, we projected the voxel loadings from the 12 ICs in the training sample onto the old-new contrast parameters from the test sample, using the 'ginv' function from the R package "MASS" [38]. Using projected values enabled us to apply our model on the fMRI data from a new sample without subjecting it to ICA. Therefore, the model can also be applied on a single participant.

The model's accuracy for each sample was assessed by comparing the predicted behavioural outcome with the observed behaviour using Pearson's correlation (*r*). Statistical test for significance was done with a *t*-test (*p*-value threshold < .05).

Additionally, the described prediction analyses were conducted two more times, for familiarity-based and recollection-based recognition memory scores as the outcome variable, separately. The procedure for these analyses was identical to the one using the overall recognition memory scores.

Anatomical labelling of functional brain networks

Anatomical labelling of grey matter brain regions was based on a population-averaged probabilistic atlas. The atlas construction is described in the Supplemental Information. The atlas consisted of 87 distinct cortical and subcortical brain regions from both hemispheres. To anatomically describe functional brain networks represented by the 12 ICs we used 5% of voxels, having most extreme voxel loadings on any of the ICs (considering the full ICA solution). For each of these voxels we extracted the probability of belonging to a given brain region according to the population-based atlas. We assigned each voxel to the anatomical brain region with the highest probability, provided the probability was higher than 25%. In case the region with the highest probability was cortical white matter, we report the anatomical region with the 2nd highest probability. Next, for each brain region we summarized the number of voxels and the percentage of voxels for the respective IC, for the left and right hemisphere separately, irrespective of the direction of task activation (task-positive and task-negative). Only brain regions with a coverage of 20% or higher are displayed in the table that describes the ICs (Suppl. Table 2).

References

1. Mandler, G., *Recognizing: The judgment of previous occurrence.* Psychological Review, 1980. **87**(3): p. 252-271.
2. Goldstein, D.G. and G. Gigerenzer, *Models of ecological rationality: The recognition heuristic.* Psychological Review, 2002. **109**(1): p. 75-90.
3. Heck, D.W. and E. Erdfelder, *Linking process and measurement models of recognition-based decisions.* , 2017. **124**(4): p. 442-471.
4. Yonelinas, A.P., *The Nature of Recollection and Familiarity: A Review of 30 Years of Research.* Journal of Memory and Language, 2002. **46**(3): p. 441-517.
5. Koen, J.D. and A.P. Yonelinas, *The Effects of Healthy Aging, Amnestic Mild Cognitive Impairment, and Alzheimer's Disease on Recollection and Familiarity: A Meta-Analytic Review.* Neuropsychology Review, 2014. **24**(3): p. 332-354.
6. Schoemaker, D., S. Gauthier, and J.C. Pruessner, *Recollection and Familiarity in Aging Individuals with Mild Cognitive Impairment and Alzheimer's Disease: A Literature Review.* Neuropsychology Review, 2014. **24**(3): p. 313-331.
7. Scalici, F., C. Caltagirone, and G.A. Carlesimo, *The contribution of different prefrontal cortex regions to recollection and familiarity: a review of fMRI data.* , 2017. **83**: p. 240-251.
8. Carlesimo, G.A., et al., *Recollection and familiarity in the human thalamus.* Neuroscience & Biobehavioral Reviews, 2015. **54**: p. 18-28.
9. Yonelinas, A.P., et al., *Separating the brain regions involved in recollection and familiarity in recognition memory.* J Neurosci, 2005. **25**(11): p. 3002-8.
10. Frithsen, A. and M.B. Miller, *The posterior parietal cortex: Comparing remember/know and source memory tests of recollection and familiarity.* Neuropsychologia, 2014. **61**: p. 31-44.
11. Horn, M., et al., *The multiple neural networks of familiarity: A meta-analysis of functional imaging studies.* Cogn Affect Behav Neurosci, 2016. **16**(1): p. 176-90.
12. Skinner, E.I. and M.A. Fernandes, *Neural correlates of recollection and familiarity: a review of neuroimaging and patient data.* Neuropsychologia, 2007. **45**(10): p. 2163-79.
13. Spaniol, J., et al., *Event-related fMRI studies of episodic encoding and retrieval: Meta-analyses using activation likelihood estimation.* Neuropsychologia, 2009. **47**(8): p. 1765-1779.
14. Vilberg, K.L. and M.D. Rugg, *Memory retrieval and the parietal cortex: a review of evidence from a dual-process perspective.* Neuropsychologia, 2008. **46**(7): p. 1787-99.
15. Kim, H., *Dissociating the roles of the default-mode, dorsal, and ventral networks in episodic memory retrieval.* Neuroimage, 2010. **50**(4): p. 1648-57.
16. de Chastelaine, M., et al., *The neural correlates of recollection and retrieval monitoring: Relationships with age and recollection performance.* Neuroimage, 2016. **138**: p. 164-175.
17. Bressler, S.L. and V. Menon, *Large-scale brain networks in cognition: emerging methods and principles.* Trends Cogn Sci, 2010. **14**(6): p. 277-90.
18. Misic, B. and O. Sporns, *From regions to connections and networks: new bridges between brain and behavior.* Curr Opin Neurobiol, 2016. **40**: p. 1-7.

19. Fox, M.D., et al., *The human brain is intrinsically organized into dynamic, anticorrelated functional networks.* Proc Natl Acad Sci U S A, 2005. **102**(27): p. 9673-8.
20. Smith, S.M., et al., *Correspondence of the brain's functional architecture during activation and rest.* Proceedings of the National Academy of Sciences, 2009. **106**(31): p. 13040-13045.
21. Damoiseaux, J.S., et al., *Consistent resting-state networks across healthy subjects.* Proceedings of the National Academy of Sciences of the United States of America, 2006. **103**(37): p. 13848-13853.
22. Egli, T., et al., *Identification of Two Distinct Working Memory-Related Brain Networks in Healthy Young Adults.* eNeuro, 2018. **5**(1).
23. Loos, E., et al., *Predicting emotional arousal and emotional memory performance from an identical brain network.* Neuroimage, 2019. **189**: p. 459-467.
24. Fornito, A., et al., *Competitive and cooperative dynamics of large-scale brain functional networks supporting recollection.* Proc Natl Acad Sci U S A, 2012. **109**(31): p. 12788-93.
25. Yarkoni, T. and J. Westfall, *Choosing Prediction Over Explanation in Psychology: Lessons From Machine Learning.* Perspect Psychol Sci, 2017. **12**(6): p. 1100-1122.
26. Gabrieli, J.D.E., S.S. Ghosh, and S. Whitfield-Gabrieli, *Prediction as a humanitarian and pragmatic contribution from human cognitive neuroscience.* Neuron, 2015. **85**(1): p. 11-26.
27. Hyvärinen, A. and E. Oja, *Independent component analysis: algorithms and applications.* Neural Networks, 2000. **13**(4): p. 411-430.
28. Poldrack, R.A. and M.J. Farah, *Progress and challenges in probing the human brain.* Nature, 2015. **526**: p. 371.
29. Darby, R.R., J. Joutsa, and M.D. Fox, *Network localization of heterogeneous neuroimaging findings.* Brain, 2018.
30. Squire, L.R., J.T. Wixted, and R.E. Clark, *Recognition memory and the medial temporal lobe: a new perspective.* Nature reviews. Neuroscience, 2007. **8**(11): p. 872-883.
31. Libby, L.A., et al., *Recollection and familiarity in schizophrenia: a quantitative review.* Biol Psychiatry, 2013. **73**(10): p. 944-50.
32. Spalek, K., et al., *Sex-dependent dissociation between emotional appraisal and memory: a large-scale behavioral and fMRI study.* J Neurosci, 2015. **35**(3): p. 920-35.
33. Heck, A., et al., *Exome sequencing of healthy phenotypic extremes links TROVE2 to emotional memory and PTSD.* Nature Human Behaviour, 2017. **1**: p. 0081.
34. J Lang, P., M. M Bradley, and B. Cuthbert, *International Affective Picture System (IAPS): Affective Ratings of Pictures and Instruction Manual (Rep. No. A-8)*. 2008.
35. Chiappetta, P., M.C. Roubaud, and B. Torresani, *Blind source separation and the analysis of microarray data.* J Comput Biol, 2004. **11**(6): p. 1090-109.
36. Kairov, U., et al., *Determining the optimal number of independent components for reproducible transcriptomic data analysis.* BMC Genomics, 2017. **18**(1): p. 712.
37. Franco, A.R., et al., *Impact of analysis methods on the reproducibility and reliability of resting-state networks.* Brain Connect, 2013. **3**(4): p. 363-74.
38. Venables, W.N., B.D. Ripley, and W.N. Venables, *Modern applied statistics with S*. 4th ed. Statistics and computing. 2002, New York: Springer. xi, 495 p.

Recognition memory performance can be estimated based on few specific brain networks

Tables and figures

Authors:

Jana Petrovska[1,3,*], Eva Loos[2,3], David Coynel[2,3], Tobias Egli[1,3], Andreas Papassotiropoulos[1,3,4,5], Dominique J.-F. de Quervain[2,3,4], Annette Milnik[1,3,4,*]

Affiliations:

1 Division of Molecular Neuroscience, Department of Psychology, University of Basel, CH-4055 Basel, Switzerland
2 Division of Cognitive Neuroscience, Department of Psychology, University of Basel, CH-4055 Basel, Switzerland
3 Transfaculty Research Platform Molecular and Cognitive Neurosciences, University of Basel, CH-4055 Basel, Switzerland
4 Psychiatric University Clinics, University of Basel, CH-4055 Basel, Switzerland
5 Department Biozentrum, Life Sciences Training Facility, University of Basel, CH-4056 Basel, Switzerland

***Corresponding authors**

Jana Petrovska and Annette Milnik

University of Basel, Divisions of Molecular Neuroscience

Birmannsgasse 8, CH-4009 Basel

Phone: + 41 61 267 0226

jana.petrovska@unibas.ch; annette.milnik@unibas.ch

Table 1: Descriptive statistics (mean and standard deviation) of recognition memory performance scores, shown separately for the training, replication and test sample.

	Training sample	Replication sample	Test sample
Recognition memory	61.59 (7.12)	61.01 (8.35)	62.20 (6.65)

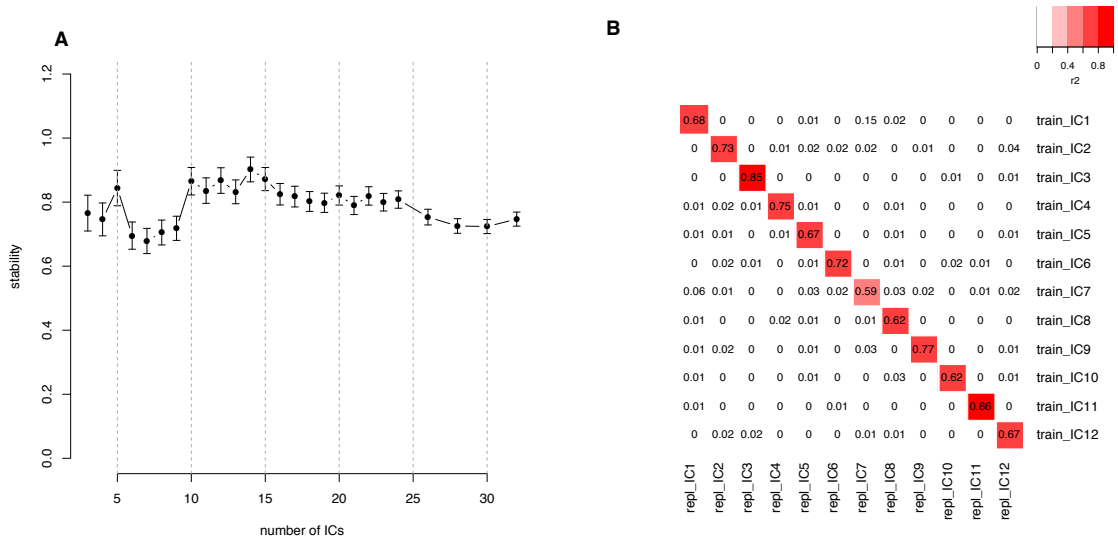

Figure 1: ICA stability and reproducibility A) Stability (y-axis) calculated as the mean correlation (r^2) of voxel loadings across 100 runs from the resampling procedure, averaged across ICs. This was done separately for different number of ICs (x-axis). The error bars represent 90% confidence intervals; B) Reproducibility, i.e., correlation (r^2) between voxel loadings in the training sample and the replication sample, of the IC solution with 12 ICs. Abbreviations: train, training sample; repl, replication sample, IC, independent component

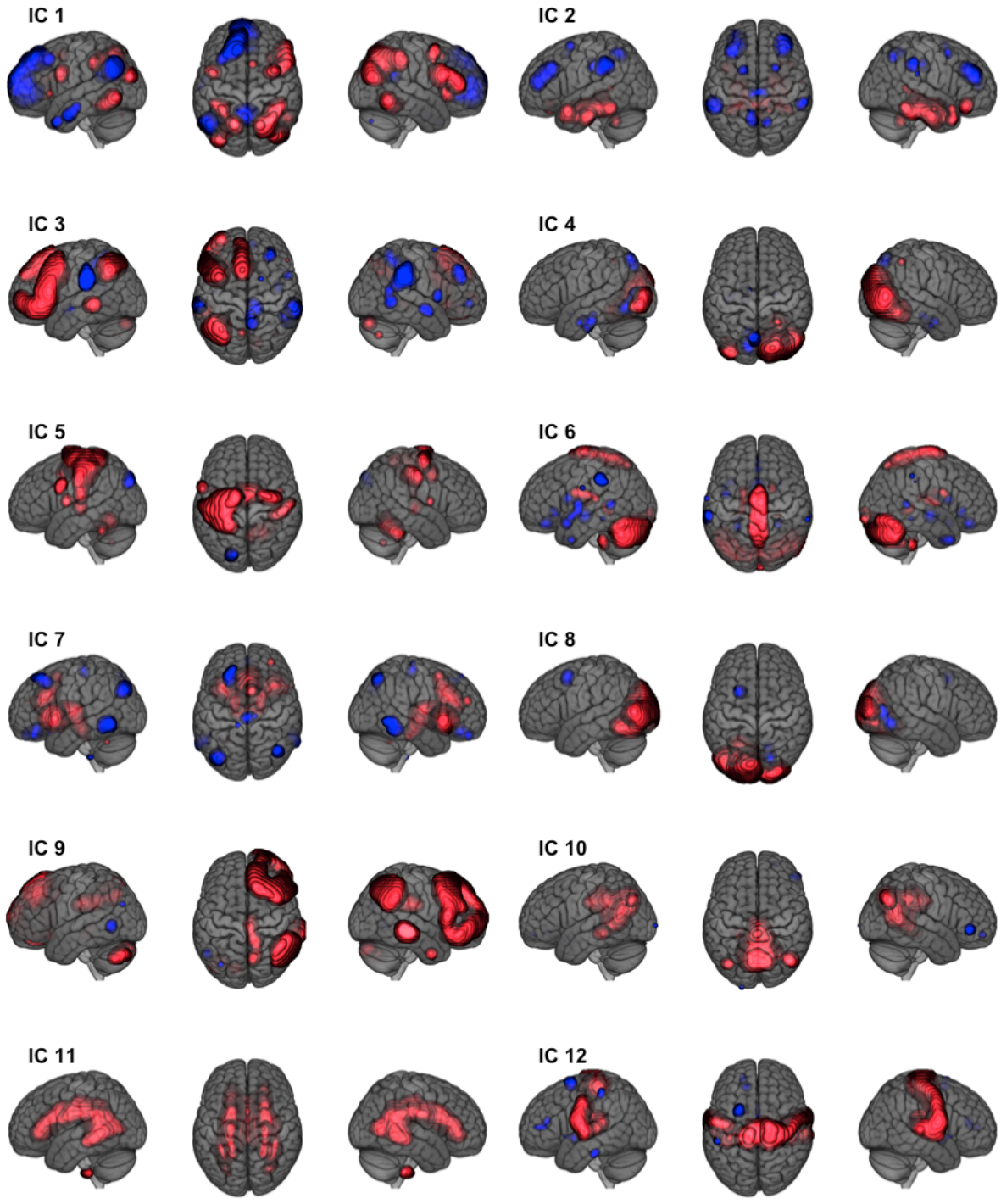

Figure 2: Anatomical localization of the voxel loadings for each of the 12 ICs in the training sample. Only voxels with the strongest loadings (overall top 5%) are depicted. Positive and negative voxels loadings are presented in red and blue, respectively.

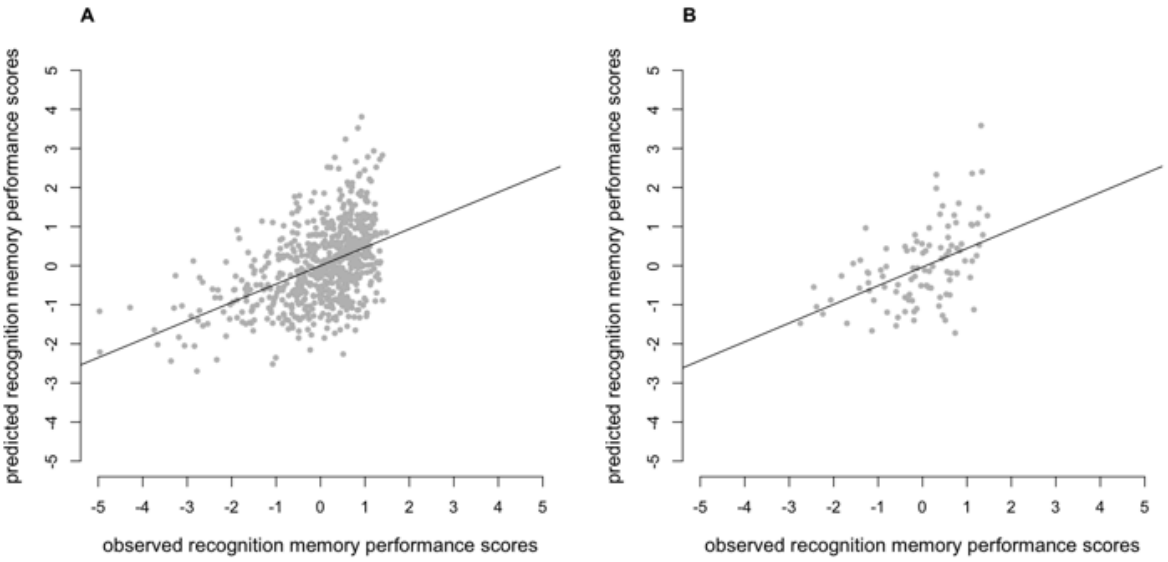

Figure 3: Scatter plot depicting the observed and predicted recognition memory performance scores in A) the replication and B) the test sample. The figure contains scaled behavioural data.

Recognition memory performance can be estimated based on few specific brain networks

Supplementary material

Authors:

Jana Petrovska[1,3,*], Eva Loos[2,3] , David Coynel[2,3], Tobias Egli[1,3], Andreas Papassotiropoulos[1,3,4,5], Dominique J.-F. de Quervain[2,3,4], Annette Milnik[1,3,4,*]

Affiliations:

1 Division of Molecular Neuroscience, Department of Psychology, University of Basel, CH-4055 Basel, Switzerland
2 Division of Cognitive Neuroscience, Department of Psychology, University of Basel, CH-4055 Basel, Switzerland
3 Transfaculty Research Platform Molecular and Cognitive Neurosciences, University of Basel, CH-4055 Basel, Switzerland
4 Psychiatric University Clinics, University of Basel, CH-4055 Basel, Switzerland
5 Department Biozentrum, Life Sciences Training Facility, University of Basel, CH-4056 Basel, Switzerland

***Corresponding authors**

Jana Petrovska and Annette Milnik

University of Basel, Divisions of Molecular Neuroscience

Birmannsgasse 8, CH-4009 Basel

Phone: + 41 61 267 0226

jana.petrovska@unibas.ch; annette.milnik@unibas.ch

Contribution of old and new picture ratings to recognition memory performance

The separate ratings for old and new pictures exhibited ceiling effects and rather narrow distributions especially for the recollection rating of new pictures (see Supplementary Table 1 and Supplementary Figure 1). Therefore, we tested in how far the separate ratings of the old and the new pictures contributed to the false-alarm corrected familiarity and recollection scores. While both performance measures contributed to the familiarity score (old and old-new: $r = 0.83$, $p < 2.2 \times 10^{-16}$; new and old-new: $r = -0.54$, $p < 2.2 \times 10^{-16}$), the recollection score was almost exclusively based on the performance of the old pictures (old and old-new: $r = 0.99$, $p < 2.2 \times 10^{-16}$; new and old-new: $r = -0.01$, $p = 0.57$) (Table 1; Figure 1).

(f)MRI data acquisition

Siemens Magnetom Verio 3 T whole-body MR unit equipped with a twelve-channel head coil was used for scanning. Blood oxygen level-dependent fMRI was acquired using a single-shot echo-planar imaging (EPI) sequence using generalized auto-calibrating partially parallel acquisition (GRAPPA). Acquisition parameters: echo time (TE) = 35 ms; field of view (FOV) = 22 cm; GRAPPA R = 2.0; voxel size = 2.75 x 2.75 x 4 mm^3. An ascending interleaved sequence with repetition time (TR) of 3000 ms ($\alpha = 82°$) was used to measure 32 contiguous axial slices placed along the anterior-posterior commissure plane based on a midsagittal scout image. A three-dimensional, high-resolution T1-weighted image were obtained using magnetization prepared rapid gradient echo (MPRAGE) sequence. Acquisition parameters: TR = 2000 ms; TE = 3.37 ms; inversion time (TI) = 1000 ms; flip angle = 8°; 176 sagittal slices; FOV = 256 mm; voxel size = 1 x 1 x 1 mm^3. Based on visual inspection by 3 raters, 38 participants with corrupted T1-weighted images (movement or anatomical abnormalities) were excluded from all subsequent analyses.

fMRI preprocessing

Preprocessing of the fMRI data was performed using the software SPM8 (Statistical Parametric Mapping, Wellcome Trust Centre for Neuroimaging; http://www.fil.ion.ucl.ac.uk/spm/) in MATLAB R2012b (MathWorks). Functional images were slice-time corrected to the first slice, adjusting for inter-voxel time of measurement variability and realigned using the 'register to mean' option. Individual images were co-registered onto high resolution structural images. The coregistered images from all participants were spatially normalized to a customized template, using the high dimensional DARTEL approach [1], which allows registration to both cortical and subcortical regions and has been shown to perform well in volume-based alignment [2]. Normalization incorporated the following four steps: (1) Structural images of each subject were segmented using the 'New Segment' procedure in SPM8. (2) The resulting gray and white matter images were used to derive a study-specific group template. The template was computed from a subgroup of 1'000 subjects, which were part of the subjects included in the present study. (3) An affine transformation was applied to map the group template to MNI space. (4) Subject-to-template and template-to-MNI transformations were combined to map the functional images to MNI space. The functional images were smoothed with an isotropic 8 mm full-width at half-maximum (FWHM) Gaussian filter.

First-level analysis

Separate regressors modelling the presentation of A) old (presented during the encoding task) and B) new (not previously presented) pictures during the recognition task were convolved with a canonical hemodynamic response function (HRF). Specifically, an

epoch/boxcar function with duration of 1 s was used for modeling. Intrinsic autocorrelations were accounted for by AR (1), and low-frequency drifts were removed via high-pass filter (time constant 128 s). Movement parameters were entered as nuisance covariates. The 4 pictures accounting for potential primacy and recency effects were excluded from the analysis.

The difference between the old and the new picture parameter estimates was calculated for each participant and voxel (first-level old-new contrast). Performance measurements were not included in the analysis.

Construction of a population-average anatomical probabilistic atlas

Automatic segmentation of the subjects' T1-weighted images was used to build a population-average probabilistic anatomical atlas. More precisely, each participant's T1-weighted image was first automatically segmented into cortical and subcortical structures using FreeSurfer(version 4.5, http://surfer.nmr.mgh.harvard.edu/) [3]. Labeling of the cortical gyri was based on the Desikan-Killiany Atlas [4], yielding 35 regions per hemisphere. We also labeled 28 subcortical regions in total (11 subcortical bilateral regions, 6 central regions comprising corpus callosum and brain stem) following Fischl et al. [3]. The segmented T1 image was then normalized to the study-specific anatomical template space using the subject's computed warp field and affine-registered to the MNI space. The normalized segmentations were finally averaged across subjects, in order to create a population-average probabilistic atlas. Each voxel of the template could consequently be assigned a probability of belonging to a given anatomical structure, based on the individual information from 1'000 subjects, which were part of the subjects included in the present study.

Supplementary Table 1: Descriptive statistics (mean and standard deviation) of the behavioural data, shown separately for old and new pictures and for the familiarity and recollection scores.

	Old	New	Old – New
Familiarity	10.64 (9.49)	7.11 (6.32)	3.53 (11.29)
Recollection	58.63 (10.85)	0.80 (1.50)	57.83 (10.77)

Supplementary Table 2: Anatomical annotation of the 12 ICs in the training and replication sample. Only voxels with the strongest loadings (top 5%) and regions with a coverage ≥ 20% in both samples are displayed. The table is sorted by the order of ICs. Abbreviations: IC, independent component; Hem., hemisphere.

IC	Lobe	Region	Hem.	Voxels N	Coverage %	
					Training sample	Replication sample
1	cingulate	Rostral anterior cingulate	left	134	61	33
1	cingulate	Rostral anterior cingulate	right	84	29	23
1	frontal	Pars opercularis	right	228	34	32
1	parietal	Inferior parietal	left	756	22	23
1	parietal	Inferior parietal	right	896	21	29
1	parietal	Superior parietal	right	731	31	42
2	subcortical	Amygdala	left	83	65	96
2	subcortical	Hippocampus	left	203	59	68
2	subcortical	Amygdala	right	87	100	99
2	subcortical	Hippocampus	right	201	64	56
2	subcortical	Ventral Diencephalon	right	219	31	41
2	temporal	Fusiform	left	414	23	32
2	temporal	Parahippocampal	left	118	58	83
2	temporal	Entorhinal	right	87	37	68
2	temporal	Fusiform	right	411	32	25
2	temporal	Parahippocampal	right	112	65	81
3	frontal	Caudal middle frontal	left	367	51	57
3	frontal	Pars opercularis	left	279	62	59
3	frontal	Pars orbitalis	left	121	51	45
3	frontal	Pars triangularis	left	197	77	66
3	frontal	Rostral middle frontal	left	972	21	32
3	frontal	Superior frontal	left	1356	22	24
3	parietal	Supramarginal	right	595	21	28
4	occipital	Pericalcarine	left	57	60	21
4	occipital	Cuneus	right	146	38	38
4	occipital	Lateral occipital	right	558	52	63
4	occipital	Lingual	right	345	58	61
4	occipital	Pericalcarine	right	66	92	94
4	temporal	Fusiform	right	411	36	31
5	frontal	Precentral	left	712	36	31
5	parietal	Postcentral	left	506	53	57
6	cerebellum	Cerebellum cortex	left	1808	45	56
6	cerebellum	Cerebellum cortex	right	1725	48	50
7	cingulate	Caudal anterior cingulate	left	93	76	57
7	cingulate	Caudal anterior cingulate	right	103	86	81
7	frontal	Pars opercularis	right	228	29	33
7	frontal	Pars triangularis	right	236	23	29
7	insula	Insula	left	317	32	25
7	insula	Insula	right	314	31	27
7	subcortical	Pallidum	right	54	57	22
8	occipital	Cuneus	left	121	42	56
8	occipital	Lateral occipital	left	610	62	48
8	occipital	Lingual	left	321	61	50

8	occipital	Pericalcarine	left	57	88	79
8	occipital	Pericalcarine	right	66	20	27
8	temporal	Fusiform	left	414	23	20
9	frontal	Caudal middle frontal	right	329	63	61
9	frontal	Pars orbitalis	right	126	79	78
9	frontal	Rostral middle frontal	right	921	43	37
9	frontal	Superior frontal	right	1304	34	21
9	parietal	Inferior parietal	right	896	47	49
9	temporal	Middle temporal	right	655	25	23
10	cingulate	Isthmus cingulate	left	115	100	94
10	cingulate	Isthmus cingulate	right	117	100	100
10	cingulate	Posterior cingulate	right	176	28	20
10	corpus callosum	Posterior	center	46	52	39
10	occipital	Cuneus	left	121	52	54
10	occipital	Cuneus	right	146	45	51
10	parietal	Precuneus	left	544	62	62
10	parietal	Precuneus	right	547	63	66
11	corpus callosum	Central	center	30	33	33
11	subcortical	Caudate	right	180	23	26
12	frontal	Precentral	right	708	41	31
12	frontoparietal	Paracentral	left	188	45	35
12	frontoparietal	Paracentral	right	222	60	47
12	insula	Insula	right	314	22	28
12	parietal	Postcentral	left	506	27	26
12	parietal	Postcentral	right	466	55	39
12	temporal	Transverse temporal	left	55	82	60
12	temporal	Transverse temporal	right	42	100	100

Supplementary Figure 1: Histograms of the behavioural data, shown for familiarity of old pictures (A), new pictures (B) and familiarity false-alarm corrected scores (C) as well as for recollection of old pictures (D), new pictures (E), and recollection false-alarm corrected scores (F).

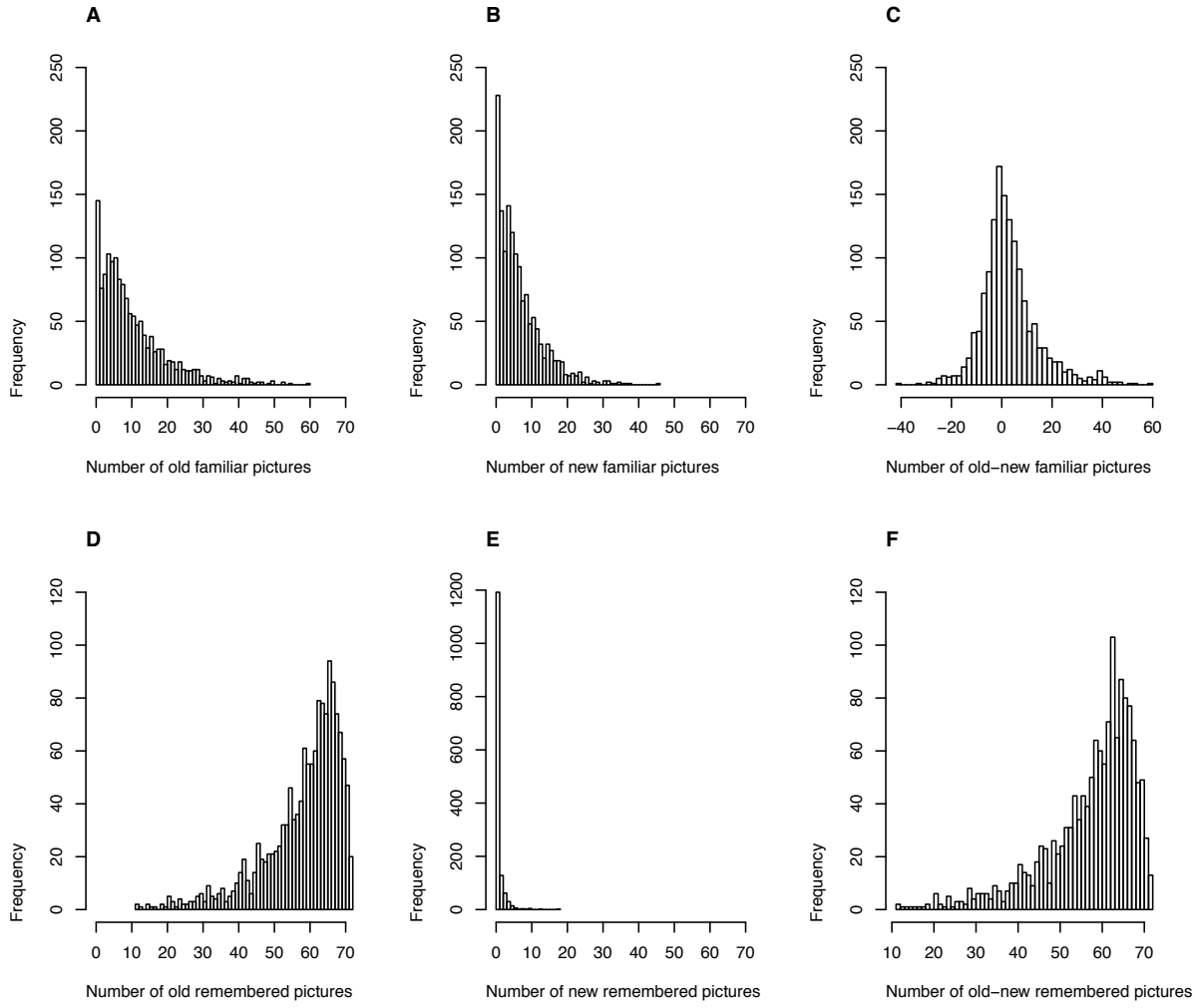

Supplementary Figure 2: ICA reproducibility between the training sample and the replication sample for the top 5 most stable solutions (5, 10, 12, 14 or 15 ICs). Abbreviations: train, training sample; repl, replication sample, IC, independent component

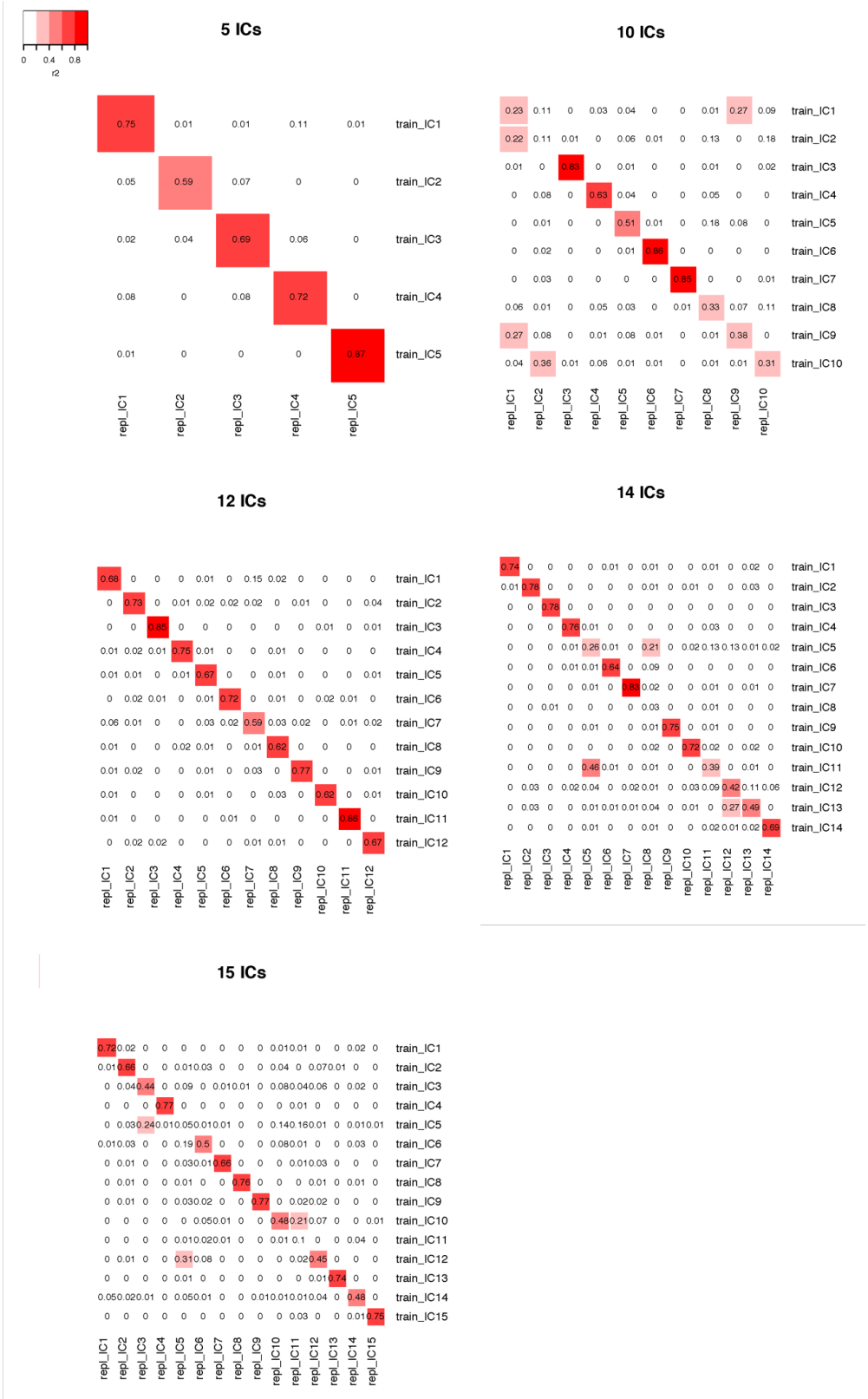

Supplementary Figure 3: Comparison of the average reproducibility metrics between the top 5 most stable ICA solutions. The difference between the mean r^2 of matched (in blue) and unmatched (in green) ICs between the training and the replication sample, "matched – unmatched ICs", was used as reproducibility metric.

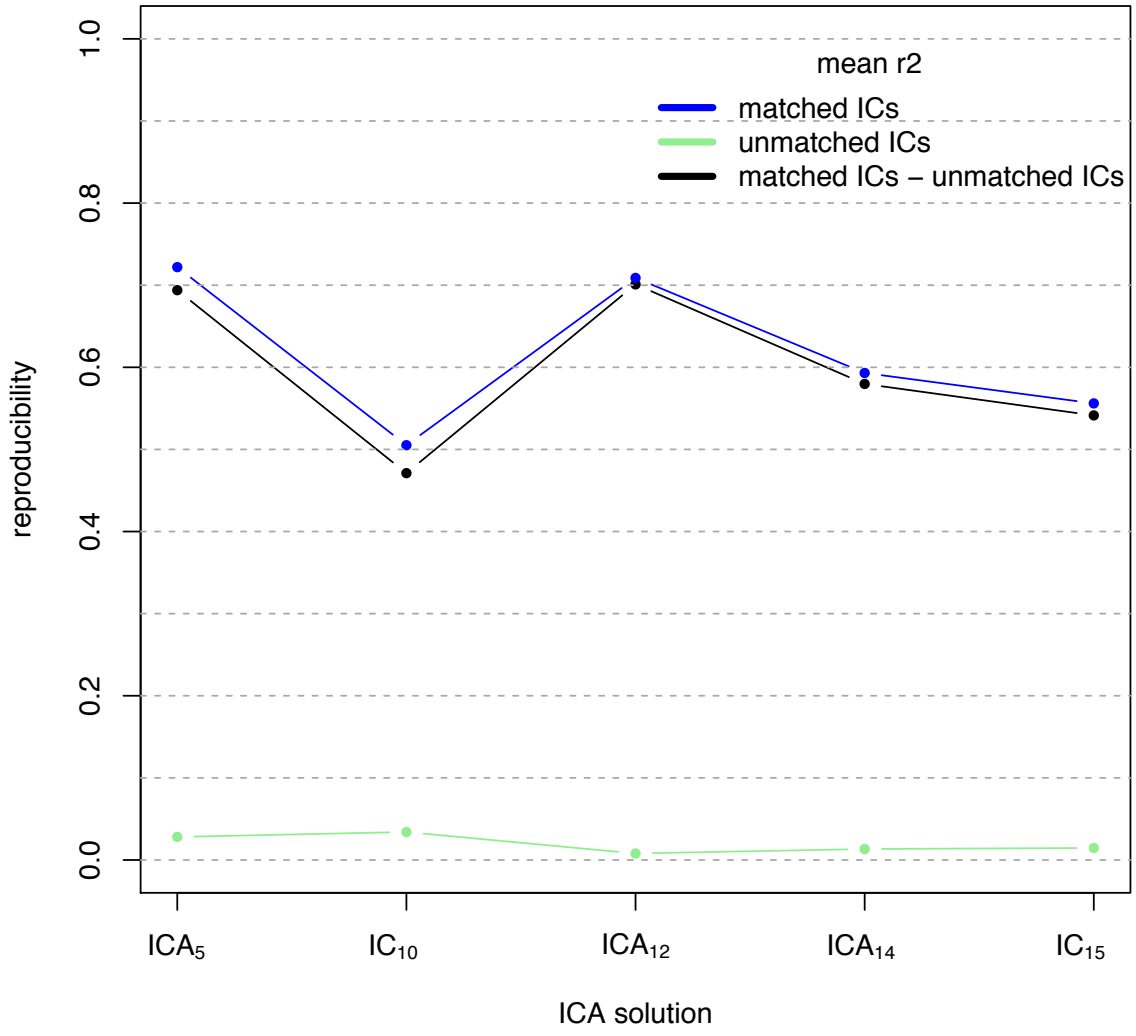

Supplementary Figure 4: Anatomical localization of ICA decomposition voxel loadings for each IC in the replication sample. Only 5% of voxels, having most extreme voxel loadings, are depicted. Positive and negative voxels loadings are presented in red and blue, respectively.

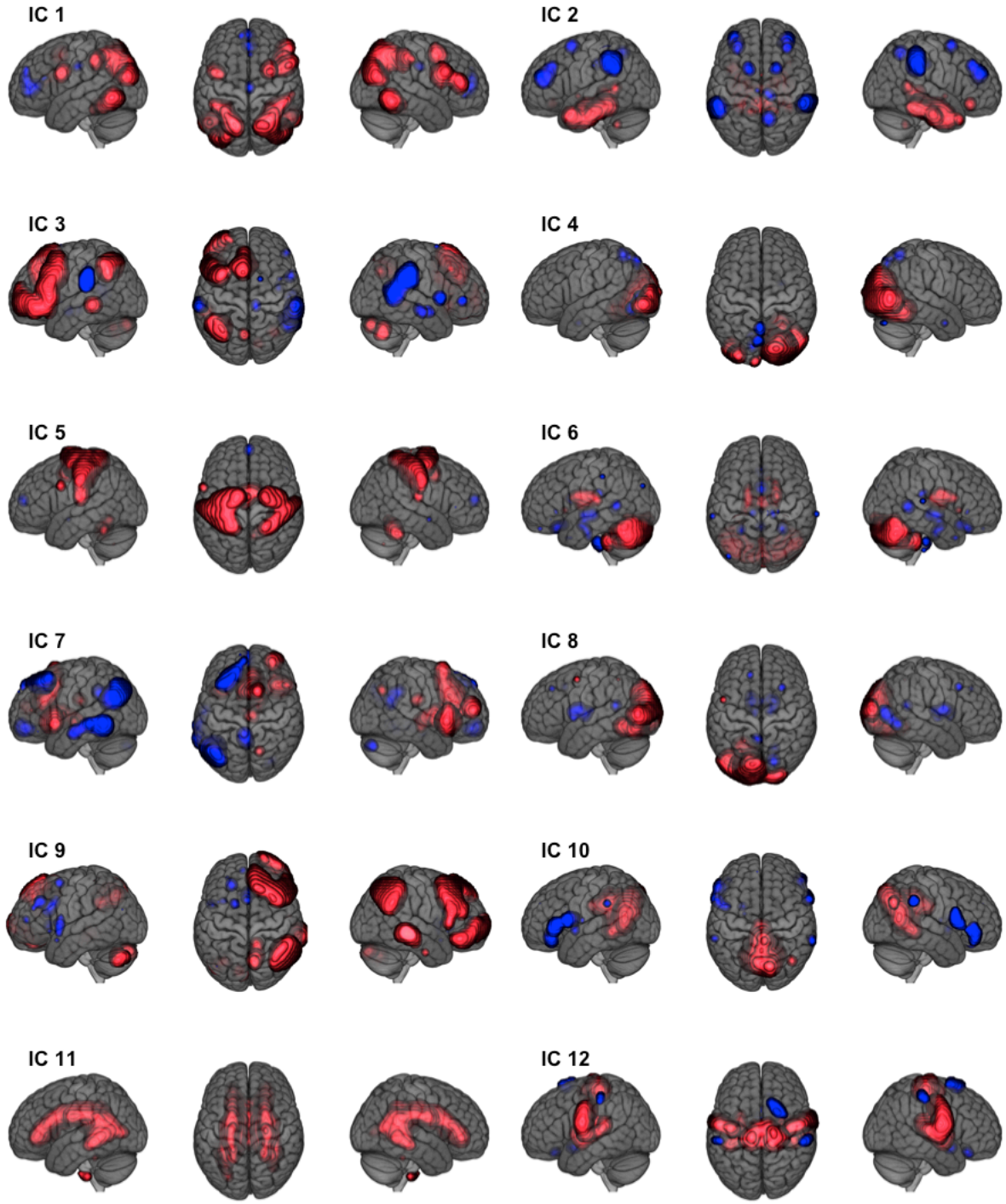

Supplementary Figure 5: Between-sample comparison of voxel loadings per IC. The overlap of voxels with most extreme loadings (top 5%) between the training sample (x-axis) and the replication sample (y-axis) is presented in green colour. Non-overlapping voxels, i.e., with IC loadings within the top 5% in one sample but not in the other, are presented in black and blue, for the training and the replication sample, respectively. Voxels with loadings < 5% in both samples are presented in grey.

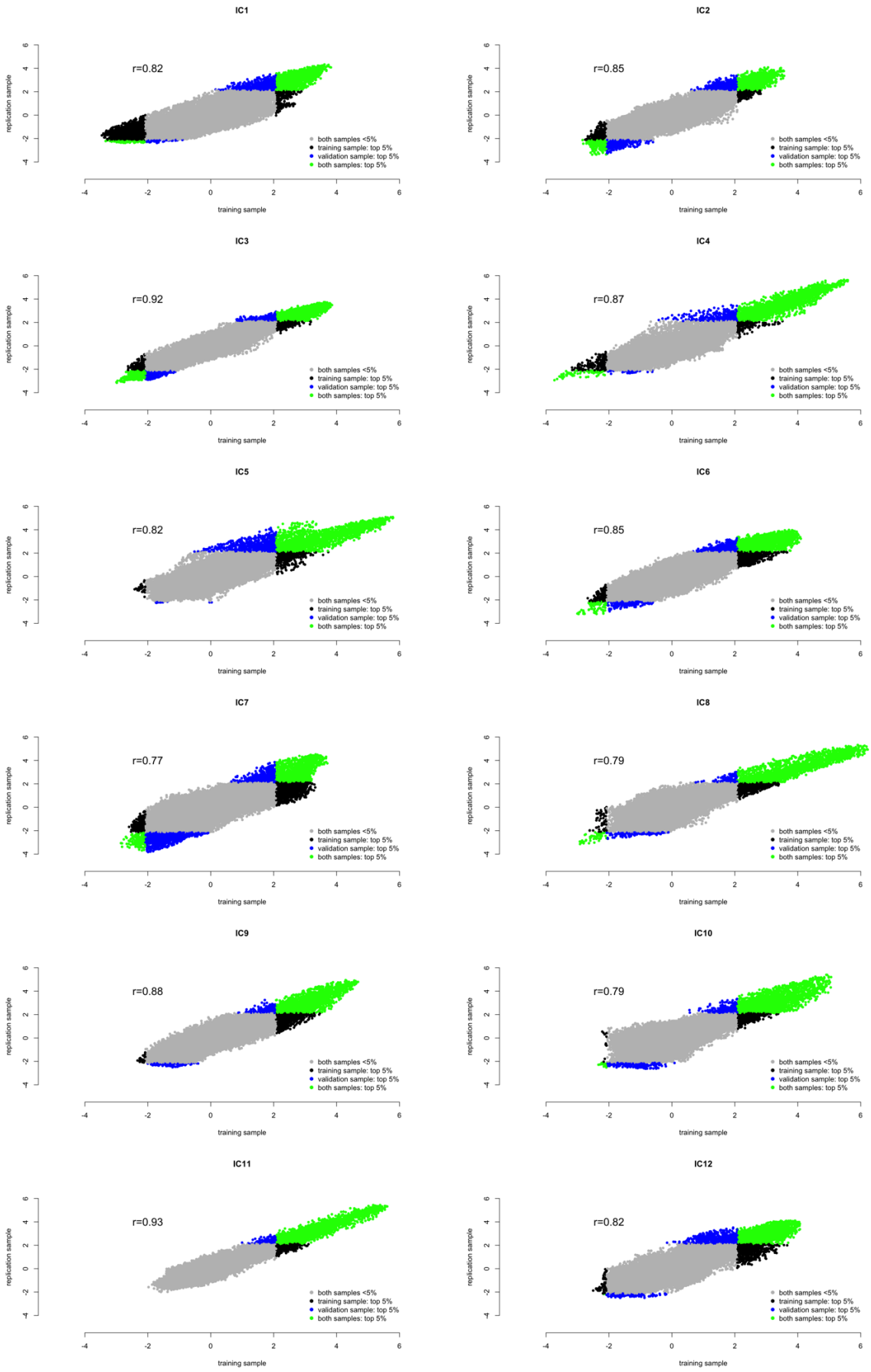
IC1
r=0.82
IC2
r=0.85
IC3
r=0.92
IC4
r=0.87
IC5
r=0.82
IC6
r=0.85
IC7
r=0.77
IC8
r=0.79
IC9
r=0.88
IC10
r=0.79
IC11
r=0.93
IC12
r=0.82
replication sample
training sample
both samples <5%
training sample: top 5%
validation sample: top 5%
both samples: top 5%

Supplementary Figure 6: Scatter plot depicting the observed and predicted familiarity and recollection performances in the replication and the test sample. A) familiarity scores and B) recollection scores in the replication sample; C) familiarity scores and D) recollection scores in the test sample. The figure contains scaled behavioural data.

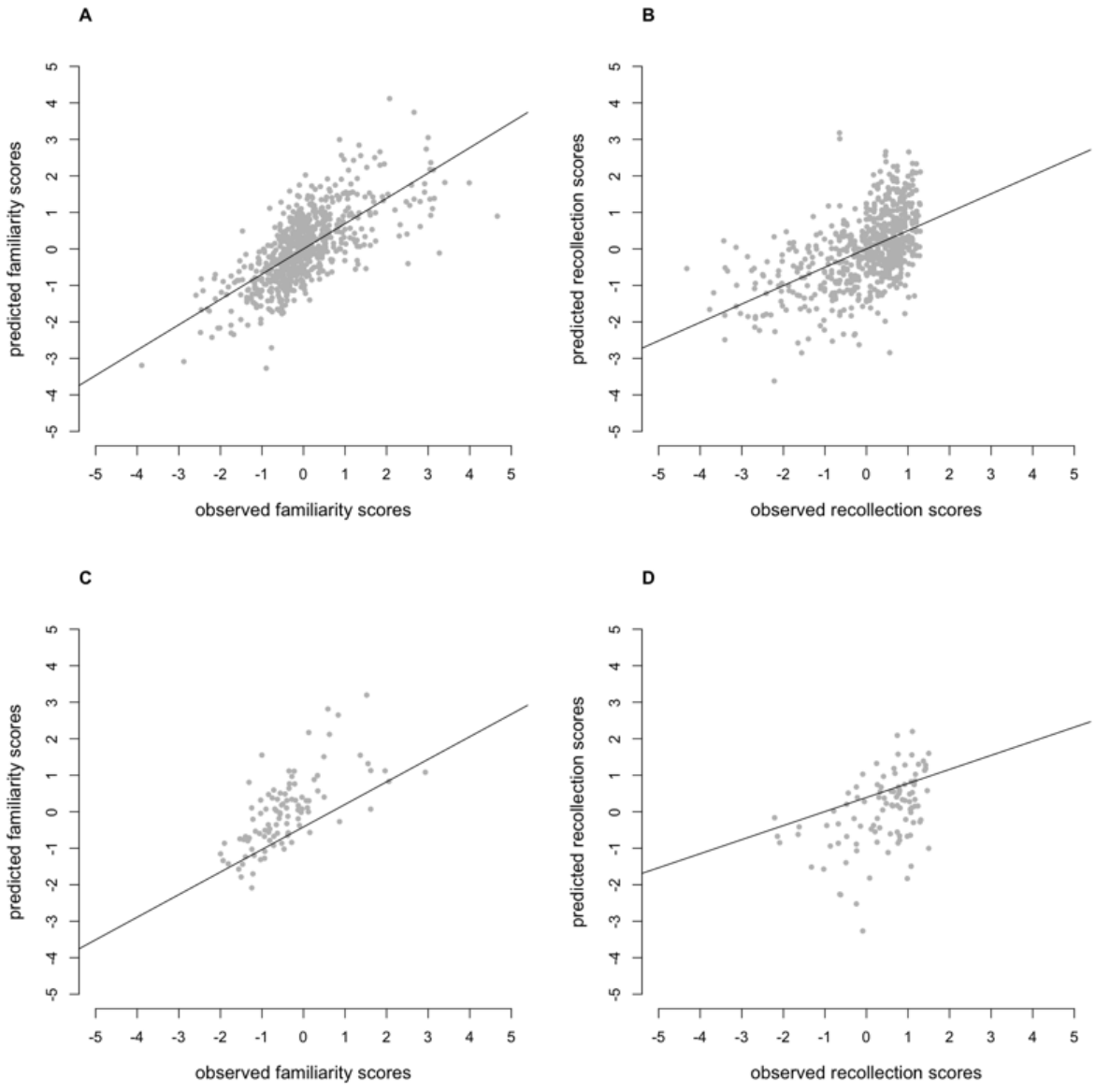

Supplementary references

1. Ashburner, J., *A fast diffeomorphic image registration algorithm.* NeuroImage, 2007. **38**(1): p. 95-113.
2. Klein, A., et al., *Evaluation of 14 nonlinear deformation algorithms applied to human brain MRI registration.* NeuroImage, 2009. **46**(3): p. 786-802.
3. Fischl, B., et al., *Whole Brain Segmentation: Automated Labeling of Neuroanatomical Structures in the Human Brain.* Neuron, 2002. **33**(3): p. 341-355.
4. Desikan, R.S., et al., *An automated labeling system for subdividing the human cerebral cortex on MRI scans into gyral based regions of interest.* NeuroImage, 2006. **31**(3): p. 968-980.

5.3. Exome sequencing of healthy phenotypic extremes links TROVE2 to emotional memory and PTSD

nature human behaviour

ARTICLES

PUBLISHED: 27 MARCH 2017 | VOLUME: 1 | ARTICLE NUMBER: 0081

Exome sequencing of healthy phenotypic extremes links *TROVE2* to emotional memory and PTSD

Angela Heck[1,2,3*], Annette Milnik[1,2,3], Vanja Vukojevic[1,2,4], Jana Petrovska[1,2], Tobias Egli[1,2], Jochen Singer[5,6], Pablo Escobar[6,7,8], Thierry Sengstag[6,7,8], David Coynel[2,9], Virginie Freytag[1,2], Matthias Fastenrath[2,9], Philippe Demougin[1,2,4], Eva Loos[2,9], Francina Hartmann[1,2], Nathalie Schicktanz[2,9], Bernardo Delarue Bizzini[1,2,4], Christian Vogler[1,2,3], Iris-Tatjana Kolassa[10], Sarah Wilker[10], Thomas Elbert[11], Torsten Schwede[6,7,8], Christian Beisel[5], Niko Beerenwinkel[5,6], Dominique J.-F. de Quervain[2,3,9†] and Andreas Papassotiropoulos[1,2,3,4*†]

Many mental disorders represent the extremes of the normal distribution of traits, which are related to multiple cognitive and emotional dimensions. By performing whole-exome sequencing of healthy, young subjects with extremely high versus extremely low aversive memory performance, we identified *TROVE2* as a gene implicated in emotional memory in health and disease. *TROVE2* encodes Ro60, a broadly expressed RNA-binding protein implicated in the regulation of inflammatory gene expression and autoimmunity. A regulatory *TROVE2* variant was linked to higher emotional memory capacity and higher emotional memory-related brain activation in healthy subjects. In addition, *TROVE2* was associated with traumatic memory and the frequency of post-traumatic stress disorder in genocide survivors.

Enhanced memory for emotional events, a common observation in animals and humans, is an evolutionary important trait, because it helps remembering both dangerous and favorable situations[1]. On the other hand, strong sensory and emotional memories of various life-threatening and aversive experiences may contribute to the development and symptoms of post-traumatic stress disorder (PTSD)[2,3], especially when such memories loose their association with the original contextual system[4,5]. In healthy humans, emotionally charged memory (that is, enhanced memory for emotional events) shows large phenotypic variability[6] and has been linked to genetic variants of well-established neuromodulatory systems and molecules in candidate gene studies[6–13]. Similarly, there is substantial variability in the individual vulnerability to develop PTSD, particularly at lower levels of trauma exposure, which can be partially explained by genetic factors[14].

Next-generation sequencing coupled with efficient DNA capture has recently enabled the use of whole-exome sequencing (WES) for the study of the genetics of human phenotypes[15]. Indeed, WES studies have been particularly successful at identifying functional variants related to complex traits[15–17]. Such variants can be identified through extreme-phenotype sampling followed by deep WES[17–20]. In extreme-phenotype sampling, samples from a carefully selected population at one or both ends of the extremes of a phenotype, which have been adjusted for known covariates, are subjected to sequencing. In these populations, causal variants are expected to be enriched. Thus, even small sample sizes may be sufficient to suggest candidate variants that can subsequently be genotyped in a larger group of phenotyped individuals, as has also been shown recently by empirical research[21].

Here we performed WES in healthy, young subjects with extreme high or extreme low emotionally charged memory performance, followed by targeted genotyping in a larger population, which showed a normal distribution of the phenotype of interest (n = 2,684). Genotype-dependent differences in emotional memory-related brain activation were studied in a homogenous sub-sample of 1,258 subjects. In addition, we assessed the effect of the identified variants on gene expression in the post-mortem human brain and on symptoms and frequency of PTSD in genocide survivors.

Results

Exome sequencing in phenotypic extremes. WES was performed in 88 healthy, young participants with extreme high or extreme low aversive memory performance carefully matched for sex (1-to-1 matching), genetic background, age and smoking behaviour (see Methods, Fig. 1, Supplementary Fig. 1 and Supplementary Table 1). Aversive memory was quantified by means of a picture delayed free-recall task. High and low extremes were defined on the basis of the distribution of aversive memory performance in n = 3,418 healthy, young subjects (see Methods).

WES was performed with the SureSelectXT human all exon V5+UTR target-enrichment kit (Agilent), which allows sequencing of exonic and near-gene regulatory variants. To avoid discarding

[1]Division of Molecular Neuroscience, Department of Psychology, University of Basel, CH-4055 Basel, Switzerland. [2]Transfaculty Research Platform Molecular and Cognitive Neurosciences, University of Basel, CH-4055 Basel, Switzerland. [3]Psychiatric University Clinics, University of Basel, CH-4055 Basel, Switzerland. [4]Department Biozentrum, Life Sciences Training Facility, University of Basel, CH-4056 Basel, Switzerland. [5]Department of Biosystems Science and Engineering, ETH Zurich, CH-4058 Basel, Switzerland. [6]SIB Swiss Institute of Bioinformatics, CH-4056 Basel, Switzerland. [7]Department Biozentrum, University of Basel, CH-4056 Basel, Switzerland. [8]sciCORE Center for Scientific Computing, University of Basel, CH-4056 Basel, Switzerland. [9]Division of Cognitive Neuroscience, Department of Psychology, University of Basel, CH-4055 Basel, Switzerland. [10]Clinical & Biological Psychology, Institute of Psychology & Education, Ulm University, D-89069 Ulm, Germany. [11]Department of Psychology, University of Konstanz, D-78457 Konstanz, Germany. †These authors jointly supervised this work. *e-mail: angela.heck@unibas.ch; andreas.papas@unibas.ch

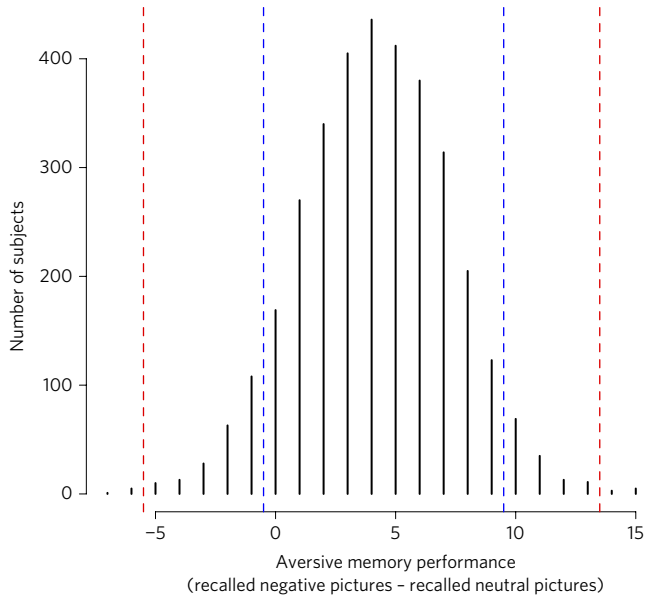

Figure 1 | Frequency histogram of aversive memory performance in 3,418 healthy, young adults. Dotted vertical blue and red lines at the right distribution tail represent the lower and upper performance margins of subjects, respectively, defined as high extremes. Dotted vertical blue and red lines at the left distribution tail represent the upper and lower performance margins of subjects, respectively, defined as low extremes.

variants that were enriched at high frequencies in the extremes[21], the empirical minor allele frequency (MAF) in the extreme dataset of $n = 88$ subjects was set to ≤0.125 (see Methods). Given that no prior information is available regarding putative differences in effect sizes of variants associated with the phenotype of interest, gene-based analyses were done using both burden and adaptive burden tests (see Methods). After adjustment for multiple testing, *TROVE2* (encoding TROVE domain family member 2; also known as Sjögren syndrome type A antigen; Ro60 KDa autoantigen), *PKD2L2* (encoding polycystin 2 like 2, also known as transient receptor potential cation channel), and *CFAP57* (also known as *WDR65*; encoding cilia and flagella associated protein 57) were significantly associated with group membership, which reflected extreme aversive memory performance (Table 1). We investigated *TROVE2* further, because this gene exceeded the adjusted significance threshold in both the burden and adaptive burden test (Table 1). In the burden test, *TROVE2* remained significant after Bonferroni correction for the entire number of genes ($n = 21{,}175$) that were analysed in the burden test ($P_{nominal} = 2 \times 10^{-6}$, $P_{Bonferroni} = 0.042$; Supplementary Fig. 2). Moreover, *TROVE2* was the best hit ($P_{nominal} = 0.0002$) in the optimized sequence kernel association test (SKAT-O)[22] (Supplementary Table 2). A detailed view of the sequencing data for *TROVE2* (Fig. 2) showed that the variant, which is mainly responsible for the results of the gene burden tests, was a 3′-UTR (untranslated region) single-nucleotide polymorphism (SNP) (rs72740218; C/T transition on chr1:193054088 according to GRCh37/hg19 coordinates). Notably, 10 of the 44 high-extreme individuals were heterozygous minor T allele carriers, whereas this was only the case for 2 of the 44 low-extreme individuals. Pyrosequencing-based genotyping confirmed this result (see Methods). According to the Exome Aggregation Consortium (ExAC) browser (version 0.3.1), rs72740218 MAF is 0.08 in European (non-Finnish) populations.

Free-recall performance for positive material relative to neutral material (termed positive memory, in analogy to aversive memory) was also significantly higher in high-extreme subjects. However, this was entirely owing to this group's lower free-recall performance for neutral pictures (Supplementary Table 1). The genetic association findings were unrelated to the difference in positive memory between extreme groups. Firstly, *TROVE2* was not significant ($P = 0.6$) when tested at the gene level (SKAT-O with positive memory as the quantitative phenotype). Secondly, *TROVE2*-variant rs6692342 was not significantly associated with positive memory ($P = 0.2$) or with free recall for positive pictures ($P = 0.9$).

Next, we tested whether the association of the T allele with increased aversive memory performance could also be detected in the entire population of healthy young subjects ($n = 2{,}684$ successfully genotyped for rs72740218, including the $n = 88$ sequenced subjects, see Methods). We identified 19 minor allele homozygotes, 369 heterozygotes, and 2,296 major allele homozygotes (empirical MAF = 0.075, Hardy–Weinberg $P > 0.1$). The T allele was significantly correlated ($P = 0.005$) with increased aversive memory performance, also after exclusion of the $n = 88$ sequenced extremes ($P = 0.035$, $n = 2{,}596$). This sample of $n = 2{,}596$ participants consisted of $n = 217$ subjects that had not been selected for exome sequencing, but nonetheless fullfilled the performance criteria for extreme high or extreme low aversive memory (Supplementary Table 3), and of 2,379 non-extreme individuals. Notably, the significant association between rs72740218 and aversive memory performance in this population of $n = 2{,}596$ participants was attributable to subjects that exhibited extreme aversive memory performance ($P = 0.0008$ for the interaction 'genotype X extreme/non-extreme group membership'; $r = 0.11$ in $n = 217$ non-sequenced extremes; $r = 0.016$ in $n = 2{,}379$ non-extremes).

Functional brain imaging. In the next step, we used functional brain imaging (functional magnetic resonance imaging, fMRI) to identify *TROVE2* rs72740218-dependent differences in brain activity related to memory encoding of aversive stimuli in $n = 1{,}258$ subjects, a sub-sample of the population of $n = 2{,}596$ healthy subjects (sequenced extremes were excluded), who participated in the behavioural genetic study. All neuroimaging data were acquired in the same MRI scanner, thereby reducing hard- and software-related methodological variance.

We first investigated encoding-related brain activation independently of whether the information was later recalled or not (see Methods). We found significant ($P < 0.05$, two-sided test, family-wise error (FWE) corrected for the whole brain (P_{FWE})) gene dose-dependent (that is, with increasing number of the minor T allele) activity increases in the middle frontal gyrus, Brodmann area 9 (peak at ((−33, 36, 48), $t = 5.39$; $P_{FWE} = 0.0015$)) (Supplementary Fig. 3). Because these activation differences may be independent of memory processes, we then investigated brain activation that was related to successful memory encoding, that is, activation that was specifically related to information that was later recalled (see Methods). We observed significant positive associations between the *TROVE2* genotype (with increasing number of the minor T allele) and aversive memory-related activity in the left medial prefrontal cortex (peak at (−5.5, 38.5, 36), superior frontal gyrus/paracingulate gyrus, Brodmann area 32, $t = 5.80$; $P_{FWE} = 0.0003$; with FWE-corrected voxels extending to the dorsal anterior cingulate) (Fig. 3 and Supplementary Fig. 4). Even after excluding the 6 minor allele homozygotes from the analysis, we still found significant *TROVE2*-dependent differences in activation between the major allele homozygotes and the heterozygotes with the peak at the same coordinate (((−5.5, 38.5, 36), $t = 5.25$; $P_{FWE} = 0.0125$)). There were no significant increases in activity with increasing number of major alleles. Additionally, we tested whether the reported association was specific for the negative valence. An analysis of *TROVE2*-dependent differences in brain activity, which were related to successful memory encoding of positive stimuli compared to neutral stimuli (see Methods), did not show significant FWE-corrected results; nevertheless the corresponding uncorrected significance level was

Table 1 | Results of gene-based analyses in phenotypic extremes.

Gene symbol	Gene name	Burden test *P* Value		Adaptive burden test *P* value	
		Nominal	Adjusted*	Nominal	Adjusted*
TROVE2	TROVE domain family member 2 (also known as Sjögren syndrome type A antigen, Ro60 KDa autoantigen)	2×10^{-6}	0.0004	4×10^{-5}	0.004
PKD2L2	Polycystin 2 like 2, transient receptor potential cation channel	0.00022	0.045	0.00288	0.317
CFAP57	Cilia and flagella associated protein 57	0.00026	0.053	0.00035	0.038

*Corrected for the number of genes reaching *i*-stat < 0.001 in the respective test (burden test: 203 genes; adaptive burden test: 110 genes).

high (((−5.5, 38.5, 36), $t = 3.44$; $P_{\text{uncorrected}} = 0.0006$; $P_{\text{FWE}} = 0.97$)). Accordingly, we did not observe significant ($P < 0.05$, two-sided test, FWE-corrected for the whole brain) associations between the number of minor *TROVE2* alleles and contrast testing for differences in brain activity between successful memory encoding of aversive compared to positive stimuli (see Methods), suggesting that, although the observed association was strongest for aversive stimuli, it was also observable for the positive valence.

In summary, the fMRI experiment showed that the minor allele of *TROVE2* SNP rs72740218, which was associated with increased memory for aversive information, was also related to increased brain activity in the medial prefrontal cortex during successful memory encoding of emotional pictures, whereby the strongest association was observed for aversive ones.

***TROVE2* expression in human frontal cortex.** Given the effect of the *TROVE2* minor allele on brain activation that is related to successful memory encoding in the prefrontal cortex, we further investigated possible minor-allele effects on *TROVE2* expression in this part of the human brain. For this analysis, we used the BRAINEAC data, a publicly available resource for the exploration of the regulatory significance of genetic variants in the human brain (http://www.braineac.org/)[23]. Brain samples specified as frontal cortex probes in the BRAINEAC database were taken from the prefrontal cortex[24], mostly Brodmann area 9/46, a region well-known for its involvement in emotional processing and emotional memory[25,26]. The 3′-UTR variant rs72740218 was significantly associated with expression of the adjacent *TROVE2* terminal coding exon (exon-specific probeset 2372955; chr1:193053788–193053828, GRCh37/hg19 coordinates) in the prefrontal cortex of 125 deceased subjects. The minor T allele predisposed to significantly higher expression values ($P = 0.005$, Fig. 4a), possibly suggesting a local effect of this variant on expression of the corresponding exon. No significance was observed at the full-transcript level (that is, the Winsorized means over all exon-specific probesets) (Supplementary Table 4).

***TROVE2* genetic variability in traumatized survivors of the Rwandan genocide.** Extremely aversive, in particular life-threatening, incidents can lead to an excessive and persisting emotional memory of the traumatic events, which can result in intrusive and distressing re-experiencing (traumatic memory), a core PTSD symptom. The heritability of re-experiencing traumatic events ranges from 23% to 51%, suggesting that naturally occurring genetic variations have an important effect on this trait[27]. Given the association of *TROVE2* with aversive memory and aversive memory-related brain activation in healthy subjects, we hypothesized that *TROVE2* would also be associated with emotional memory for traumatic events reflected in increased re-experiencing symptoms. We tested this hypothesis in 271 refugees who have fled from the Rwandan civil war, who have been living in the Nakivale refugee camp in Uganda during the time of investigation, and from whom lifetime data on the prevalence of PTSD were available (137 females; 134 males; mean age, 35 years; range, 18–68 years; see Methods). All subjects had experienced highly aversive situations and were examined

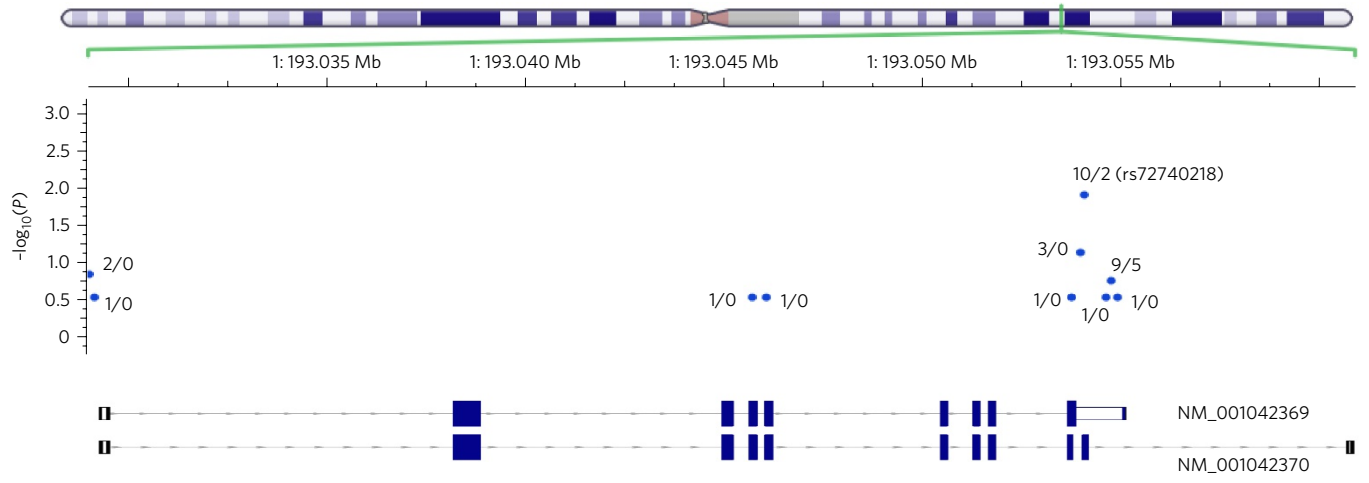

Figure 2 | Sequencing results of *TROVE2* (positions according to the GRCh37/hg19 coordinates). Blue dots indicate variants with MAF ≤ 0.125 detected in the sample of 88 individuals with extreme aversive memory performance. Solidus-separated numbers accompanying each dot indicate the frequency of the occurrence of the respective minor allele in subjects with extremely high and extremely low performance (high/low). The minor allele of variant rs72740218 was observed in 10 high extremes and in 2 low extremes. The *y* axis indicates $-\log_{10}$ of the *P* value of genetic association tests that were performed separately for each variant. For illustration purposes, two *TROVE2* transcript variants (see also Fig. 4) are shown in the lower part of the figure. Blue filled rectangles represent coding exons, empty rectangles represent non-coding exons and UTRs.

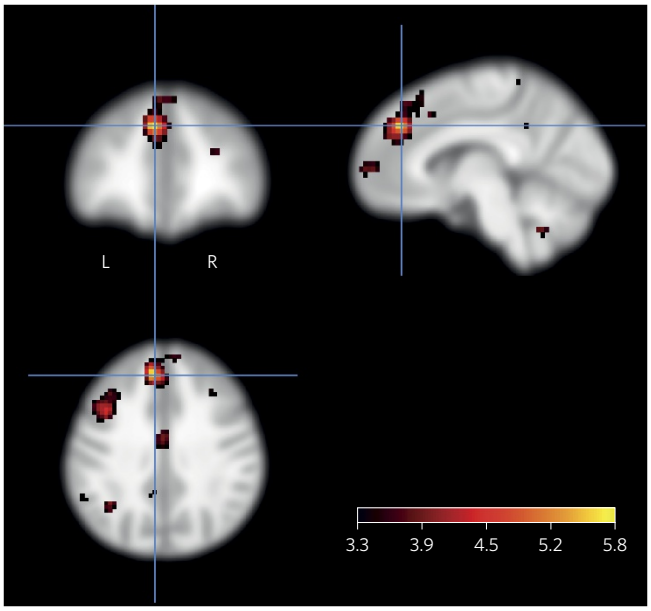

Figure 3 | *TROVE2* rs72740218 genotype-dependent differences in brain activity related to successful memory encoding of aversive stimuli compared with neutral stimuli in 1,258 healthy young subjects. Displayed are positive associations between genotype (the number of minor T alleles) and activity. The blue cross indicates the peak genotype-dependent activation ($t = 5.80$; $P_{FWE} = 0.0003$) in the left medial prefrontal cortex at (−5.5, 38.5, 36). Activations are overlaid on coronal, sagittal and axial sections of brain images, displayed at $t \geq 3.1$ ($P_{nominal} < 0.001$) and using colour-coded t values. L, left side of the brain; R, right side of the brain.

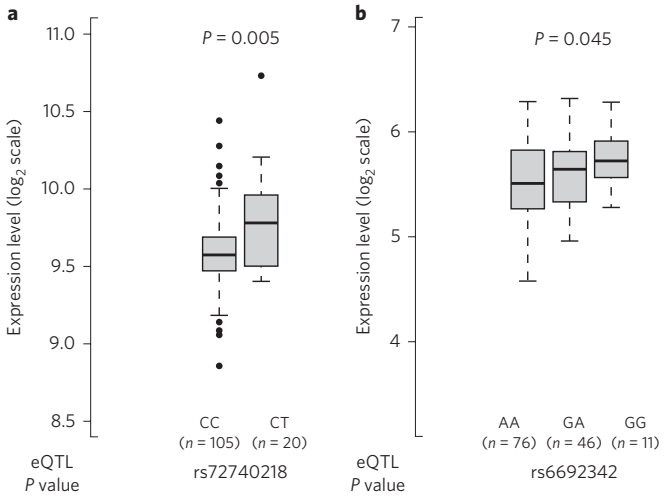

Figure 4 | Association of *TROVE2* SNPs rs72740218 and rs6692342 in the human frontal cortex. a,**b**, Association of *TROVE2* SNPs rs72740218 (**a**) and rs6692342 (**b**) with gene expression. **a**, Expression values of exon-specific probeset 2372955 (chr1:193053788–193053828). **b**, Expression values of exon-specific probeset 2372928 (chr1:193028950–193029112; GRCh37/hg19 coordinates). Data and box plots were retrieved from the BRAINEAC project server[23] (http://www.braineac.org/, accessed on 7 October 2016). Box plots demarcate the 25th and 75th percentile (middle line is median), and bars represent the minimum and maximum values. Filled circles represent outliers. eQTL, expression quantitative trait locus.

by trained experts with a structured interview based on the Post-traumatic Diagnostic Scale[28] with the help of trained interviewers chosen from the refugee community. Traumatic events were assessed using a checklist of 36 reported war- and non-war-related traumatic event types (such as, injury by a weapon, rape, accidents) (Supplementary Table 5). In sub-Saharan African samples, the rs72740218 variant is rare (MAF < 0.01, according to dbSNP). Therefore, we analysed all *TROVE2*–spanning common SNPs that were present on the Human SNP Array 6.0 with an empirical MAF ≥ 0.05 in the Rwandan sample ($n = 5$ tagging SNPs, Table 2). None of these variants was significantly associated with age, sex, the number of experienced traumatic event types, or with the occurrence of any of the 36 distinct traumatic event types (Table 2 and Supplementary Table 5). *TROVE2* SNPs were significantly associated with traumatic memory (that is, lifetime symptoms of re-experiencing the traumatic event) and with frequency of lifetime PTSD (Table 2). Variant rs6692342, which is located 555 and 1,007 bases upstream of the respective *TROVE2* transcript variants (Fig. 5), showed the strongest association: the minor allele G was associated with increased traumatic memory ($P = 0.007$) and with increased PTSD frequency ($P = 0.0004$). Linkage disequilibrium between variants rs6692342 and rs72740218 was not calculated in the PTSD sample, given the very low frequency of rs72740218 in the Rwandan population. In the healthy, young population sample, variants rs72740218 and rs6692342 were unlinked ($r^2 = 0.02$). Because the occurrence of some of the traumatic event types was unevenly distributed between rs6692342 genotype groups (albeit without reaching corrected statistical significance; Supplementary Table 5), we reran the analyses by controlling for such uneven distributions and obtained nearly identical results (Supplementary Table 6). The minor allele G of variant rs6692342 was also moderately associated with increased expression of the adjacent *TROVE2* non-coding exon 1 of transcript variants NM_004600, NM_001173525, NM_001042369 and NM_001042370 (exon-specific probeset 2372928, chr1:193028950–193029112, GRCh37/hg19 coordinates) in the prefrontal cortex of 123 deceased subjects of the BRAINEAC study ($P = 0.045$, Fig. 4b), possibly suggesting a local effect of this variant on expression of the corresponding exon. No significance was observed at the full-transcript level (that is, the Winsorized means over all exon-specific probesets) (Supplementary Table 4). The frequency of the minor G allele of rs6692342 was nearly identical in the BRAINEAC and Rwandan samples (25.6% and 24.6%, respectively). Accordingly, genotype frequencies of rs6692342 did not differ between these samples ($P = 0.5$, χ^2 test). Notably, genotype and allele frequencies in the BRAINEAC and Rwandan samples for rs6692342 were in close agreement with the reported values for European and Sub-Saharan populations, respectively, in the 1000 genomes project (Phase 3).

Discussion

The present study suggests that variants related to increased expression of *TROVE2* transcripts in the human frontal cortex are linked to emotional memory capacity and emotional memory-related brain activation in healthy subjects, and to traumatic memory and risk for PTSD in traumatized genocide survivors.

TROVE2 is widely expressed in human tissues, including the brain and its frontal cortex[23,29]. *TROVE2* undergoes complex transcriptional regulation, such as alternative splicing with several coding transcript variants and a range of 8–11 coding and non-coding exons[30,31] (Fig. 5). SNP rs72740218 was associated with emotional memory performance and brain activation related to successful memory encoding of emotionally charged information in the medial prefrontal cortex, one of the key brain regions related to emotional processing[32], although it does not belong to one of the typical localizations found to be activated by emotional memory encoding in genotype-independent studies[33]. It is important to note, however, that genotype-independent analyses may not reveal brain regions for which different genotype groups show opposite activation patterns, for example when major-allele

Table 2 | Associations between common *TROVE2* SNPs and traumatic memory (P_{memory}), lifetime PTSD (P_{PTSD}), sex (P_{sex}), age (P_{age}), and the number of traumatic event types (P_{events}).

SNP ID	Localization	MAF	P_{sex}	P_{age}	P_{events}	P_{memory}	P_{PTSD}
rs6692342	Upstream	0.25	0.868	0.952	0.712	0.007	0.0004
rs4657842	Upstream	0.35	0.895	0.328	0.652	0.191	0.023
rs7554496	Intronic	0.15	0.323	0.800	0.318	0.169	0.581
rs10801173	3′-UTR; intronic	0.47	0.235	0.316	0.746	0.186	0.024
rs41520747	Downstream; intronic	0.18	0.360	0.669	0.791	0.587	0.017

homozygotes show a deactivation, whereas the other genotype groups show an activation, as was the case with SNP rs72740218 (Supplementary Fig. 5). Notably, it has been shown that PTSD patients, when compared to controls, have an increased response in the left dorsal anterior cingulate/medial prefrontal cortex at almost identical coordinate positions (peak at −3, 39, 39) during encoding of later remembered negative verbal information[34]. Of note, there is evidence for a dissociative subtype of PTSD patients, who typically show increased activation in the anterior cingulate/medial prefrontal cortex[35].

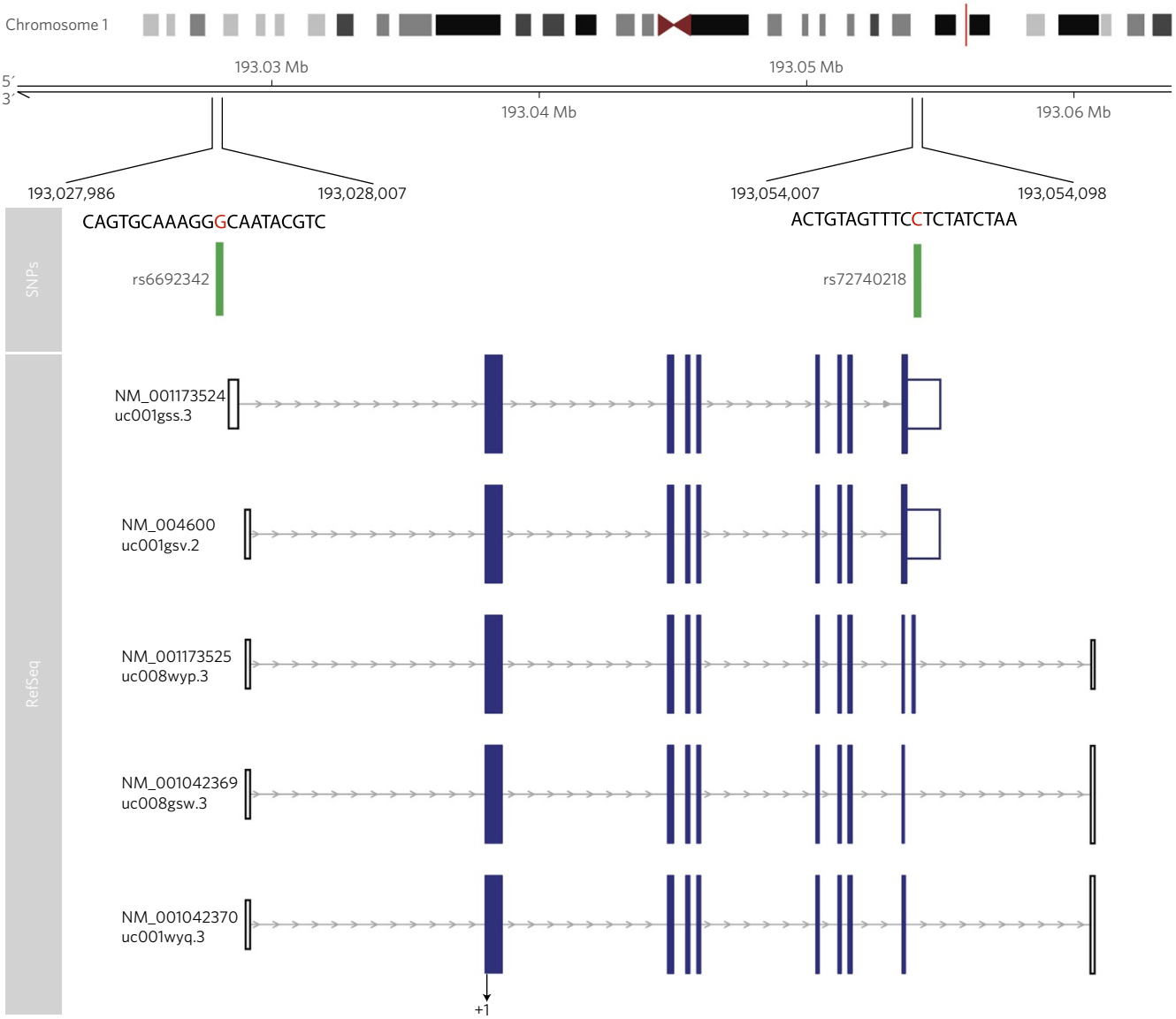

Figure 5 | Schematic representation of selected *TROVE2* RefSeq transcript variants (positions according to GRCh37/hg19 coordinates). UCSC (University of California Santa-Cruz) identifiers are also given beneath each RefSeq identifier. Blue filled rectangles represent coding exons, empty rectangles represent non-coding exons and UTRs. SNPs rs6692342 and rs72740218 are zoomed in with 10 bases up- and downstream; +1: first coding base in the first coding exon.

SNP rs72740218 is located within the 3′-UTR of transcripts NM_001173524 and NM_004600 (Fig. 5), and is significantly associated with expression levels of the terminal coding exon of these variants in the prefrontal cortex (Fig. 4). SNP rs6692342, which was associated with traumatic memory and PTSD frequency, is located 555 bases upstream of transcript variant NM_001173524 and 1,007 bases upstream of transcript variants NM_004600, NM_001173525, NM_001042369, and NM_001042370, and is moderately, albeit significantly associated with expression levels of the adjacent non-coding exon 1 of the latter four variants in the prefrontal cortex (Fig. 4). Taken together, the minor alleles of these *TROVE2* SNPs were associated with increased expression of adjacent exons and with gain of emotional (in the case of rs72740218) and traumatic (in the case of rs6692342) memory-related phenotypes. Given that free recall was assessed shortly after encoding in this study, further research will be needed to study the role of this gene on emotional memory capacity related to the longer-term (such as, hours, days) consolidation processes.

TROVE2 encodes Ro60, an RNA-binding protein that binds to misfolded, non-coding RNAs, pre-5S rRNA (ribosomal RNA) and Y RNA (small non-coding RNA)[31]. Autoantibodies to Ro60 are prevalent in autoimmune disorders including Sjögren's syndrome and systemic lupus erythematosus[36–38], and recent research supports the idea of a direct link between Ro60 autoantibody production, type I interferon, and autoimmunity[39]. The findings of the present study support a genetic link between *TROVE2* and emotional memory-related traits, possibly by regulation of specific transcripts. Although speculative, one might hypothesize that *TROVE2* has a role in a possible link between the regulation of immune-related processes and the regulation of emotional memory-related traits, given the crucial involvement of *TROVE2* in autoimmunity. Notably, recent genetic and epidemiological data point to a link between autoimmunity and PTSD: a retrospective cohort study of 666,269 Iraq and Afghanistan veterans revealed significant associations between PTSD and risk for autoimmune disorders, whereby shared etiology was one of the possible explanations for this observation[40]. Recently, a large genome-wide association study (GWAS) of PTSD has shown a significantly increased enrichment ratio for immune-related expression quantitative trait loci in PTSD[41]. In addition, abnormal cytokine regulation and a proinflammatory milieu are present in PTSD[42–45]. Thus, a link between the regulation of immune functions and emotional memory-related neuropsychiatric phenotypes probably exists. Despite the known, direct connection between the human brain and peripheral tissues relevant to the function of the immune system[46], it is not yet possible to draw any causal inferences about the mechanistic nature of this link and about a putative involvement of *TROVE2*. Notably, recent animal research identified meningeal immunity as a direct player in the regulation of complex brain functions, such as learning, memory and social behaviour[47,48].

A number of—mostly small—PTSD GWAS in civilian and military or veteran samples have been published[41,49–55]. *TROVE2* has not been reported as one of the top hits in these GWAS. Of note, the published GWAS results do not converge so far. It is widely acknowledged that substantial within- and between-sample differences in traumatic event type, duration and rate, time of trauma onset, ancestry, sociodemographic factors and social support render comparability of GWAS results in the PTSD field inherently difficult[56]. The possibility exists that some of the reported findings might prove specific to a certain population. Therefore, the replication issue of genetic studies of PTSD will remain challenging and might be resolved by future large collaborative efforts, which should include different subgroups of large homogenous samples. Notably, a recent study that has reported on combined genetic and transcriptomic findings in human and *C. elegans* identified *TROVE2* as one of the top scoring genes involved in mood regulation and stress response[57].

In the present study, we used exome sequencing in healthy phenotypic extremes to detect genes that were linked to emotionally charged memory capacity. Notably, the extreme phenotype design proved to be essential for the identification of *TROVE2*, because the effect size of the minor allele T of rs72740218 was considerably higher in the extremes, also in the non-sequenced samples, compared to the largest, middle part of the phenotypic distribution. It is important to stress that the success of the genetic search presented herein is not necessarily generalizable to every genetically complex cognitive and/or emotional trait. A synergy of factors, such as meticulous matching of phenotypic extremes with a particular focus on genetic background[15], a relatively high MAF for the implicated variant and the specific genetic architecture of the phenotype of interest, gave rise to the identification of *TROVE2*. Nevertheless, our experience with this approach and the statistical features of our findings are in close analogy to the observations of a recent study, which identified a genetic modifier of a Mendelian trait (cystic fibrosis) by means of exome sequencing in phenotypic extremes[21].

In conclusion, *TROVE2*, a gene implicated in autoimmunity, is linked to emotionally charged memory in health and psychiatric disease, particularly in PTSD. Specifically, the present findings suggest that the drawback of the *TROVE2* variant-related enhancement of emotional memory is increased enhancement of intrusive and distressing memory for traumatic events. Given that many mental disorders represent the extremes of a normal distribution of traits on multiple cognitive and emotional dimensions[58], we believe that appropriate genetic methodologies in healthy phenotypic extremes may help uncover disease dimensions with different symptom patterns, a subtyping that may be necessary to improve understanding and treatment of psychopathology.

Methods

Definition of phenotypic extremes. Aversive memory was assessed in $n = 3,418$ subjects who participated in ongoing behavioural and imaging genetics studies of healthy, young adults in the city of Basel, Switzerland (data lock April 2015). The ethics committee of the Cantons of Basel-Stadt and Basel-Landschaft approved the experiments. All participants received general information about the study and gave their written, informed consent for participation. Participants were free of any neurological or psychiatric illness, and did not take any medication at the time of the experiment (except hormonal contraceptives).

Aversive memory was quantified by means of a picture delayed free-recall task. Stimuli consisted of 72 pictures that were selected from the International Affective Picture System[59], as well as from in-house standardized picture sets that allowed us to equate the pictures for visual complexity and content (such as human presence). On the basis of normative valence scores (from 1 to 9), pictures were assigned to emotionally negative (2.3 ± 0.6), emotionally neutral (5.0 ± 0.3), and emotionally positive (7.6 ± 0.4) conditions, resulting in 24 pictures for each emotional valence. Four additional pictures that showed neutral objects were used to control for primacy and recency effects in memory. Two of these pictures were presented at the beginning and two at the end of the picture task. These pictures were not included in the analysis. The pictures were presented for 2.5 s in a quasi-randomized order. To ensure that the ratio between valence categories was kept constant across consecutive parts of the entire picture sequence, each twelfth part of the sequence contained exactly two positive, two negative and two neutral pictures. Thus, maximally four pictures of the same category occurred consecutively. Ten minutes after picture presentation, memory performance was tested using a free-recall task, which required participants to write down a short description (a few words) of the previously seen pictures. Remembered primacy and recency pictures as well as training pictures were excluded from the analysis. No time limit was set for this task. A picture was scored as correctly recalled, if the rater could identify the presented picture on the basis of the subject's description. Two trained investigators rated the descriptions independently for recall success (inter-rater reliability >99%). A third independent rater decided on those pictures that had been rated differently[7]. For the purpose of selecting phenotypic extremes, aversive memory performance was calculated by subtracting the number of the freely recalled neutral pictures from the number of freely recalled negative pictures. In a sub-sample of 1,900 subjects with data on a second assessment of free-recall performance 24 h after the first presentation of the identical picture set, both phenotypes showed high levels of inter-trial correlation (Pearson's $r = 0.73$ and $r = 0.78$ for free recall of negative and neutral pictures, respectively). On the basis of the observed phenotypic distribution, subjects with aversive memory performance ≥ 10 and ≤ 13 were classified as high-extreme subjects (HES), and subjects with aversive memory performance ≥ -5 and ≤ -1 were classified as

low-extreme subjects (LES). We adopted an almost-extreme sampling approach, because the very extremes of cognitive phenotypes are vulnerable to potential measurement errors and phenotype heterogeneity[18]. For example, performance at the very extreme low end of the distribution might be related to erroneous understanding of task instructions or to gross errors in task execution. Moreover, the additive polygenic mode of inheritance of common phenotypes breaks down at the very extremes of the distribution tails[60,61]. Thus, subjects at the very extreme ends, as identified upon visual inspection of the frequency histogram (that is, aversive memory performance <-5, $n = 6$; aversive memory performance >13, $n = 8$), were not considered for further analysis (Fig. 1).

Next, we selected all subjects who had been genotyped on the Genome-Wide Human SNP Array 6.0 (Affymetrix) and performed standard quality control with PLINK (https://atgu.mgh.harvard.edu/plinkseq/) including sex check and identity by descent analysis as described in ref. [62], resulting in $n = 2{,}991$ subjects with quality-controlled SNP array data.

The next steps were performed to calculate each subject's genetic background, to select a homogeneous group of participants of European ancestry, and to compute an individual parameter in order to match the to-be-sequenced extremes for genetic similarity. Thus, we analysed the SNP array data of seven Swiss and German samples[62–64] (total $n = 5{,}172$) including our target sample. Genetic data of these subjects was projected onto the first two principal components (PCs) of genetic variation in the HapMap3 reference sample (consisting of African, Asian and European samples) using SMARTPCA[65]. Participants scoring for PC1 < 0.012 and for PC2 < 0.065 were then filtered out to obtain a cluster of broad European ancestry (Supplementary Fig. 1a, b). Genetic data of the subjects composing this cluster was also checked for the presence of duplicates and cryptic relatedness (identity by descent: $\hat{p} < 0.2$). Before performing the final principal component analysis within this European sample, genetic quality control (MAF > 0.02, call rate > 0.95, Hardy–Weinberg $P > 0.001$) was applied within each of the seven sub-samples separately. We also excluded SNPs within regions of long-range linkage disequilibrium as has been suggested in ref. [66]. The remaining autosomal SNPs of the combined sample were then pruned using PLINK (indep-pairwise command; window-size 200 SNPs, 5 SNP steps, $r^2 < 0.2$). We next used SMARTPCA[65] to estimate the PCs of genetic variation within this broad European cluster (Supplementary Fig. 1a, b). The resulting first two PCs were used as parameters for genetic similarity.

After these steps, $n = 2{,}739$ subjects of European ancestry remained for further selection of pairs of subjects from the high- and low extreme groups that: (1) have a similar genetic background; (2) have the same sex; (3) were investigated at a similar time point; (4) are of similar age; (5) have similar smoking behaviour. The latter matching criterion was included given the borderline significant correlation between smoking status and being a member of the high or low extreme performance group ($P = 0.08$ before matching). Matching was done separately for females and males with the library Matching (Version 4.8–3.4) in R[67]. Membership in the low or high extreme group was used as treatment vector. Matching was done without replacement, the sequence of the subjects entering the matching procedure was chosen randomly. Time point of investigation, age, smoking behaviour and the two results of the first two PCs from the genetic similarity analysis were used as variables to match on. For each HES, the best-matching LES was identified, separately for females and males. Finally, these high extreme–low extreme pairs were randomly assigned on the plate for subsequent exome sequencing. In line with the circumstance that emotionally arousing information is often remembered at the expense of neutral background information[68], HES had significantly increased mean free-recall performance for aversive pictures ($P = 3 \times 10^{-17}$) and significantly, albeit orders of magnitude weaker, decreased mean free-recall performance for neutral pictures ($P = 1 \times 10^{-12}$) than LES (Supplementary Table 1). No difference in mean free-recall performance for positive pictures ($P = 0.6$) was observed between HES and LES. Overall memory capacity was very similar between extreme groups ($P = 0.5$). No significant group difference in arousal and valence ratings for any of the 3 picture categories was observed (all comparisons: $P > 0.05$).

Exome sequencing: blood sampling, DNA isolation and related quality controls. Blood samples were collected between midday and evening (mean time of day: 14:30, range 13:00–20.00) using BD Vacutainer Push Button blood collection sets and 10.0-mL BD Vacutainer Plus plastic whole blood tubes, BD Hemogard closure with spray-coated K_2EDTA (Becton, Dickinson and Company, New Jersey, USA). Standard haematological analysis, including blood-cell counting, was performed with a Sysmex pocH-100i Automated Hematology Analyzer (Sysmex Co, Kobe, Japan.) DNA was isolated from the remaining fraction, upon plasma removal. The isolation was performed with the QIAmp Blood Maxi Kit (Qiagen AG, Hilden, Germany), using the recommended spin protocol. In order to obtain high purity DNA, isolated DNA samples were additionally re-purified. For this purpose, 2 µg of DNA isolated with the QIAmp/Oragene procedure, was incubated overnight at 50 °C with proteinase K (lysis buffer: 30 mM TrisCl, 10 mM EDTA, 1% SDS pH 8.0, 150 ng µl^{-1} Proteinase K), agitated by gentle orbital shaking. Next, DNA was purified using the Genomic DNA Clean & Concentrate Kit (Zymo Research, Irvine, California, USA). The quality and concentration of DNA were assessed using gel electrophoresis, NanoDrop ND-1000 (Thermo Scientific, Waltham, Massachusetts, USA) and fluorometry measurements (Qubit dsDNA BR Assay Kit; Invitrogen, Carlsbad, California, USA), respectively. DNA samples of high integrity and purity were further normalized to 24 ng µl^{-1} and randomly assigned to a 96-well plate for library preparation.

Exome sequencing: library preparation. Quality checks of the genomic DNA samples and intermediate products of the library preparation (efficiency of DNA fragmentation, pre- and post-capture libraries) were done with the Fragment Analyzer, using the DNF-467 Genomic DNA 50 kb Analysis Kit and DNF-473 Standard Sensitivity NGS Fragment Analysis Kit, respectively (Advanced Analytical Technologies, Ankeny, Iowa, USA). Library preparation for WES was performed with the Agilent SureSelectXT Human All Exon V5+UTR kit using the SureSelectXT automated target enrichment for Illumina paired-end multiplexed sequencing protocol on the Agilent NGS workstation, option B (Agilent Technologies Inc, Santa Clara, California, USA). In brief, 200 ng of genomic DNA was fragmented with the Covaris E220 focused-ultrasonicator (Covaris Inc, Woburn, Massachusetts, USA), with the following settings: duty factor: 10%; peak incident power: 175; cycles per burst: 200; treatment time: 360 s; bath temperature: 4–8 °C. The target DNA fragment size was 150–200 bp. After quality assessment the libraries were further prepared by using the SureSelect XT Library Prep Kit ILM (Agilent, USA; SureSelectXT target enrichment system for Illumina paired-end multiplexed sequencing library protocol version B3). AMPure XP bead purification was always implemented between the library preparation steps. First, the 3′ ends of the DNA fragments were adenylated, followed by paired-end adaptor ligation and adaptor-ligated library amplification. After library quality assessment, samples were hybridized to the target-specific capture library and the hybridized DNA was captured with streptavidin-coated beads. The libraries with 8-bp indexing primers were then amplified, assayed for quality and quantity and finally pooled for multiplexed sequencing.

Whole-exome sequencing. Libraries were clustered on the Illumina cBot cluster station (HiSeq PE Cluster Kit v4). WES was done on an Illumina HiSeq 2500 machine (paired-end reads, 101 bp per read). The libraries were mixed in 4 pools ($3 \times 24 + 1 \times 22$). Each pool was sequenced in 6 lanes. A fifth pool was mixed with 27 of the samples and this Pool 5 was sequenced in an extra lane. For each sample, over 12 Gb of sequence were generated.

The SureSelectXT Human All Exon V5+UTR kit (Agilent) used in this study targets 359,555 exons in 21,522 genes (that is, 75 Mb of sequence) included in the following databases: CCDS, RefSeq, GENCODE, miRBase, TCGA and UCSC. The sequence of each sample was mapped to the hg19 human reference genome, downloaded from http://genome.ucsc.edu, using BWA 0.7.12 (Burrow–Wheeler Alignment)[69]. Duplicates were flagged with Picard 1.135 (http://picard.sourceforge.net). Analysis of coverage was done with Picard CalculateHSmetrics and Bedtools[70] version 2.18.1. Finally, 98% of the target bases had a coverage equal or greater than 20× and approximately 50% of target bases had 100× coverage (Bedtools; Supplementary Fig. 6). Base quality score recalibration and local realignment around indels was done with GATK[71] version 3.4-0 following the standard GATK protocol[72]. Single nucleotide variants (SNVs) were called with the Haplotype Caller. No padding was used for variant calling outside non-target regions to prevent false-positive SNV calls. Following the recommendation of ref. [73], variant quality score recalibration was used. We chose 99% sensitivity for a variant to be 'true' on the basis of an adaptive error model and filtered out false-positive variants using this threshold.

Exome sequencing: callset quality control. The final callset was evaluated using variant-level concordance (that is, the percentage of variants in the study sample that matched a defined gold standard) and genotype concordance (that is, the percentage of variants that matched the genotypes derived from the same samples using a different genotyping technique). After defining dbSNP 138.b37 as the gold standard, we ran the VariantEval toolkit of GATK. The variant-level concordance rate between our callset and dbSNP was high (98.33%). Two genotype concordance measures can be derived from comparing sequencing data with array data: non-reference sensitivity (NRS, that is, the rate at which non-reference alleles in the array data are also identified in the sequenced genotypes) and the non-reference discrepancy (NRD; that is, the rate at which sequenced genotypes differ from array genotypes) rate. We used the GATK toolkit GenotypeConcordance for these calculations. 18,709 bi-allelic overlapping variants were identified for both WES data and array genotype data of the Affymetrix 6.0 human SNP array. NRS was 97.5%, suggesting a high sensitivity for common variants, and NRD was 2.4%. The ratio between transitions to transversions (T_i/T_v ratio) was 2.61, which matched the expected value of 2.5–2.8 well, for sequences covering both exonic and non-exonic 3′ and 5′ UTRs[74], like the SureSelectXT Human All Exon V5+UTR kit (Agilent), which targets 75 Mb of the human genome. We furthermore checked the rate of novel missense SNPs (that is, not included in dbSNP 138.b37) in our callset. The mean over all samples was low ($n = 57.8$), suggesting a low number of false-positive calls. Another quality indicator is the het/hom ratio (that is, the ratio between heterozygous and homozygous

non-reference variants). In our callset, the het/hom ratio, which is expected to be approximately 1.5 for European populations[75,76], was 1.57 for all SNPs and 1.54 for known SNPs (that is, dbSNP SNPs). Variant call format data were annotated with the reference genome GRCh37.75 using SnpEff software version 4.1l (build 2015-10-03)[77].

Pyrosequencing. Targeted genotyping of *TROVE2* SNP rs72740218 was done with pyrosequencing on a PyroMark ID System. The following primers were used: 5′-TACTAAACTAGCTCTTGGGGAAAT-3′ (forward primer, 5′-biotinylated), 5′-CAAAGCAAAACTATTTTACAGTGT-3′ (reverse primer), 5′-CAAAAAGTTCTCTATTAGAT-3′ (sequencing primer). $n = 2{,}684$ subjects were successfully genotyped for rs72740218. One-sided genetic-association testing (additive model) was used for hypothesis confirmation purposes. Researcher team members involved in genotyping were blinded to group allocation.

Burden testing. Genotype–phenotype associations were calculated with PLINK/SEQ version 0.10 (https://atgu.mgh.harvard.edu/plinkseq/). We calculated gene-based tests falling into two categories: burden tests[78] and adaptive burden tests (variable threshold test)[79]. Burden tests perform optimally when assuming that a large proportion of variants are causal and the effects are in the same direction. Adaptive burden tests, which use data-adaptive weights or thresholds, are thought to be more robust than burden tests that use fixed weights or thresholds[80]. Following power analyses done in studies of phenotypic extremes with similar sample size as in the present one, we set the empirical MAF as MAF ≤ 0.125 to avoid eliminating variants enriched to high frequency in the extremes[21]. To correct for multiple testing we used the *i*-stat statistic (that is, the smallest possible empirical *P* value of a gene), which is implemented in PLINKSeq. According to previous recommendations[15], the *i*-stat threshold was set to <0.001. Burden-test-derived significances were then Bonferroni-corrected for the number of genes with an *i*-stat below this threshold.

fMRI experiment. Subjects were right-handed, free of any lifetime neurological or psychiatric illness, and did not take any medication (except hormonal contraceptives) at the time of the experiment, which was approved by the ethics committee of the Cantons of Basel-Stadt and Basel-Landschaft. Written, informed consent was obtained from all subjects before participation. After receiving general information about the study and giving their informed consent, participants were instructed and then trained on the picture task they later performed in the scanner. After training, they were positioned in the scanner. The participants received earplugs and headphones to reduce scanner noise. Their head was fixated in the coil using small cushions, and they were told not to move their heads. Functional magnetic resonance images were acquired during the performance of the picture task in two separate sessions (total scanning time, approximately 30 min). After finishing the tasks, participants left the scanner and were taken to a separate room for free recall of the pictures. Finally, participants filled out questionnaires, gave saliva for genotype analysis and were debriefed. The total length of the experimental procedure was approximately 3 hours. We excluded 54 subjects from the fMRI experiment. Reasons for exclusion were defined as follows: corrupted or missing data ($n = 40$), subjects recalling less than one picture in one of the valence categories ($n = 10$), failed co-registration ($n = 4$).

Measurements were performed on a Siemens Magnetom Verio 3 T wholebody MR unit equipped with a twelve-channel head coil. Functional time series were acquired with a single-shot echo-planar sequence using parallel imaging (GRAPPA). We used the following acquisition parameters: TE (echo time) = 35 ms, FOV (field of view) = 22 cm, acquisition matrix = 80 × 80, interpolated to 128 × 128, voxel size: 2.75 × 2.75 × 4 mm^3, GRAPPA acceleration factor $R = 2.0$. Using a midsagittal scout image, 32 contiguous axial slices were placed along the anterior–posterior commissure (AC–PC) plane covering the entire brain with a TR = 3,000 ms ($\alpha = 82°$). The first two acquisitions were discarded owing to T_1 saturation effects. A high-resolution T_1-weighted anatomical image was acquired using a magnetization prepared gradient echo sequence (MPRAGE, TR = 2,000 ms; TE = 3.37 ms; TI = 1,000 ms; flip angle = 8; 176 slices; FOV = 256 mm; voxel size = 1 × 1 × 1 mm^3).

Preprocessing and data analysis was performed using SPM8 (Statistical Parametric Mapping, Wellcome Department of Cognitive Neurology, London, UK; http://www.fil.ion.ucl.ac.uk/spm/) implemented in Matlab (Mathworks Inc., Natick, Massachusetts, USA). Volumes were slice-time corrected to the first slice and realigned to the first acquired volume. Both functional and structural images were spatially normalized by applying DARTEL, which leads to an improved registration between subjects. Normalization incorporated the following steps: (1) Structural images of each subject were segmented using the 'New Segment' procedure in SPM8. (2) The resulting gray- and white-matter images were used to derive a study-specific group template. The template was computed from a subpopulation of 1,000 subjects from this study. (3) An affine transformation was applied to map the group template to MNI space. (4) Subject-to-template and template-to-MNI transformations were combined to map the functional images to MNI space. The functional images were smoothed with an isotropic 8 mm full width at half maximum Gaussian filter. Serial correlations were removed using a first-order autoregressive model. A high-pass filter (128 s) was applied to remove low-frequency noise.

Normalized functional images were masked using information from their respective T_1 anatomical file as follows: a partial volume effect file obtained from the SPM-VBM8 toolbox (http://dbm.neuro.uni-jena.de/vbm8/) was used as a starting point to define the brain mask. This volume represents the three-tissue classification results of the segmentation process (GM, WM, CSF), with two additional mixed classes (GM–WM, GM–CSF). It was binarized, dilated and eroded with a 3 × 3 × 3 voxels kernel using fslmaths (FSL) to fill in potential small holes in the mask. The previously computed DARTEL flowfield was used to normalize the brain mask to MNI space, at the spatial resolution of the functional images. The mask was finally thresholded at 10% and applied to the normalized functional images. Consequently, the implicit intensity-based masking threshold usually that was employed to compute a brain mask from the functional data during the first level specification (by default fixed at mask.thresh = 0.8) was not needed any longer and set to a lower value of 0.05.

For each subject, analyses were conducted in the framework of the general linear model. Regressors, which modelled the onset and duration of stimulus events, were convolved with a canonical haemodynamic response function. More precisely, the model comprised regressors for button presses that were modelled as stick/delta functions, picture presentations that were modelled with an epoch/boxcar function (duration: 2.5 s), and rating scales that were modelled with an epoch/boxcar function of variable duration (depending on when the subsequent button press occured). Six movement parameters were also entered as nuisance covariates. Pictures accounting for possible primacy and recency effects were modelled separately.

Brain activity contrasts were calculated individually using a fixed-effects model (first level analysis). The following contrasts were specified: (1) brain activity related to memory encoding of aversive stimuli compared to neutral stimuli, independent of whether the information was later recalled or not (aversive pictures − neutral pictures); (2) brain activity related to successful memory encoding of aversive stimuli compared to neutral stimuli (aversive pictures recalled − aversive pictures not recalled) − (neutral pictures recalled − neutral pictures not recalled); (3) differences in brain activity between successful memory encoding of aversive compared to positive stimuli (aversive pictures recalled − aversive pictures not recalled) − (positive pictures recalled − positive pictures not recalled); (4) brain activity related to successful memory encoding of positive stimuli compared to neutral stimuli (positive pictures recalled − positive pictures not recalled) − (neutral pictures recalled − neutral pictures not recalled). The resulting contrast parameters were then used for genotype-dependent analyses in a random-effects model (second level analysis). Specifically, we used a regression model to analyse differences in brain activity, whereas the number of alleles served as covariate in our analysis. We controlled for the effects of sex and age by including them as covariates. Significance peaks were assigned to anatomical labels based on the Harvard–Oxford Cortical Structural Atlas[81]. Brodmann areas are given based on ref. [82].

Rwanda sample. Study participants were survivors of the Rwandan genocide who were living as refugees in the Nakivale refugee settlement. As the Nakivale refugee settlement has grown over the last decade and is spread over a large area, participants were sampled proportionally to the population size from each zone. To exclude genetic relatives in the samples, only one person per household was interviewed. Interviewers had been trained to detect current alcohol abuse and acute psychotic symptoms; candidates exhibiting these signs were excluded. All subjects had experienced highly aversive traumatic situations (including life-threatening situations) and were examined in 2006/2007 by psychologists of the University of Konstanz with the help of trained interpreters, or by intensely trained local interviewers using a structured interview that was based on the Post-traumatic Diagnostic Scale[28] with the help of trained interpreters. This procedure has been validated for implementation in East-African crisis regions[83]. Traumatic events were assessed with a checklist of 36 war- and non-war-related traumatic event types, such as, injury by weapon, rape, accident, which have also been employed in previous studies[7]. Traumatic load was estimated by assessing the number of different traumatic event types experienced or witnessed. This measure has been shown to be more reliable than assessing the frequency of traumatic events[84]. The procedures and study protocols were approved by the Ethics Committees of the University of Konstanz, Germany, and the Mbarara University of Science and Technology (MUST), Mbarara, Uganda.

Instruments were translated into Kinyarwanda using several steps of translations, blind back-translations, and subsequent corrections by independent groups of translators. Following the translations, the psychometric properties of the translated scales were investigated in a validation study including a retest spanning a two-week period and a cross-validation with expert rating[85]. To avoid known ceiling effects (that is, the phenomenon that almost everybody will develop PTSD at extreme levels of trauma load)[86,87], subjects were selected to have experienced no more than 16 different traumatic event types. Subjects that lacked sufficient data for the estimation of the prevalence of lifetime PTSD were excluded from this study. The significance level of genetic associations with traumatic memory and PTSD risk was calculated by performing forward and backward linear and logistic

regressions, respectively, under inclusion of age, sex, trauma load, and—wherever indicated—occurrence of specific traumatic event types. The significance level of genetic associations with trauma load and the occurrence of specific traumatic events was calculated by performing forward and backward linear and logistic regressions, respectively, under inclusion of age and sex. The significance level of genetic associations with age and sex was calculated by performing linear regressions and χ^2 tests, respectively. Saliva samples were obtained from each person using the Oragen DNA Self-Collection Kit (DNA Genotek, Ottawa, Ontario, Canada). DNA was extracted from saliva using standard protocols.

Data availability. The data that support the findings of this study are available from the corresponding author upon request.

Received 7 October 2016; accepted 27 February 2017; published 27 March 2017

References

1. McGaugh, J. L. in *Memory and Emotion* (Weidenfeld and Nicolson, 2003).
2. Pitman, R. K. Post-traumatic stress disorder, hormones, and memory. *Biol. Psychiatry* **26,** 221–223 (1989).
3. Phelps, E. A. & LeDoux, J. E. Contributions of the amygdala to emotion processing: from animal models to human behavior. *Neuron* **48,** 175–187 (2005).
4. Brewin, C. R., Dalgleish, T. & Joseph, S. A dual representation theory of posttraumatic stress disorder. *Psychol. Rev.* **103,** 670–686 (1996).
5. Brewin, C. R., Gregory, J. D., Lipton, M. & Burgess, N. Intrusive images in psychological disorders: characteristics, neural mechanisms, and treatment implications. *Psychol. Rev.* **117,** 210–232 (2010).
6. de Quervain, D. J. *et al.* A deletion variant of the α2b-adrenoceptor is related to emotional memory in Europeans and Africans. *Nat. Neurosci.* **10,** 1137–1139 (2007).
7. de Quervain, D. J. *et al.* PKCα is genetically linked to memory capacity in healthy subjects and to risk for posttraumatic stress disorder in genocide survivors. *Proc. Natl Acad. Sci. USA* **109,** 8746–8751 (2012).
8. Todd, R. M. *et al.* Deletion variant in the *ADRA2B* gene increases coupling between emotional responses at encoding and later retrieval of emotional memories. *Neurobiol. Learn Mem.* **112,** 222–229 (2014).
9. Todd, R. M., Palombo, D. J., Levine, B. & Anderson, A. K. Genetic differences in emotionally enhanced memory. *Neuropsychologia* **49,** 734–744 (2011).
10. Papassotiropoulos, A. *et al.* Human genome-guided identification of memory-modulating drugs. *Proc. Natl Acad. Sci. USA* **110,** E4369–E4374 (2013).
11. Ackermann, S., Heck, A., Rasch, B., Papassotiropoulos, A. & de Quervain, D. J. The BclI polymorphism of the glucocorticoid receptor gene is associated with emotional memory performance in healthy individuals. *Psychoneuroendocrinology* **38,** 1203–1207 (2013).
12. Gibbs, A. A., Bautista, C. E., Mowlem, F. D., Naudts, K. H. & Duka, T. Alpha 2B adrenoceptor genotype moderates effect of reboxetine on negative emotional memory bias in healthy volunteers. *J. Neurosci.* **33,** 17023–17028 (2013).
13. Cheung, J. & Bryant, R. A. FKBP5 risk alleles and the development of intrusive memories. *Neurobiol. Learn. Mem.* **125,** 258–264 (2015).
14. Wilker, S., Elbert, T. & Kolassa, I.-T. The downside of strong emotional memories: how human memory-related genes influence the risk for posttraumatic stress disorder—a selective review. *Neurobiol. Learn. Mem.* **112,** 75–86 (2014).
15. Kiezun, A. *et al.* Exome sequencing and the genetic basis of complex traits. *Nat. Genet.* **44,** 623–630 (2012).
16. Wang, Z., Liu, X., Yang, B. Z. & Gelernter, J. The role and challenges of exome sequencing in studies of human diseases. *Front. Genet.* **4,** 160 (2013).
17. Peloso, G. M. *et al.* Phenotypic extremes in rare variant study designs. *Eur. J. Hum. Genet.* **24,** 924–930 (2016).
18. Li, D., Lewinger, J. P., Gauderman, W. J., Murcray, C. E. & Conti, D. Using extreme phenotype sampling to identify the rare causal variants of quantitative traits in association studies. *Genet. Epidemiol.* **35,** 790–799 (2011).
19. Auer, P. L. & Lettre, G. Rare variant association studies: considerations, challenges and opportunities. *Genome Med.* **7,** 16 (2015).
20. Guey, L. T. *et al.* Power in the phenotypic extremes: a simulation study of power in discovery and replication of rare variants. *Genet. Epidemiol.* **35,** 236–246 (2011).
21. Emond, M. J. *et al.* Exome sequencing of extreme phenotypes identifies *DCTN4* as a modifier of chronic *Pseudomonas aeruginosa* infection in cystic fibrosis. *Nat. Genet.* **44,** 886–889 (2012).
22. Lee, S. *et al.* Optimal unified approach for rare-variant association testing with application to small-sample case-control whole-exome sequencing studies. *Am. J. Hum. Genet.* **91,** 224–237 (2012).
23. Ramasamy, A. *et al.* Genetic variability in the regulation of gene expression in ten regions of the human brain. *Nat. Neurosci.* **17,** 1418–1428 (2014).
24. Trabzuni, D. *et al.* Quality control parameters on a large dataset of regionally dissected human control brains for whole genome expression studies. *J. Neurochem.* **119,** 275–282 (2011).
25. LaBar, K. S. & Cabeza, R. Cognitive neuroscience of emotional memory. *Nat. Rev. Neurosci.* **7,** 54–64 (2006).
26. Buchanan, T. W. Retrieval of emotional memories. *Psychol. Bull.* **133,** 761–779 (2007).
27. Stein, M. B., Jang, K. L., Taylor, S., Vernon, P. A. & Livesley, W. J. Genetic and environmental influences on trauma exposure and posttraumatic stress disorder symptoms: a twin study. *Am. J. Psychiatry* **159,** 1675–1681 (2002).
28. Foa, E. B., Cashman, L., Jaycox, L. & Perry, K. The validation of a self-report measure of posttraumatic stress disorder: The posttraumatic diagnostic scale. *Psychol. Assess.* **9,** 445–451 (1997).
29. Hawrylycz, M. J. *et al.* An anatomically comprehensive atlas of the adult human brain transcriptome. *Nature* **489,** 391–399 (2012).
30. Speir, M. L. *et al.* The UCSC genome browser database: 2016 update. *Nucleic Acids Res.* **44,** D717–D725 (2016).
31. UniProt, C. UniProt: a hub for protein information. *Nucleic Acids Res.* **43,** D204–D212 (2015).
32. Etkin, A., Egner, T. & Kalisch, R. Emotional processing in anterior cingulate and medial prefrontal cortex. *Trends Cogn. Sci.* **15,** 85–93 (2011).
33. Murty, V. P., Ritchey, M., Adcock, R. A. & LaBar, K. S. fMRI studies of successful emotional memory encoding: a quantitative meta-analysis. *Neuropsychologia* **48,** 3459–3469 (2010).
34. Thomaes, K. *et al.* Increased anterior cingulate cortex and hippocampus activation in complex PTSD during encoding of negative words. *Soc. Cogn. Affect. Neurosci.* **8,** 190–200 (2013).
35. Lanius, R. A. *et al.* Emotion modulation in PTSD: clinical and neurobiological evidence for a dissociative subtype. *Am. J. Psychiatry* **167,** 640–647 (2010).
36. Schulte-Pelkum, J., Fritzler, M. & Mahler, M. Latest update on the Ro/SS-A autoantibody system. *Autoimmun. Rev.* **8,** 632–637 (2009).
37. Alspaugh, M. & Maddison, P. Resolution of the identity of certain antigen–antibody systems in systemic lupus erythematosus and Sjogren's syndrome: an interlaboratory collaboration. *Arthritis Rheum.* **22,** 796–798 (1979).
38. Clark, G., Reichlin, M. & Tomasi, T. B. Jr. Characterization of a soluble cytoplasmic antigen reactive with sera from patients with systemic lupus erythmatosus. *J. Immunol.* **102,** 117–122 (1969).
39. Hung, T. *et al.* The Ro60 autoantigen binds endogenous retroelements and regulates inflammatory gene expression. *Science* **350,** 455–459 (2015).
40. O'Donovan, A. *et al.* Elevated risk for autoimmune disorders in Iraq and Afghanistan veterans with posttraumatic stress disorder. *Biol. Psychiatry* **77,** 365–374 (2015).
41. Stein, M. B. *et al.* Genome-wide association studies of posttraumatic stress disorder in 2 cohorts of US army soldiers. *JAMA Psychiatry* **73,** 695–704 (2016).
42. Eraly, S. A. *et al.* Assessment of plasma C-reactive protein as a biomarker of posttraumatic stress disorder risk. *JAMA Psychiatry* **71,** 423–431 (2014).
43. Michopoulos, V. *et al.* Association of *CRP* genetic variation and CRP level with elevated PTSD symptoms and physiological responses in a civilian population with high levels of trauma. *Am. J. Psychiatry* **172,** 353–362 (2015).
44. Smith, A. K. *et al.* Differential immune system DNA methylation and cytokine regulation in post-traumatic stress disorder. *Am. J. Med. Genet. B Neuropsychiatr. Genet.* **156B,** 700–708 (2011).
45. Lindqvist, D. *et al.* Proinflammatory milieu in combat-related PTSD is independent of depression and early life stress. *Brain Behav. Immun.* **42,** 81–88 (2014).
46. Louveau, A. *et al.* Structural and functional features of central nervous system lymphatic vessels. *Nature* **523,** 337–341 (2015).
47. Derecki, N. C. *et al.* Regulation of learning and memory by meningeal immunity: a key role for IL-4. *J. Exp. Med.* **207,** 1067–1080 (2010).
48. Filiano, A. J. *et al.* Unexpected role of interferon-γ in regulating neuronal connectivity and social behaviour. *Nature* **535,** 425–429 (2016).
49. Kilaru, V. *et al.* Genome-wide gene-based analysis suggests an association between Neuroligin 1 (*NLGN1*) and post-traumatic stress disorder. *Transl. Psychiatry* **6,** e820 (2016).
50. Ashley-Koch, A. E. *et al.* Genome-wide association study of posttraumatic stress disorder in a cohort of Iraq–Afghanistan era veterans. *J. Affect. Disord.* **184,** 225–234 (2015).
51. Nievergelt, C. M. *et al.* Genomic predictors of combat stress vulnerability and resilience in U.S. marines: a genome-wide association study across multiple ancestries implicates *PRTFDC1* as a potential PTSD gene. *Psychoneuroendocrinology* **51,** 459–471 (2015).
52. Almli, L. M. *et al.* A genome-wide identified risk variant for PTSD is a methylation quantitative trait locus and confers decreased cortical activation to fearful faces. *Am. J. Med. Genet. B Neuropsychiatr. Genet.* **168B,** 327–336 (2015).

53. Logue, M. W. *et al.* A genome-wide association study of post-traumatic stress disorder identifies the retinoid-related orphan receptor alpha (*RORA*) gene as a significant risk locus. *Mol. Psychiatry* **18,** 937–942 (2013).
54. Xie, P. *et al.* Genome-wide association study identifies new susceptibility loci for posttraumatic stress disorder. *Biol. Psychiatry* **74,** 656–663 (2013).
55. Guffanti, G. *et al.* Genome-wide association study implicates a novel RNA gene, the lincRNA *AC068718.1*, as a risk factor for post-traumatic stress disorder in women. *Psychoneuroendocrinology* **38,** 3029–3038 (2013).
56. Logue, M. W. *et al.* The psychiatric genomics consortium posttraumatic stress disorder workgroup: posttraumatic stress disorder enters the age of large-scale genomic collaboration. *Neuropsychopharmacology* **40,** 2287–2297 (2015).
57. Rangaraju, S. *et al.* Mood, stress and longevity: convergence on *ANK3*. *Mol. Psychiatry* **21,** 1037–1049 (2016).
58. Papassotiropoulos, A. & de Quervain, D. J. Failed drug discovery in psychiatry: time for human genome-guided solutions. *Trends Cogn. Sci.* **19,** 183–187 (2015).
59. Lang, P. J., Bradley, M. M. & Cuthbert, B. N. *International Affective Pictures System (IAPS): Affective Ratings of Pictures and Instruction Manual* (Univ. Florida, 2008).
60. Wood, A. R. *et al.* Defining the role of common variation in the genomic and biological architecture of adult human height. *Nat. Genet.* **46,** 1173–1186 (2014).
61. Locke, A. E. *et al.* Genetic studies of body mass index yield new insights for obesity biology. *Nature* **518,** 197–206 (2015).
62. Heck, A. *et al.* Genetic analysis of association between calcium signaling and hippocampal activation, memory performance in the young and old, and risk for sporadic Alzheimer disease. *JAMA Psychiatry* **72,** 1029–1036 (2015).
63. Heck, A. *et al.* Converging genetic and functional brain imaging evidence links neuronal excitability to working memory, psychiatric disease, and brain activity. *Neuron* **81,** 1203–1213 (2014).
64. Hauer, D. *et al.* Relationship of a common polymorphism of the glucocorticoid receptor gene to traumatic memories and posttraumatic stress disorder in patients after intensive care therapy. *Crit. Care Med.* **39,** 643–650 (2011).
65. Price, A. L. *et al.* Principal components analysis corrects for stratification in genome-wide association studies. *Nat. Genet.* **38,** 904–909 (2006).
66. Price, A. L. *et al.* Long-range LD can confound genome scans in admixed populations. *Am. J. Hum. Genet.* **83,** 132–135 (2008); author reply **83,** 135–139 (2008).
67. Sekhon, J. S. Multivariate and propensity score matching software with automated balance optimization: the matching package for R. *J. Stat. Softw.* **42,** 1–52 (2011).
68. Reisberg, D. & Heuer, F. in *Memory and Emotion* (eds Reisberg, D. & Hertel, P.) 3–40 (Oxford Univ. Press, 2004).
69. Li, H. & Durbin, R. Fast and accurate short read alignment with Burrows–Wheeler transform. *Bioinformatics* **25,** 1754–1760 (2009).
70. Quinlan, A. R. & Hall, I. M. BEDTools: a flexible suite of utilities for comparing genomic features. *Bioinformatics* **26,** 841–842 (2010).
71. McKenna, A. *et al.* The genome analysis toolkit: a MapReduce framework for analyzing next-generation DNA sequencing data. *Genome Res.* **20,** 1297–1303 (2010).
72. Van der Auwera, G. A. *et al.* From FastQ data to high confidence variant calls: the Genome Analysis Toolkit best practices pipeline. *Curr. Protoc. Bioinformatics* **43,** 11.10.1–11.10.33 (2013).
73. DePristo, M. A. *et al.* A framework for variation discovery and genotyping using next-generation DNA sequencing data. *Nat. Genet.* **43,** 491–498 (2011).
74. Guo, Y., Ye, F., Sheng, Q., Clark, T. & Samuels, D. C. Three-stage quality control strategies for DNA re-sequencing data. *Brief. Bioinform.* **15,** 879–889 (2014).
75. McKernan, K. J. *et al.* Sequence and structural variation in a human genome uncovered by short-read, massively parallel ligation sequencing using two-base encoding. *Genome Res.* **19,** 1527–1541 (2009).
76. Schuster, S. C. *et al.* Complete Khoisan and Bantu genomes from southern Africa. *Nature* **463,** 943–947 (2010).
77. Cingolani, P. *et al.* A program for annotating and predicting the effects of single nucleotide polymorphisms, SnpEff: SNPs in the genome of *Drosophila melanogaster* strain w^{1118}; iso-2; iso-3. *Fly* **6,** 80–92 (2012).
78. Madsen, B. E. & Browning, S. R. A groupwise association test for rare mutations using a weighted sum statistic. *PLoS Genet.* **5,** e1000384 (2009).
79. Price, A. L. *et al.* Pooled association tests for rare variants in exon-resequencing studies. *Am. J. Hum. Genet.* **86,** 832–838 (2010).
80. Lee, S., Abecasis, G. R., Boehnke, M. & Lin, X. Rare-variant association analysis: study designs and statistical tests. *Am. J. Hum. Genet.* **95,** 5–23 (2014).
81. Desikan, R. S. *et al.* An automated labeling system for subdividing the human cerebral cortex on MRI scans into gyral based regions of interest. *Neuroimage* **31,** 968–980 (2006).
82. Damasio, H & Damasio, A. R. *Lesion Analysis in Neuropsychology*, (Oxford Univ. Press, 1989).
83. Ertl, V. *et al.* Validation of a mental health assessment in an African conflict population. *Psychol. Assess.* **22,** 318–324 (2010).
84. Wilker, S. *et al.* How to quantify exposure to traumatic stress? Reliability and predictive validity of measures for cumulative trauma exposure in a post-conflict population. *Eur. J. Psychotraumatol.* **6,** 28306 (2015).
85. Onyut, L. P. *et al.* Trauma, poverty and mental health among Somali and Rwandese refugees living in an African refugee settlement — an epidemiological study. *Confl. Health* **3,** 6 (2009).
86. Kolassa, I.-T., Kolassa, S., Ertl, V., Papassotiropoulos, A. & De Quervain, D. J. The risk of posttraumatic stress disorder after trauma depends on traumatic load and the catechol-o-methyltransferase Val(158)Met polymorphism. *Biol. Psychiatry* **67,** 304–308 (2010).
87. Neuner, F. *et al.* Psychological trauma and evidence for enhanced vulnerability for posttraumatic stress disorder through previous trauma among West Nile refugees. *BMC Psychiatry* **4,** 34 (2004).

Acknowledgements

This work was funded by the University of Basel, the Swiss National Science Foundation (grants 163434, 147570 and 159740 to D.J.-F.d.Q. and A.P.), the European Community's Seventh Framework Programme (FP7/2007–2013) under grant agreement 602450 (IMAGEMEND; grant to A.P. and D.J.-F.d.Q.), the Novartis Foundation for medical-biological Research (grant 15C219 to A.P.), and by the German Research Foundation (Deutsche Forschungsgemeinschaft; grants to I.-T.K. and T.El.).
The funders had no role in study design, data collection and analysis, decision to publish or preparation of the manuscript.

Author contributions

A.P., D.J.-F.d.Q., A.H., A.M. and M.F. conceived and designed the study. A.H., A.M., V.V., J.P., T.Eg., J.S., D.C., V.F., M.F., P.D., E.L., F.H., N.S., B.D.B., C.V., I.-T.K., S.W., T.El., D.J.-F.d.Q. and A.P. analysed the data. P.E., T.Se., T.Sc., C.B. and N.B. provided bioinformatic support. A.P., A.H. and D.J.-F.d.Q. wrote the manuscript. All authors reviewed and approved the final manuscript.

Additional information

Supplementary information is available for this paper.

Reprints and permissions information is available at www.nature.com/reprints.

Correspondence and requests for materials should be addressed to A.P. or A.H.

How to cite this article: Heck, A. *et al.*, Exome sequencing of healthy phenotypic extremes links *TROVE2* to emotional memory and PTSD. *Nat. Hum. Behav.* **1,** 0081 (2017).

Competing interests

The authors declare no competing interests.

6 Discussion

Large datasets of genetic variability, brain structure and brain function hold great potential for investigating the biological substrates of complex human behavior. There is an ever-growing expansion of diverse approaches for analyzing such datasets. In this PhD thesis, some of those approaches were discussed in the context of specific research questions. It was also illustrated that the initial analyses need to be incorporated into comprehensive analytical pipelines including multiple additional steps for insuring the robustness of findings, such as results replication and study-specific validation procedures. To this end, I presented two studies investigating the biological underpinnings of complex behavioral traits in healthy young adults using extensive genomics and brain imaging data, respectively. In both studies, the initial analyses were placed in the context of robust analytical pipelines for obtaining high-confidence findings.

In Study 1, we aggregated genome-wide SNP data to predefined gene sets and used inferential statistics to associate each gene set with depressive symptoms. Furthermore, we applied an appropriate correction for multiple testing, replicated the results in an independent sample and used imagining genetics to validate and extend our initial findings. Taking these steps, we found that the NCAM1 Interactions gene set is related to depressive symptoms and their structural brain correlates in healthy young individuals.

In Study 2, we decomposed the brain-wide voxel-wise brain activation contrast of looking at previously seen vs. new pictures into 12 independent components, which can also be considered as functional brain networks. Next, we evaluated recognition memory performance based on our 12 components using prediction analysis. Of note,

we used stable and reproducible data decomposition, insuring the robustness of the resulting components. Furthermore, we trained and tested our prediction model in different samples, avoiding overfitting and thus increasing the generalizability of our results. We found that recognition memory performance can be estimated with high accuracy based on our 12 robust components of brain activation.

In both studies, we substantially reduced the initial number of variables by restructuring our respective genome-wide and brain-wide datasets, but using different approaches. Namely, in Study 1 we relied on previous biological knowledge regarding the gene sets to which we aggregated our SNP data, while in Study 2 we obtained our brain activation components in a data-driven manner. The knowledge-guided creation of gene sets in Study 1 goes in line with the aim of the analysis, i.e., identifying biologically meaningful groups of genes relevant to our behavioral trait, and aids the interpretation of the results. Inevitably, it also makes the results dependent on the particular gene set annotations used (Wadi et al., 2016). In contrast, the decomposition of voxel-wise brain activation in Study 2 was driven by patterns found within our dataset, without being directed by previous findings.

Importantly, in Study 2 we also applied prediction, rather than the traditional inferential approach, increasing the generalizability of our findings. While predictive models are often associated with complex machine learning algorithms, e.g., deep neural networks, in Study 2 we opted for a linear model, having higher transparency and interpretability (Bzdok & Ioannidis, 2019). Interestingly, more complex pattern-learning algorithms do not necessarily outperform simpler predictive models in brain imaging research of complex cognitive traits (e.g. He et al., 2018). This may be due to the low signal-to-noise ratio intrinsic to brain imagining and cognitive measurements

and/or insufficient sample sizes for the application of highly complex algorithms (Arbabshirani et al., 2017; Bzdok & Ioannidis, 2019).

After establishing our analytical model, we took further steps to reduce the likelihood of false positive findings in each study. Unfortunately, false positive findings, reflected in failed replication of the results, are commonly encountered across scientific disciplines (Begley & Ellis, 2012; Ioannidis, 2005; Open Science Collaboration, 2015; Prinz et al., 2011). Some common issues contributing to false positive findings, such as overfitting and multiple testing, have been discussed in this PhD thesis, along with examples of how to overcome them.

Of note, the analytical pipelines presented in this thesis can also be further validated and extended upon. For example, it can be investigated to which extent certain findings depend on the specific analytical algorithms used. In Study 1, we conducted GSA using the Meta-Analysis Gene-set Enrichment of variaNT Associations (MAGENTA) software package (Segre et al., 2010). MAGENTA has been previously used for identification of robust gene set associations with complex behavioral traits in our samples (Heck et al., 2014, 2015). Nevertheless, one can also investigate if GSA results replicate with algorithms provided by different software packages such as INterval enRICHment analysis (INRICH) (Lee et al., 2012), Multi-marker Analysis of GenoMic Annotation (MAGMA) (de Leeuw et al., 2015) or Versatile Gene-based Association Study (VEGAS) 2 (Mishra & MacGregor, 2017). In Study 2, the dimensionality reduction of our brain imaging data was performed by ICA, which deconstructs the brain-wide fMRI signal into statistically independent components and has been used for identification of distinct brain networks in previous studies (Smith et al., 2009; Vanasse et al., 2018). However, alternative data-driven dimensionality reduction techniques can also be applied when working with highly dimensional

neuroscientific data. Some of them can be used prior to the prediction analysis, such as principal component analysis and factor analysis, and others as part of the prediction algorithm, like in the case of penalized regression (Huys et al., 2016). Given the variety of algorithms for utilization of large genomics and brain imaging data, repeating the initial analysis with well-chosen alternative analytical tools may further validate and/or add additional insight into the findings.

The generalizability of findings to more diverse populations and settings can also be further investigated. In Study 1, while we replicated our initial results in an independent sample with similar demographic characteristics, one could further test if our findings extend beyond healthy young adults of European ancestry. Although we did not find an association between the NCAM1 Interactions gene set and MDD diagnosis in a large case-control sample (Ripke et al., 2013), its association with continuously measured depressive symptoms in MDD and other (clinical) samples remains to be investigated. Using continuous measurements, rather than clinical cutoffs, can increase the power for identifying genetic variants implicated in polygenic traits (van der Sluis et al., 2013) and thus impact the GSA. Importantly, it remains to be seen if the identified genetic associations can be generalized to populations of non-European ancestry. While non-European samples have been mostly underrepresented in genomics studies, large GWASes including samples of diverse ancestry are becoming increasingly available (Hindorff et al., 2018; Popejoy & Fullerton, 2016; Wojcik et al., 2019). In Study 2, the prediction model remains to be externally validated. For example, one can investigate if the estimation of our model can be generalized to brain activation data obtained by a different scanner, while performing a comparable, but not identical task, in samples with different demographic characteristics or in clinical samples.

In summary, this PhD thesis has presented two studies in which large genomics and brain imaging datasets were successfully utilized for investigating the biological underpinnings of complex behavioral traits using genome-wide and brain-wide analyses. Importantly, the applied analyses were carefully tailored to the specific research question and integrated into robust pipelines for replication and validation of the initial results. These pipelines can also be further extended upon.

7 References

Amrhein, V., & Greenland, S. (2018). Remove, rather than redefine, statistical significance. *Nature Human Behaviour*, *2*(1), 4–4. https://doi.org/10.1038/s41562-017-0224-0

Arbabshirani, M. R., Plis, S., Sui, J., & Calhoun, V. D. (2017). Single subject prediction of brain disorders in neuroimaging: Promises and pitfalls. *NeuroImage*, *145*(Pt B), 137–165. PubMed. https://doi.org/10.1016/j.neuroimage.2016.02.079

Assary, E., Vincent, J. P., Keers, R., & Pluess, M. (2018). Gene-environment interaction and psychiatric disorders: Review and future directions. *Seminars in Cell & Developmental Biology*, *77*, 133–143. https://doi.org/10.1016/j.semcdb.2017.10.016

Ayuso-Mateos, J. L., Nuevo, R., Verdes, E., Naidoo, N., & Chatterji, S. (2010). From depressive symptoms to depressive disorders: The relevance of thresholds. *The British Journal of Psychiatry: The Journal of Mental Science*, *196*(5), 365–371. https://doi.org/10.1192/bjp.bp.109.071191

Basser, P. J. (1995). Inferring microstructural features and the physiological state of tissues from diffusion-weighted images. *NMR in Biomedicine*, *8*(7), 333–344.

Beaulieu, C. (2002). The basis of anisotropic water diffusion in the nervous system—A technical review. *NMR in Biomedicine*, *15*(7–8), 435–455. https://doi.org/10.1002/nbm.782

Beck, A. T., Steer, R. A., & Brown, G. K. (1996). Beck depression inventory-II. *San Antonio*, *78*(2), 490–498.

Begley, C. G., & Ellis, L. M. (2012). Raise standards for preclinical cancer research. *Nature*, *483*(7391), 531–533. https://doi.org/10.1038/483531a

Belliveau, J., Kennedy, D., McKinstry, R., Buchbinder, B., Weisskoff, R., Cohen, M., Vevea, J., Brady, T., & Rosen, B. (1991). Functional mapping of the human visual cortex by magnetic resonance imaging. *Science*, *254*(5032), 716. https://doi.org/10.1126/science.1948051

Benjamin, D. J., Berger, J. O., Johannesson, M., Nosek, B. A., Wagenmakers, E.-J., Berk, R., Bollen, K. A., Brembs, B., Brown, L., Camerer, C., Cesarini, D., Chambers, C. D., Clyde, M., Cook, T. D., De Boeck, P., Dienes, Z., Dreber, A., Easwaran, K., Efferson, C., … Johnson, V. E. (2018). Redefine statistical

significance. *Nature Human Behaviour*, *2*(1), 6–10. https://doi.org/10.1038/s41562-017-0189-z

Boekel, W., Wagenmakers, E.-J., Belay, L., Verhagen, J., Brown, S., & Forstmann, B. U. (2015). A purely confirmatory replication study of structural brain-behavior correlations. *Cortex*, *66*, 115–133. https://doi.org/10.1016/j.cortex.2014.11.019

Bogdan, R., Salmeron, B. J., Carey, C. E., Agrawal, A., Calhoun, V. D., Garavan, H., Hariri, A. R., Heinz, A., Hill, M. N., Holmes, A., Kalin, N. H., & Goldman, D. (2017). Imaging Genetics and Genomics in Psychiatry: A Critical Review of Progress and Potential. *Biological Psychiatry*, *82*(3), 165–175. https://doi.org/10.1016/j.biopsych.2016.12.030

Bressler, S. L., & Menon, V. (2010). Large-scale brain networks in cognition: Emerging methods and principles. *Trends in Cognitive Sciences*, *14*(6), 277–290. https://doi.org/10.1016/j.tics.2010.04.004

Brown, P. O., & Botstein, D. (1999). Exploring the new world of the genome with DNA microarrays. *Nature Genetics*, *21*(1), 33–37. https://doi.org/10.1038/4462

Bumgarner, R. (2013). Overview of DNA microarrays: Types, applications, and their future. *Current Protocols in Molecular Biology*, *Chapter 22*, Unit 22.1. https://doi.org/10.1002/0471142727.mb2201s101

Bycroft, C., Freeman, C., Petkova, D., Band, G., Elliott, L. T., Sharp, K., Motyer, A., Vukcevic, D., Delaneau, O., O'Connell, J., Cortes, A., Welsh, S., Young, A., Effingham, M., McVean, G., Leslie, S., Allen, N., Donnelly, P., & Marchini, J. (2018). The UK Biobank resource with deep phenotyping and genomic data. *Nature*, *562*(7726), 203–209. https://doi.org/10.1038/s41586-018-0579-z

Bzdok, D., & Ioannidis, J. P. A. (2019). Exploration, Inference, and Prediction in Neuroscience and Biomedicine. *Trends in Neurosciences*, *42*(4), 251–262. https://doi.org/10.1016/j.tins.2019.02.001

Carlesimo, G. A., Lombardi, M. G., Caltagirone, C., & Barban, F. (2015). Recollection and familiarity in the human thalamus. *Neuroscience and Biobehavioral Reviews*, *54*, 18–28. https://doi.org/10.1016/j.neubiorev.2014.09.006

Chee, M., Yang, R., Hubbell, E., Berno, A., Huang, X. C., Stern, D., Winkler, J., Lockhart, D. J., Morris, M. S., & Fodor, S. P. (1996). Accessing genetic

information with high-density DNA arrays. *Science (New York, N.Y.)*, *274*(5287), 610–614. https://doi.org/10.1126/science.274.5287.610

Chen, J. E., & Glover, G. H. (2015). Functional Magnetic Resonance Imaging Methods. *Neuropsychology Review*, *25*(3), 289–313. PubMed. https://doi.org/10.1007/s11065-015-9294-9

Chen, J. J., Roberson, P. K., & Schell, M. J. (2010). The false discovery rate: A key concept in large-scale genetic studies. *Cancer Control : Journal of the Moffitt Cancer Center*, *17*(1), 58–62. https://doi.org/10.1177/107327481001700108

Corvin, A., Craddock, N., & Sullivan, P. F. (2010). Genome-wide association studies: A primer. *Psychological Medicine*, *40*(7), 1063–1077. https://doi.org/10.1017/S0033291709991723

Coynel, D., Gschwind, L., Fastenrath, M., Freytag, V., Milnik, A., Spalek, K., Papassotiropoulos, A., & de Quervain, D. J.-F. (2017). Picture free recall performance linked to the brain's structural connectome. *Brain and Behavior*, *7*(7), e00721. https://doi.org/10.1002/brb3.721

Craig, D. W., Goor, R. M., Wang, Z., Paschall, J., Ostell, J., Feolo, M., Sherry, S. T., & Manolio, T. A. (2011). Assessing and managing risk when sharing aggregate genetic variant data. *Nature Reviews Genetics*, *12*(10), 730–736. https://doi.org/10.1038/nrg3067

Damoiseaux, J. S., Rombouts, S. A. R. B., Barkhof, F., Scheltens, P., Stam, C. J., Smith, S. M., & Beckmann, C. F. (2006). Consistent resting-state networks across healthy subjects. *Proceedings of the National Academy of Sciences of the United States of America*, *103*(37), 13848–13853. https://doi.org/10.1073/pnas.0601417103

Das, S., Forer, L., Schönherr, S., Sidore, C., Locke, A. E., Kwong, A., Vrieze, S. I., Chew, E. Y., Levy, S., McGue, M., Schlessinger, D., Stambolian, D., Loh, P.-R., Iacono, W. G., Swaroop, A., Scott, L. J., Cucca, F., Kronenberg, F., Boehnke, M., … Fuchsberger, C. (2016). Next-generation genotype imputation service and methods. *Nature Genetics*, *48*(10), 1284–1287. https://doi.org/10.1038/ng.3656

de Chastelaine, M., Mattson, J. T., Wang, T. H., Donley, B. E., & Rugg, M. D. (2016). The neural correlates of recollection and retrieval monitoring: Relationships with age and recollection performance. *NeuroImage*, *138*, 164–175. https://doi.org/10.1016/j.neuroimage.2016.04.071

de Leeuw, C. A., Mooij, J. M., Heskes, T., & Posthuma, D. (2015). MAGMA: generalized gene-set analysis of GWAS data. *PLoS Computational Biology*, *11*(4), e1004219.

de Leeuw, C. A., Neale, B. M., Heskes, T., & Posthuma, D. (2016). The statistical properties of gene-set analysis. *Nature Reviews Genetics*, *17*, 353.

de Quervain, D. J.-F., Kolassa, I.-T., Ackermann, S., Aerni, A., Boesiger, P., Demougin, P., Elbert, T., Ertl, V., Gschwind, L., Hadziselimovic, N., Hanser, E., Heck, A., Hieber, P., Huynh, K.-D., Klarhofer, M., Luechinger, R., Rasch, B., Scheffler, K., Spalek, K., … Papassotiropoulos, A. (2012). PKCalpha is genetically linked to memory capacity in healthy subjects and to risk for posttraumatic stress disorder in genocide survivors. *Proceedings of the National Academy of Sciences of the United States of America*, *109*(22), 8746–8751. https://doi.org/10.1073/pnas.1200857109

Egli, T., Coynel, D., Spalek, K., Fastenrath, M., Freytag, V., Heck, A., Loos, E., Auschra, B., Papassotiropoulos, A., de Quervain, D. J.-F., & Milnik, A. (2018). Identification of Two Distinct Working Memory-Related Brain Networks in Healthy Young Adults. *ENeuro*, *5*(1). https://doi.org/10.1523/ENEURO.0222-17.2018

Fastenrath, M., Coynel, D., Spalek, K., Milnik, A., Gschwind, L., Roozendaal, B., Papassotiropoulos, A., & de Quervain, D. J. F. (2014). Dynamic modulation of amygdala-hippocampal connectivity by emotional arousal. *The Journal of Neuroscience: The Official Journal of the Society for Neuroscience*, *34*(42), 13935–13947. PubMed. https://doi.org/10.1523/JNEUROSCI.0786-14.2014

Fornito, A., Harrison, B. J., Zalesky, A., & Simons, J. S. (2012). Competitive and cooperative dynamics of large-scale brain functional networks supporting recollection. *Proceedings of the National Academy of Sciences of the United States of America*, *109*(31), 12788–12793. https://doi.org/10.1073/pnas.1204185109

Fox, M. D., Snyder, A. Z., Vincent, J. L., Corbetta, M., Van Essen, D. C., & Raichle, M. E. (2005). The human brain is intrinsically organized into dynamic, anticorrelated functional networks. *Proceedings of the National Academy of Sciences of the United States of America*, *102*(27), 9673. https://doi.org/10.1073/pnas.0504136102

Franco, A. R., Mannell, M. V., Calhoun, V. D., & Mayer, A. R. (2013). Impact of analysis methods on the reproducibility and reliability of resting-state networks. *Brain Connectivity*, *3*(4), 363–374. https://doi.org/10.1089/brain.2012.0134

Freytag, V., Carrillo-Roa, T., Milnik, A., Samann, P. G., Vukojevic, V., Coynel, D., Demougin, P., Egli, T., Gschwind, L., Jessen, F., Loos, E., Maier, W., Riedel-Heller, S. G., Scherer, M., Vogler, C., Wagner, M., Binder, E. B., de Quervain, D. J.-F., & Papassotiropoulos, A. (2017). A peripheral epigenetic signature of immune system genes is linked to neocortical thickness and memory. *Nature Communications*, *8*, 15193. https://doi.org/10.1038/ncomms15193

Friston, K. J. (2011). Functional and effective connectivity: A review. *Brain Connectivity*, *1*(1), 13–36. https://doi.org/10.1089/brain.2011.0008

Frithsen, A., & Miller, M. B. (2014). The posterior parietal cortex: Comparing remember/know and source memory tests of recollection and familiarity. *Neuropsychologia*, *61*, 31–44. https://doi.org/10.1016/j.neuropsychologia.2014.06.011

Fuchsberger, C., Flannick, J., Teslovich, T. M., Mahajan, A., Agarwala, V., Gaulton, K. J., Ma, C., Fontanillas, P., Moutsianas, L., McCarthy, D. J., Rivas, M. A., Perry, J. R. B., Sim, X., Blackwell, T. W., Robertson, N. R., Rayner, N. W., Cingolani, P., Locke, A. E., Tajes, J. F., … McCarthy, M. I. (2016). The genetic architecture of type 2 diabetes. *Nature*, *536*(7614), 41–47. https://doi.org/10.1038/nature18642

Fuster, J. M. (2000). The Module: Crisis of a Paradigm. *Neuron*, *26*(1), 51–53. https://doi.org/10.1016/S0896-6273(00)81137-X

Gabrieli, J. D. E., Ghosh, S. S., & Whitfield-Gabrieli, S. (2015). Prediction as a humanitarian and pragmatic contribution from human cognitive neuroscience. *Neuron*, *85*(1), 11–26. https://doi.org/10.1016/j.neuron.2014.10.047

Gauthier, C. J., & Fan, A. P. (2019). BOLD signal physiology: Models and applications. *NeuroImage*, *187*, 116–127. https://doi.org/10.1016/j.neuroimage.2018.03.018

Gibbs, R. A., Belmont, J. W., Hardenbol, P., Willis, T. D., Yu, F., Yang, H., Ch'ang, L.-Y., Huang, W., Liu, B., Shen, Y., Tam, P. K.-H., Tsui, L.-C., Waye, M. M. Y., Wong, J. T.-F., Zeng, C., Zhang, Q., Chee, M. S., Galver, L. M., Kruglyak,

S., … Methods Group. (2003). The International HapMap Project. *Nature*, *426*(6968), 789–796. https://doi.org/10.1038/nature02168

Goeman, J. J., & Solari, A. (2014). Multiple hypothesis testing in genomics. *Statistics in Medicine*, *33*(11), 1946–1978. https://doi.org/10.1002/sim.6082

Goodwin, S., McPherson, J. D., & McCombie, W. R. (2016). Coming of age: Ten years of next-generation sequencing technologies. *Nature Reviews Genetics*, *17*(6), 333–351. https://doi.org/10.1038/nrg.2016.49

Hasin, Y., Seldin, M., & Lusis, A. (2017). Multi-omics approaches to disease. *Genome Biology*, *18*(1), 83–83. PubMed. https://doi.org/10.1186/s13059-017-1215-1

He, T., Kong, R., Holmes, A. J., Sabuncu, M. R., Eickhoff, S. B., Bzdok, D., Feng, J., & Yeo, B. T. (2018). Is deep learning better than kernel regression for functional connectivity prediction of fluid intelligence? In 2018 *International Workshop on Pattern Recognition in Neuroimaging (PRNI),* IEEE. 1–4.

Heck, A., Fastenrath, M., Ackermann, S., Auschra, B., Bickel, H., Coynel, D., Gschwind, L., Jessen, F., Kaduszkiewicz, H., Maier, W., Milnik, A., Pentzek, M., Riedel-Heller, S. G., Ripke, S., Spalek, K., Sullivan, P., Vogler, C., Wagner, M., Weyerer, S., … Papassotiropoulos, A. (2014). Converging Genetic and Functional Brain Imaging Evidence Links Neuronal Excitability to Working Memory, Psychiatric Disease, and Brain Activity. *Neuron*, *81*(5), 1203–1213. https://doi.org/10.1016/j.neuron.2014.01.010

Heck, A., Fastenrath, M., Coynel, D., Auschra, B., Bickel, H., Freytag, V., Gschwind, L., Hartmann, F., Jessen, F., Kaduszkiewicz, H., Maier, W., Milnik, A., Pentzek, M., Riedel-Heller, S. G., Spalek, K., Vogler, C., Wagner, M., Weyerer, S., Wolfsgruber, S., … Papassotiropoulos, A. (2015). Genetic Analysis of Association Between Calcium Signaling and Hippocampal Activation, Memory Performance in the Young and Old, and Risk for Sporadic Alzheimer Disease. *JAMA Psychiatry*, *72*(10), 1029–1036. PubMed. https://doi.org/10.1001/jamapsychiatry.2015.1309

Heck, A., Milnik, A., Vukojevic, V., Petrovska, J., Egli, T., Singer, J., Escobar, P., Sengstag, T., Coynel, D., & Freytag, V. (2017). Exome sequencing of healthy phenotypic extremes links TROVE2 to emotional memory and PTSD. *Nature Human Behaviour*, *1*(4), 0081.

Hindorff, L. A., Bonham, V. L., Brody, L. C., Ginoza, M. E. C., Hutter, C. M., Manolio, T. A., & Green, E. D. (2018). Prioritizing diversity in human genomics research. *Nature Reviews Genetics*, *19*(3), 175–185. https://doi.org/10.1038/nrg.2017.89

Horn, M., Jardri, R., D'Hondt, F., Vaiva, G., Thomas, P., & Pins, D. (2016). The multiple neural networks of familiarity: A meta-analysis of functional imaging studies. *Cognitive, Affective & Behavioral Neuroscience*, *16*(1), 176–190. https://doi.org/10.3758/s13415-015-0392-1

Horwitz, T., Lam, K., Chen, Y., Xia, Y., & Liu, C. (2019). A decade in psychiatric GWAS research. *Molecular Psychiatry*, *24*(3), 378–389. https://doi.org/10.1038/s41380-018-0055-z

Huys, Q. J. M., Maia, T. V., & Frank, M. J. (2016). Computational psychiatry as a bridge from neuroscience to clinical applications. *Nature Neuroscience*, *19*(3), 404–413. https://doi.org/10.1038/nn.4238

Hyvarinen, A., & Oja, E. (2000). Independent component analysis: Algorithms and applications. *Neural Networks : The Official Journal of the International Neural Network Society*, *13*(4–5), 411–430. https://doi.org/10.1016/s0893-6080(00)00026-5

Ioannidis, J. P. A. (2005). Why most published research findings are false. *PLoS Medicine*, *2*(8), e124. https://doi.org/10.1371/journal.pmed.0020124

Jasny, B. R., Chin, G., Chong, L., & Vignieri, S. (2011). Again, and Again, and Again …. *Science*, *334*(6060), 1225. https://doi.org/10.1126/science.334.6060.1225

Jiang, J., Zhao, Y.-J., Hu, X.-Y., Du, M.-Y., Chen, Z.-Q., Wu, M., Li, K.-M., Zhu, H.-Y., Kumar, P., & Gong, Q.-Y. (2017). Microstructural brain abnormalities in medication-free patients with major depressive disorder: A systematic review and meta-analysis of diffusion tensor imaging. *Journal of Psychiatry & Neuroscience : JPN*, *42*(3), 150–163. https://doi.org/10.1503/jpn.150341

Kairov, U., Cantini, L., Greco, A., Molkenov, A., Czerwinska, U., Barillot, E., & Zinovyev, A. (2017). Determining the optimal number of independent components for reproducible transcriptomic data analysis. *BMC Genomics*, *18*(1), 712. https://doi.org/10.1186/s12864-017-4112-9

Kannan, L., Ramos, M., Re, A., El-Hachem, N., Safikhani, Z., Gendoo, D. M. A., Davis, S., Gomez-Cabrero, D., Castelo, R., Hansen, K. D., Carey, V. J., Morgan, M., Culhane, A. C., Haibe-Kains, B., & Waldron, L. (2016). Public

data and open source tools for multi-assay genomic investigation of disease. *Briefings in Bioinformatics*, *17*(4), 603–615. PubMed. https://doi.org/10.1093/bib/bbv080

Kelly, S., Jahanshad, N., Zalesky, A., Kochunov, P., Agartz, I., Alloza, C., Andreassen, O. A., Arango, C., Banaj, N., Bouix, S., Bousman, C. A., Brouwer, R. M., Bruggemann, J., Bustillo, J., Cahn, W., Calhoun, V., Cannon, D., Carr, V., Catts, S., … Donohoe, G. (2018). Widespread white matter microstructural differences in schizophrenia across 4322 individuals: Results from the ENIGMA Schizophrenia DTI Working Group. *Molecular Psychiatry*, *23*(5), 1261–1269. https://doi.org/10.1038/mp.2017.170

Kiezun, A., Garimella, K., Do, R., Stitziel, N. O., Neale, B. M., McLaren, P. J., Gupta, N., Sklar, P., Sullivan, P. F., Moran, J. L., Hultman, C. M., Lichtenstein, P., Magnusson, P., Lehner, T., Shugart, Y. Y., Price, A. L., de Bakker, P. I. W., Purcell, S. M., & Sunyaev, S. R. (2012). Exome sequencing and the genetic basis of complex traits. *Nature Genetics*, *44*(6), 623–630. https://doi.org/10.1038/ng.2303

Kim, H. (2010). Dissociating the roles of the default-mode, dorsal, and ventral networks in episodic memory retrieval. *NeuroImage*, *50*(4), 1648–1657. https://doi.org/10.1016/j.neuroimage.2010.01.051

Laird, A. R., Lancaster, J. L., & Fox, P. T. (2005). BrainMap: The social evolution of a human brain mapping database. *Neuroinformatics*, *3*(1), 65–78. https://doi.org/10.1385/ni:3:1:065

Lam, M., Chen, C.-Y., Li, Z., Martin, A. R., Bryois, J., Ma, X., Gaspar, H., Ikeda, M., Benyamin, B., Brown, B. C., Liu, R., Zhou, W., Guan, L., Kamatani, Y., Kim, S.-W., Kubo, M., Kusumawardhani, A. A. A. A., Liu, C.-M., Ma, H., … Genetic REsearch on schizophreniA neTwork-China and the Netherlands (GREAT-CN). (2019). Comparative genetic architectures of schizophrenia in East Asian and European populations. *Nature Genetics*, *51*(12), 1670–1678. https://doi.org/10.1038/s41588-019-0512-x

Laruelle, M., Gelernter, J., & Innis, R. (1998). D 2 receptors binding potential is not affected by Taq1 polymorphism at the D 2 receptor gene. *Molecular Psychiatry*, *3*(3), 261.

Lazar, N. (2016). The big picture: Imagining genetics: A tale of two modalities. *Chance*, *29*(2), 61–63.

Lee, P. H., O'Dushlaine, C., Thomas, B., & Purcell, S. M. (2012). INRICH: interval-based enrichment analysis for genome-wide association studies. *Bioinformatics (Oxford, England)*, *28*(13), 1797–1799. https://doi.org/10.1093/bioinformatics/bts191

Legon, W., Punzell, S., Dowlati, E., Adams, S. E., Stiles, A. B., & Moran, R. J. (2016). Altered Prefrontal Excitation/Inhibition Balance and Prefrontal Output: Markers of Aging in Human Memory Networks. *Cerebral Cortex (New York, N.Y. : 1991)*, *26*(11), 4315–4326. https://doi.org/10.1093/cercor/bhv200

Lerch, J. P., van der Kouwe, A. J. W., Raznahan, A., Paus, T., Johansen-Berg, H., Miller, K. L., Smith, S. M., Fischl, B., & Sotiropoulos, S. N. (2017). Studying neuroanatomy using MRI. *Nature Neuroscience*, *20*(3), 314–326. https://doi.org/10.1038/nn.4501

Li, Z., Chen, J., Yu, H., He, L., Xu, Y., Zhang, D., Yi, Q., Li, C., Li, X., Shen, J., Song, Z., Ji, W., Wang, M., Zhou, J., Chen, B., Liu, Y., Wang, J., Wang, P., Yang, P., … Shi, Y. (2017). Genome-wide association analysis identifies 30 new susceptibility loci for schizophrenia. *Nature Genetics*, *49*, 1576.

Lips, E. S., Cornelisse, L. N., Toonen, R. F., Min, J. L., Hultman, C. M., Holmans, P. A., O'Donovan, M. C., Purcell, S. M., Smit, A. B., Verhage, M., Sullivan, P. F., Visscher, P. M., Posthuma, D., & the International Schizophrenia Consortium. (2012). Functional gene group analysis identifies synaptic gene groups as risk factor for schizophrenia. *Molecular Psychiatry*, *17*(10), 996–1006. https://doi.org/10.1038/mp.2011.117

Locke, A. E., Kahali, B., Berndt, S. I., Justice, A. E., Pers, T. H., Day, F. R., Powell, C., Vedantam, S., Buchkovich, M. L., Yang, J., Croteau-Chonka, D. C., Esko, T., Fall, T., Ferreira, T., Gustafsson, S., Kutalik, Z., Luan, J., Mägi, R., Randall, J. C., … Speliotes, E. K. (2015). Genetic studies of body mass index yield new insights for obesity biology. *Nature*, *518*, 197.

Loos, E., Egli, T., Coynel, D., Fastenrath, M., Freytag, V., Papassotiropoulos, A., de Quervain, D. J.-F., & Milnik, A. (2019). Predicting emotional arousal and emotional memory performance from an identical brain network. *NeuroImage*, *189*, 459–467. https://doi.org/10.1016/j.neuroimage.2019.01.028

Luciano, M., Hagenaars, S. P., Davies, G., Hill, W. D., Clarke, T.-K., Shirali, M., Harris, S. E., Marioni, R. E., Liewald, D. C., Fawns-Ritchie, C., Adams, M. J., Howard, D. M., Lewis, C. M., Gale, C. R., McIntosh, A. M., & Deary, I. J.

(2018). Association analysis in over 329,000 individuals identifies 116 independent variants influencing neuroticism. *Nature Genetics*, *50*(1), 6–11. https://doi.org/10.1038/s41588-017-0013-8

Lusebrink, F., Sciarra, A., Mattern, H., Yakupov, R., & Speck, O. (2017). T1-weighted in vivo human whole brain MRI dataset with an ultrahigh isotropic resolution of 250 mum. *Scientific Data*, *4*, 170032. https://doi.org/10.1038/sdata.2017.32

Mandler, G. (1980). Recognizing: The judgment of previous occurrence. *Psychological Review*, *87*(3), 252–271. https://doi.org/10.1037/0033-295X.87.3.252

Marchini, J., Howie, B., Myers, S., McVean, G., & Donnelly, P. (2007). A new multipoint method for genome-wide association studies by imputation of genotypes. *Nature Genetics*, *39*(7), 906–913. https://doi.org/10.1038/ng2088

Marigorta, U. M., Rodriguez, J. A., Gibson, G., & Navarro, A. (2018). Replicability and Prediction: Lessons and Challenges from GWAS. *Trends in Genetics : TIG*, *34*(7), 504–517. https://doi.org/10.1016/j.tig.2018.03.005

McIntosh, A. R., Rajah, M. N., & Lobaugh, N. J. (1999). Interactions of prefrontal cortex in relation to awareness in sensory learning. *Science (New York, N.Y.)*, *284*(5419), 1531–1533. https://doi.org/10.1126/science.284.5419.1531

Metzker, M. L. (2010). Sequencing technologies—The next generation. *Nature Reviews Genetics*, *11*(1), 31–46. https://doi.org/10.1038/nrg2626

Mishra, A., & MacGregor, S. (2017). A Novel Approach for Pathway Analysis of GWAS Data Highlights Role of BMP Signaling and Muscle Cell Differentiation in Colorectal Cancer Susceptibility. *Twin Research and Human Genetics : The Official Journal of the International Society for Twin Studies*, *20*(1), 1–9. https://doi.org/10.1017/thg.2016.100

Misic, B., & Sporns, O. (2016). From regions to connections and networks: New bridges between brain and behavior. *Current Opinion in Neurobiology*, *40*, 1–7. https://doi.org/10.1016/j.conb.2016.05.003

Montgomery, S. A., & Asberg, M. (1979). A new depression scale designed to be sensitive to change. *The British Journal of Psychiatry : The Journal of Mental Science*, *134*, 382–389. https://doi.org/10.1192/bjp.134.4.382

Murray, R. M., Bhavsar, V., Tripoli, G., & Howes, O. (2017). 30 Years on: How the Neurodevelopmental Hypothesis of Schizophrenia Morphed Into the

Developmental Risk Factor Model of Psychosis. *Schizophrenia Bulletin*, *43*(6), 1190–1196. PubMed. https://doi.org/10.1093/schbul/sbx121

Nagel, M., Jansen, P. R., Stringer, S., Watanabe, K., de Leeuw, C. A., Bryois, J., Savage, J. E., Hammerschlag, A. R., Skene, N. G., Munoz-Manchado, A. B., White, T., Tiemeier, H., Linnarsson, S., Hjerling-Leffler, J., Polderman, T. J. C., Sullivan, P. F., van der Sluis, S., & Posthuma, D. (2018). Meta-analysis of genome-wide association studies for neuroticism in 449,484 individuals identifies novel genetic loci and pathways. *Nature Genetics*, *50*(7), 920–927. https://doi.org/10.1038/s41588-018-0151-7

Nichols, T. E., Das, S., Eickhoff, S. B., Evans, A. C., Glatard, T., Hanke, M., Kriegeskorte, N., Milham, M. P., Poldrack, R. A., Poline, J.-B., Proal, E., Thirion, B., Van Essen, D. C., White, T., & Yeo, B. T. T. (2017). Best practices in data analysis and sharing in neuroimaging using MRI. *Nature Neuroscience*, *20*(3), 299–303. https://doi.org/10.1038/nn.4500

Nurnberger, J. I., Jr, Koller, D. L., Jung, J., Edenberg, H. J., Foroud, T., Guella, I., Vawter, M. P., Kelsoe, J. R., & for the Psychiatric Genomics Consortium Bipolar Group. (2014). Identification of Pathways for Bipolar Disorder: A Meta-analysis. *JAMA Psychiatry*, *71*(6), 657–664. https://doi.org/10.1001/jamapsychiatry.2014.176

Open Science Collaboration. (2015). Estimating the reproducibility of psychological science. *Science*, *349*(6251), aac4716.

Otte, C., Gold, S. M., Penninx, B. W., Pariante, C. M., Etkin, A., Fava, M., Mohr, D. C., & Schatzberg, A. F. (2016). Major depressive disorder. *Nature Reviews. Disease Primers*, *2*, 16065. https://doi.org/10.1038/nrdp.2016.65

Papassotiropoulos, A., Henke, K., Stefanova, E., Aerni, A., Muller, A., Demougin, P., Vogler, C., Sigmund, J. C., Gschwind, L., Huynh, K.-D., Coluccia, D., Mondadori, C. R., Hanggi, J., Buchmann, A., Kostic, V., Novakovic, I., van den Bussche, H., Kaduszkiewicz, H., Weyerer, S., … de Quervain, D. J.-F. (2011). A genome-wide survey of human short-term memory. *Molecular Psychiatry*, *16*(2), 184–192. https://doi.org/10.1038/mp.2009.133

Papassotiropoulos, A., Stefanova, E., Vogler, C., Gschwind, L., Ackermann, S., Spalek, K., Rasch, B., Heck, A., Aerni, A., Hanser, E., Demougin, P., Huynh, K.-D., Luechinger, R., Klarhofer, M., Novakovic, I., Kostic, V., Boesiger, P., Scheffler, K., & de Quervain, D. J.-F. (2013). A genome-wide survey and

functional brain imaging study identify CTNNBL1 as a memory-related gene. *Molecular Psychiatry*, *18*(2), 255–263. https://doi.org/10.1038/mp.2011.148

Papassotiropoulos, Andreas, & de Quervain, D. J.-F. (2011). Genetics of human episodic memory: Dealing with complexity. *Trends in Cognitive Sciences*, *15*(9), 381–387. https://doi.org/10.1016/j.tics.2011.07.005

Papassotiropoulos, Andreas, Stephan, D. A., Huentelman, M. J., Hoerndli, F. J., Craig, D. W., Pearson, J. V., Huynh, K.-D., Brunner, F., Corneveaux, J., Osborne, D., Wollmer, M. A., Aerni, A., Coluccia, D., Hanggi, J., Mondadori, C. R. A., Buchmann, A., Reiman, E. M., Caselli, R. J., Henke, K., & de Quervain, D. J.-F. (2006). Common Kibra alleles are associated with human memory performance. *Science (New York, N.Y.)*, *314*(5798), 475–478. https://doi.org/10.1126/science.1129837

Pardinas, A. F., Holmans, P., Pocklington, A. J., Escott-Price, V., Ripke, S., Carrera, N., Legge, S. E., Bishop, S., Cameron, D., Hamshere, M. L., Han, J., Hubbard, L., Lynham, A., Mantripragada, K., Rees, E., MacCabe, J. H., McCarroll, S. A., Baune, B. T., Breen, G., … Walters, J. T. R. (2018). Common schizophrenia alleles are enriched in mutation-intolerant genes and in regions under strong background selection. *Nature Genetics*, *50*(3), 381–389. https://doi.org/10.1038/s41588-018-0059-2

Pe'er, I., Yelensky, R., Altshuler, D., & Daly, M. J. (2008). Estimation of the multiple testing burden for genomewide association studies of nearly all common variants. *Genetic Epidemiology*, *32*(4), 381–385. https://doi.org/10.1002/gepi.20303

Petrovska, J., Coynel, D., Fastenrath, M., Milnik, A., Auschra, B., Egli, T., Gschwind, L., Hartmann, F., Loos, E., Sifalakis, K., Vogler, C., de Quervain, D. J.-F., Papassotiropoulos, A., & Heck, A. (2017). The NCAM1 gene set is linked to depressive symptoms and their brain structural correlates in healthy individuals. *Journal of Psychiatric Research*, *91*, 116–123. https://doi.org/10.1016/j.jpsychires.2017.03.007

Plewes, D. B., & Kucharczyk, W. (2012). Physics of MRI: a primer. *Journal of Magnetic Resonance Imaging : JMRI*, *35*(5), 1038–1054. https://doi.org/10.1002/jmri.23642

Plomin, R., DeFries, J. C., Knopik, V. S., & Neiderhiser, J. M. (2016). Top 10 Replicated Findings From Behavioral Genetics. *Perspectives on*

Psychological Science : A Journal of the Association for Psychological Science, *11*(1), 3–23. https://doi.org/10.1177/1745691615617439

Pohjalainen, T., Rinne, J. O., Nagren, K., Lehikoinen, P., Anttila, K., Syvalahti, E. K., & Hietala, J. (1998). The A1 allele of the human D2 dopamine receptor gene predicts low D2 receptor availability in healthy volunteers. *Molecular Psychiatry*, *3*(3), 256–260. https://doi.org/10.1038/sj.mp.4000350

Poldrack, R. A., Baker, C. I., Durnez, J., Gorgolewski, K. J., Matthews, P. M., Munafò, M. R., Nichols, T. E., Poline, J.-B., Vul, E., & Yarkoni, T. (2017). Scanning the horizon: Towards transparent and reproducible neuroimaging research. *Nature Reviews Neuroscience*, *18*(2), 115–126. https://doi.org/10.1038/nrn.2016.167

Poldrack, R. A., & Farah, M. J. (2015). Progress and challenges in probing the human brain. *Nature*, *526*(7573), 371–379. https://doi.org/10.1038/nature15692

Popejoy, A. B., & Fullerton, S. M. (2016). Genomics is failing on diversity. *Nature News*, *538*(7624), 161.

Price, A. L., Spencer, C. C. A., & Donnelly, P. (2015). Progress and promise in understanding the genetic basis of common diseases. *Proceedings. Biological Sciences*, *282*(1821), 20151684. https://doi.org/10.1098/rspb.2015.1684

Prinz, F., Schlange, T., & Asadullah, K. (2011). Believe it or not: How much can we rely on published data on potential drug targets? *Nature Reviews Drug Discovery*, *10*(9), 712–712. https://doi.org/10.1038/nrd3439-c1

Reid, A. T., Headley, D. B., Mill, R. D., Sanchez-Romero, R., Uddin, L. Q., Marinazzo, D., Lurie, D. J., Valdés-Sosa, P. A., Hanson, S. J., Biswal, B. B., Calhoun, V., Poldrack, R. A., & Cole, M. W. (2019). Advancing functional connectivity research from association to causation. *Nature Neuroscience*, *22*(11), 1751–1760. https://doi.org/10.1038/s41593-019-0510-4

Ripke, S., Neale, B. M., Corvin, A., Walters, J. T. R., Farh, K.-H., Holmans, P. A., Lee, P., Bulik-Sullivan, B., Collier, D. A., Huang, H., Pers, T. H., Agartz, I., Agerbo, E., Albus, M., Alexander, M., Amin, F., Bacanu, S. A., Begemann, M., Belliveau Jr, R. A., … O'Donovan, M. C. (2014). Biological insights from 108 schizophrenia-associated genetic loci. *Nature*, *511*, 421.

Ripke, S., Wray, N. R., Lewis, C. M., Hamilton, S. P., Weissman, M. M., Breen, G., Byrne, E. M., Blackwood, D. H. R., Boomsma, D. I., Cichon, S., Heath, A. C.,

Holsboer, F., Lucae, S., Madden, P. A. F., Martin, N. G., McGuffin, P., Muglia, P., Noethen, M. M., Penninx, B. P., … Major Depressive Disorder Working Group of the Psychiatric GWAS Consortium. (2013). A mega-analysis of genome-wide association studies for major depressive disorder. *Molecular Psychiatry*, *18*(4), 497–511. https://doi.org/10.1038/mp.2012.21

Roalf, D. R., & Gur, R. C. (2017). Functional brain imaging in neuropsychology over the past 25 years. *Neuropsychology*, *31*(8), 954–971. https://doi.org/10.1037/neu0000426

Rosen, B. R., & Savoy, R. L. (2012). fMRI at 20: Has it changed the world? *NeuroImage*, *62*(2), 1316–1324. https://doi.org/10.1016/j.neuroimage.2012.03.004

Salimpoor, V. N., van den Bosch, I., Kovacevic, N., McIntosh, A. R., Dagher, A., & Zatorre, R. J. (2013). Interactions between the nucleus accumbens and auditory cortices predict music reward value. *Science (New York, N.Y.)*, *340*(6129), 216–219. https://doi.org/10.1126/science.1231059

Sanders, S. J., Neale, B. M., Huang, H., Werling, D. M., An, J.-Y., Dong, S., Abecasis, G., Arguello, P. A., Blangero, J., Boehnke, M., Daly, M. J., Eggan, K., Geschwind, D. H., Glahn, D. C., Goldstein, D. B., Gur, R. E., Handsaker, R. E., McCarroll, S. A., Ophoff, R. A., … Freimer, N. B. (2017). Whole genome sequencing in psychiatric disorders: The WGSPD consortium. *Nature Neuroscience*, *20*(12), 1661–1668. https://doi.org/10.1038/s41593-017-0017-9

Scalici, F., Caltagirone, C., & Carlesimo, G. A. (2017). The contribution of different prefrontal cortex regions to recollection and familiarity: A review of fMRI data. *Neuroscience and Biobehavioral Reviews*, *83*, 240–251. https://doi.org/10.1016/j.neubiorev.2017.10.017

Schmidt, S. (2009). Shall we Really do it Again? The Powerful Concept of Replication is Neglected in the Social Sciences. *Review of General Psychology*, *13*(2), 90–100. https://doi.org/10.1037/a0015108

Segre, A. V., Groop, L., Mootha, V. K., Daly, M. J., & Altshuler, D. (2010). Common inherited variation in mitochondrial genes is not enriched for associations with type 2 diabetes or related glycemic traits. *PLoS Genetics*, *6*(8). https://doi.org/10.1371/journal.pgen.1001058

Skinner, E. I., & Fernandes, M. A. (2007). Neural correlates of recollection and familiarity: A review of neuroimaging and patient data. *Neuropsychologia*, *45*(10), 2163–2179. https://doi.org/10.1016/j.neuropsychologia.2007.03.007

Smith, S. M., Fox, P. T., Miller, K. L., Glahn, D. C., Fox, P. M., Mackay, C. E., Filippini, N., Watkins, K. E., Toro, R., Laird, A. R., & Beckmann, C. F. (2009). Correspondence of the brain's functional architecture during activation and rest. *Proceedings of the National Academy of Sciences of the United States of America*, *106*(31), 13040–13045. https://doi.org/10.1073/pnas.0905267106

Spalek, K., Coynel, D., Freytag, V., Hartmann, F., Heck, A., Milnik, A., de Quervain, D., & Papassotiropoulos, A. (2016). A common NTRK2 variant is associated with emotional arousal and brain white-matter integrity in healthy young subjects. *Translational Psychiatry*, *6*(3), e758–e758. PubMed. https://doi.org/10.1038/tp.2016.20

Spaniol, J., Davidson, P. S. R., Kim, A. S. N., Han, H., Moscovitch, M., & Grady, C. L. (2009). Event-related fMRI studies of episodic encoding and retrieval: Meta-analyses using activation likelihood estimation. *Neuropsychologia*, *47*(8–9), 1765–1779. https://doi.org/10.1016/j.neuropsychologia.2009.02.028

Spielberg, J. M., Miller, G. A., Heller, W., & Banich, M. T. (2015). Flexible brain network reconfiguration supporting inhibitory control. *Proceedings of the National Academy of Sciences of the United States of America*, *112*(32), 10020–10025. https://doi.org/10.1073/pnas.1500048112

Squire, L. R., Wixted, J. T., & Clark, R. E. (2007). Recognition memory and the medial temporal lobe: A new perspective. *Nature Reviews Neuroscience*, *8*(11), 872.

Stephan, K. E., Marshall, J. C., Friston, K. J., Rowe, J. B., Ritzl, A., Zilles, K., & Fink, G. R. (2003). Lateralized cognitive processes and lateralized task control in the human brain. *Science (New York, N.Y.)*, *301*(5631), 384–386. https://doi.org/10.1126/science.1086025

Sullivan, P. F. (2010). The psychiatric GWAS consortium: Big science comes to psychiatry. *Neuron*, *68*(2), 182–186. https://doi.org/10.1016/j.neuron.2010.10.003

Sullivan, P. F., Agrawal, A., Bulik, C. M., Andreassen, O. A., Børglum, A. D., Breen, G., Cichon, S., Edenberg, H. J., Faraone, S. V., Gelernter, J., Mathews, C. A., Nievergelt, C. M., Smoller, J. W., O'Donovan, M. C., & Psychiatric Genomics

Consortium. (2018). Psychiatric Genomics: An Update and an Agenda. *The American Journal of Psychiatry*, *175*(1), 15–27. PubMed. https://doi.org/10.1176/appi.ajp.2017.17030283

Takeuchi, H., Taki, Y., Sassa, Y., Hashizume, H., Sekiguchi, A., Fukushima, A., & Kawashima, R. (2011). Verbal working memory performance correlates with regional white matter structures in the frontoparietal regions. *Neuropsychologia*, *49*(12), 3466–3473. https://doi.org/10.1016/j.neuropsychologia.2011.08.022

Thompson, P. M., Stein, J. L., Medland, S. E., Hibar, D. P., Vasquez, A. A., Renteria, M. E., Toro, R., Jahanshad, N., Schumann, G., Franke, B., Wright, M. J., Martin, N. G., Agartz, I., Alda, M., Alhusaini, S., Almasy, L., Almeida, J., Alpert, K., Andreasen, N. C., … Drevets, W. (2014). The ENIGMA Consortium: Large-scale collaborative analyses of neuroimaging and genetic data. *Brain Imaging and Behavior*, *8*(2), 153–182. https://doi.org/10.1007/s11682-013-9269-5

van der Sluis, S., Posthuma, D., Nivard, M. G., Verhage, M., & Dolan, C. V. (2013). Power in GWAS: lifting the curse of the clinical cut-off. *Molecular Psychiatry*, *18*(1), 2–3. https://doi.org/10.1038/mp.2012.65

Van Essen, D. C., Smith, S. M., Barch, D. M., Behrens, T. E. J., Yacoub, E., & Ugurbil, K. (2013). The WU-Minn Human Connectome Project: An overview. *NeuroImage*, *80*, 62–79. https://doi.org/10.1016/j.neuroimage.2013.05.041

Vanasse, T. J., Fox, P. M., Barron, D. S., Robertson, M., Eickhoff, S. B., Lancaster, J. L., & Fox, P. T. (2018). BrainMap VBM: An environment for structural meta-analysis. *Human Brain Mapping*, *39*(8), 3308–3325. https://doi.org/10.1002/hbm.24078

Vilberg, K. L., & Rugg, M. D. (2008). Memory retrieval and the parietal cortex: A review of evidence from a dual-process perspective. *Neuropsychologia*, *46*(7), 1787–1799. https://doi.org/10.1016/j.neuropsychologia.2008.01.004

Visscher, P. M., Wray, N. R., Zhang, Q., Sklar, P., McCarthy, M. I., Brown, M. A., & Yang, J. (2017). 10 Years of GWAS Discovery: Biology, Function, and Translation. *American Journal of Human Genetics*, *101*(1), 5–22. https://doi.org/10.1016/j.ajhg.2017.06.005

Vossel, S., Weidner, R., Moos, K., & Fink, G. R. (2016). Individual attentional selection capacities are reflected in interhemispheric connectivity of the

parietal cortex. *NeuroImage*, *129*, 148–158. https://doi.org/10.1016/j.neuroimage.2016.01.054

Vukojevic, V., Kolassa, I.-T., Fastenrath, M., Gschwind, L., Spalek, K., Milnik, A., Heck, A., Vogler, C., Wilker, S., Demougin, P., Peter, F., Atucha, E., Stetak, A., Roozendaal, B., Elbert, T., Papassotiropoulos, A., & de Quervain, D. J.-F. (2014). Epigenetic modification of the glucocorticoid receptor gene is linked to traumatic memory and post-traumatic stress disorder risk in genocide survivors. *The Journal of Neuroscience : The Official Journal of the Society for Neuroscience*, *34*(31), 10274–10284. https://doi.org/10.1523/JNEUROSCI.1526-14.2014

Wadi, L., Meyer, M., Weiser, J., Stein, L. D., & Reimand, J. (2016). Impact of outdated gene annotations on pathway enrichment analysis. *Nature Methods*, *13*(9), 705–706. https://doi.org/10.1038/nmeth.3963

Wang, K., Li, M., & Hakonarson, H. (2010). Analysing biological pathways in genome-wide association studies. *Nature Reviews Genetics*, *11*(12), 843–854. https://doi.org/10.1038/nrg2884

Whelan, R., Watts, R., Orr, C. A., Althoff, R. R., Artiges, E., Banaschewski, T., Barker, G. J., Bokde, A. L. W., Buchel, C., Carvalho, F. M., Conrod, P. J., Flor, H., Fauth-Buhler, M., Frouin, V., Gallinat, J., Gan, G., Gowland, P., Heinz, A., Ittermann, B., … Garavan, H. (2014). Neuropsychosocial profiles of current and future adolescent alcohol misusers. *Nature*, *512*(7513), 185–189. https://doi.org/10.1038/nature13402

Wojcik, G. L., Graff, M., Nishimura, K. K., Tao, R., Haessler, J., Gignoux, C. R., Highland, H. M., Patel, Y. M., Sorokin, E. P., Avery, C. L., Belbin, G. M., Bien, S. A., Cheng, I., Cullina, S., Hodonsky, C. J., Hu, Y., Huckins, L. M., Jeff, J., Justice, A. E., … Carlson, C. S. (2019). Genetic analyses of diverse populations improves discovery for complex traits. *Nature*, *570*(7762), 514–518. https://doi.org/10.1038/s41586-019-1310-4

Wojcik, G. L., Kao, W. H. L., & Duggal, P. (2015). Relative performance of gene- and pathway-level methods as secondary analyses for genome-wide association studies. *BMC Genetics*, *16*, 34. https://doi.org/10.1186/s12863-015-0191-2

Woo, C.-W., Chang, L. J., Lindquist, M. A., & Wager, T. D. (2017). Building better biomarkers: Brain models in translational neuroimaging. *Nature Neuroscience*, *20*(3), 365.

Wood, A. R., Esko, T., Yang, J., Vedantam, S., Pers, T. H., Gustafsson, S., Chu, A. Y., Estrada, K., Luan, J., Kutalik, Z., Amin, N., Buchkovich, M. L., Croteau-Chonka, D. C., Day, F. R., Duan, Y., Fall, T., Fehrmann, R., Ferreira, T., Jackson, A. U., … Frayling, T. M. (2014). Defining the role of common variation in the genomic and biological architecture of adult human height. *Nature Genetics*, *46*(11), 1173–1186. https://doi.org/10.1038/ng.3097

Wray, N. R., Ripke, S., Mattheisen, M., Trzaskowski, M., Byrne, E. M., Abdellaoui, A., Adams, M. J., Agerbo, E., Air, T. M., Andlauer, T. M. F., Bacanu, S.-A., Bækvad-Hansen, M., Beekman, A. F. T., Bigdeli, T. B., Binder, E. B., Blackwood, D. R. H., Bryois, J., Buttenschøn, H. N., Bybjerg-Grauholm, J., … the Major Depressive Disorder Working Group of the Psychiatric Genomics Consortium. (2018). Genome-wide association analyses identify 44 risk variants and refine the genetic architecture of major depression. *Nature Genetics*, *50*(5), 668–681. https://doi.org/10.1038/s41588-018-0090-3

Xu, M., Wang, T., Chen, S., Fox, P. T., & Tan, L. H. (2015). Effective connectivity of brain regions related to visual word recognition: An fMRI study of Chinese reading. *Human Brain Mapping*, *36*(7), 2580–2591. https://doi.org/10.1002/hbm.22792

Yahata, N., Kasai, K., & Kawato, M. (2017). Computational neuroscience approach to biomarkers and treatments for mental disorders. *Psychiatry and Clinical Neurosciences*, *71*(4), 215–237. https://doi.org/10.1111/pcn.12502

Yarkoni, T., & Westfall, J. (2017). Choosing Prediction Over Explanation in Psychology: Lessons From Machine Learning. *Perspectives on Psychological Science : A Journal of the Association for Psychological Science*, *12*(6), 1100–1122. https://doi.org/10.1177/1745691617693393

Yonelinas, A. P. (2002). The nature of recollection and familiarity: A review of 30 years of research. *Journal of Memory and Language*, *46*(3), 441–517.

Yonelinas, A. P., Otten, L. J., Shaw, K. N., & Rugg, M. D. (2005). Separating the brain regions involved in recollection and familiarity in recognition memory. *The Journal of Neuroscience : The Official Journal of the Society for Neuroscience*, *25*(11), 3002–3008. https://doi.org/10.1523/JNEUROSCI.5295-04.2005